2016

Interference Mitigation and Measurement Quality Assessment for Multi-Antenna GNSS Receivers

Vagle, Niranjana

UNIVERSITY OF CALGARY

Interference Mitigation and Measurement Quality Assessment for Multi-Antenna GNSS Receivers

by

Niranjana Vagle

A THESIS

SUBMITTED TO THE FACULTY OF GRADUATE STUDIES

IN PARTIAL FULFILMENT OF THE REQUIREMENTS FOR THE

DEGREE OF DOCTOR OF PHILOSOPHY

GRADUATE PROGRAM IN GEOMATICS ENGINEERING

CALGARY, ALBERTA

DECEMBER, 2016

Abstract

This research focuses on performance improvement of antenna array based GNSS receivers under interference with focus on code and carrier phase measurements. Despite the remarkable amount of research on antenna array processing in wireless communications, application of these techniques to GNSS has not been studied extensively. In the case of GNSS, apart from interference mitigation, it is important to generate good estimates of code and carrier phase measurements. Array based processing techniques induce measurement distortions in the presence of interference, which is not acceptable for high precision carrier phase based applications, an issue that is not relevant for communications. An extensive analysis of GNSS measurement and position quality is performed.

In order to analyze performance in a controlled environment, a novel method of simulating multi-antenna GNSS signals is proposed, with simulation of different types of electronic interference and multipath. The simulator is tested for high fidelity applications and is used to characterize measurement distortions. The performance of different beamforming techniques is evaluated in specular multipath conditions using simulated and actual data. It is shown that significant reduction in multipath errors can be obtained using a practically realizable antenna array by using the receiver processing approaches suggested herein. Calibration is the first step towards implementing many distortionless beamforming techniques. Yet, calibration using actual signals is challenging in multipath environments. A method is proposed and tested to reduce calibration parameter estimation errors in multipath environments. Finally, array based receiver measurement and position

distortions are evaluated under different electronic interference using simulated and actual data.

Preface

Some parts of this thesis contain materials from two previously published conference papers and two journal papers which are being accepted for publication. These papers are as follows:

Vagle, N., A. Broumandan, and G. Lachapelle (2016) “Analysis of Multi-antenna GNSS Receiver Performance under Jamming Attacks”, in *SENSORS, MPDI,* doi:10.3390/s16111937.

Vagle, N., A. Broumandan, A. Jafarnia-Jahromi and G. Lachapelle (2016) “Performance Analysis of Multipath Mitigation using Antenna Arrays”, in *The Journal of Global Positioning Systems*, DOI: 10.1186/s41445-016-0004-6.

Vagle, N., A. Broumandan, A. Jafarnia-Jahromi and G. Lachapelle (2016) “Performance of Antenna Array Calibration in Multipath Environments”, in *Proceedings of ION International Technical Meeting (ITM) 2016,* 25-28 January, Monterey, California, The Institute of Navigation, 9 Pages [Peer Reviewed].

Vagle, N., A. Broumandan, A. Jafarnia-Jahromi and G. Lachapelle (2014) “Characterization of GNSS Measurement Distortions Due to Antenna Array Processing in the Presence of Interference Signals”, in *Proceedings of UPINLBS 2014,* 20-21 November, Corpus Christi, Texas, IEEE, 10 Pages [Peer Reviewed].

Acknowledgements

I would like to thank all people who have been supporting me in this unforgettable journey of my life. First, I would like to express my sincere gratitude to my supervisor, Professor Gérard Lachapelle for his continuous guidance, financial support, care and encouragement throughout my studies. His pro-active nature, passion for the outdoors and enthusiasm to learn new things have motivated me in studies as well as in life. It was an honour and privilege to be your student.

My sincere thanks to my advisor, Dr. Ali Broumandan for his continuous advice and guidance. This research would have been more challenging without your continuous constructive feedback, encouragement and technical discussions. Thank you for constantly motivating me to focus and complete the research in a timely manner.

I also thank Dr. Ali Jafarnia-Jahroomi, Dr. Saeed Daneshmand and Dr. Tao Lin for their suggestions during the course work and research. Also, many thanks to Prof Mark Petovello, Professor John Nielsen and Professor Noureldin for their excellent teaching.

I thank Accord Software and Systems for introducing me to the field of GNSS through interesting projects. I acknowledge Dr. Vyasaraj Gururao and all technical managers at Accord for their guidance and sharing their knowledge.

My past three and half years have been an enjoyable and exciting experience. I thank all past and current students of the PLAN Group for providing a friendly atmosphere during my studies. Specially, the wonderful environment created by Vijay, Suvarna, Sujay, Naveen G S, Thyagaraja Marathe, Srinivas Bhaskar, Ranjeeth, Vimal, Rakesh, Ashwitha, Srinivas Tantry, Shashidharan, Pavana, Aruna, Kavya, Sajan, Jyothi, Sahasra, made my stay in Calgary more enjoyable. Thank you all.

This research would not have been possible without blessings from my parents, the unconditional love and care from my lovely wife Shruthi, the continued support from my brothers, my in-laws and all family members. Finally, special thanks and lots of love to my little princess Aaradhya who brought bundle of joy to the family.

Dedicated to my parents: Shivarama Vagle and Rajashree Vagle

Table of Contents

List of Tables

List of Figures and Illustrations

List of Abbreviations

Abbreviation	Expansion
ADC	Analog to Digital Conversion
AGC	Automatic Gain Control
BPF	Band Pass Filter
BWGN	Bandlimited White Gaussian Noise
C/A	Coarse/Acquisition
CDMA	Code Division Multiple Access
C/N_0	Carrier to Noise Density Ratio
CRPA	Controlled Reception Pattern Antenna
CW	Continuous Wave
CWI	Continuous Wave Interference
DAS	Delay And Sum
DD	Double Delta
DLL	Delay Locked Loop
DME	Distance Measuring Equipment
DOA	Direction of Arrival
DOP	Dilution of Precision
DRC	Doppler Removal and Correlation
DSSS	Direct Sequence Spread Spectrum
DVB-T	Digital Video Broadcasting – Terrestrial
ECEF	Earth Centered Earth Fixed
EML	Early Minus Late
ENU	East North Up
FLL	Frequency Locked Loop
FRPA	Fixed Reception Pattern Antenna
GLONASS	GLObalnaya Navigazionnaya Sputnikovaya Sistema
GNSS	Global Navigation Satellite System
GPS	Global Positioning System
I&D	Integrate & Dump
IF	Intermediate Frequency
INS	Inertial Navigation System
J/S	Jamming to Signal Ratio
LNA	Low Noise Amplifier
LO	Local Oscillator
LOS	Line of Sight
MEDLL	Multipath Estimating Delay Lock Loop
MPDR	Minimum Power Distortionless Response
MPDRSS	Minimum Power Distortionless Response with Spatial Smoothing
NBP	Narrow Band Power
NCO	Numerically Controlled Oscillator
NLOS	Non Line of Sight
OCXO	Oven Controlled Crystal Oscillator
PDOP	Position Dilution of Precision

PLI	Phase Lock Indicator
PLL	Phase Locked Loop
PM	Power Minimization
PRN	Pseudo Random Number
PVT	Position Velocity Time
RF	Radio Frequency
RFI	Radio Frequency Interference
RMS	Root Mean Square
RMSE	Root Mean Square Error
RTK	Real Time Kinematic
SFP	Space Frequency Processing
SINR	Signal to Interference plus Noise Ratio
SNR	Signal to Noise Ratio
SOP	Space Only Processing
STP	Space Time Processing
TACAN	Tactical Air Navigation
UHF	Ultra High Frequency
VHF	Very High Frequency
WBP	Wide Band Power

List of Symbols

Symbol	Definition
t	Time variable
$s_i(t)$	Signal received from i^{th} satellite
P_i	Received signal power of i^{th} satellite
d_i	Navigation data bit of i^{th} satellite
c_i	Spreading code of i^{th} satellite
τ_i	Transit delay of i^{th} satellite
f_{IF}	Intermediate carrier frequency
f_d^i	Carrier Doppler of i^{th} satellite
φ_i	Carrier phase of i^{th} satellite
η_i	Additive white Gaussian noise considering single satellite
P_{cw}	Power of the CW interference [W]
f_{cw}	CW interference frequency
φ_{cw}	Phase of the CW interference
$j_{cw}(t)$	CW interference signal
$j_{chirp}(t)$	Chirp interference signal
P_{chirp}	Power of the chirp interference
$f_{chirp}(t)$	Frequency of the chirp interference
φ_{chirp}	Phase of the chirp interference
k_{chirp}	Chirp rate
f_{chirp_0}	Initial frequency of the chirp interference
$\eta(t)$	Additive white Gaussian noise considering GNSS signals and interference
J	Number of interference sources
K	Sum of LOS and multipath signals
L	Number of satellites and also number of receiver channels
μ	Narrow band power to wide band power ratio
T_c	Coherent integration time
$I_{p,acc}^i$	1 ms prompt correlator in phase accumulated value of i^{th} satellite
$Q_{p,acc}^i$	1 ms prompt correlator quadrature accumulated value of i^{th} satellite
Δd_1, Δd_2	Correlator spacing

$M \times N$	Number of antenna elements in a rectangular array
λ	Wavelength of GNSS carrier signal
$\mathbf{k}$	Vector wave number
$\mathbf{a}$	Steering vector
$\mathbf{p}_m$	Relative position of the m^{th} antenna
e_m	East relative position of m^{th} antenna with respect to reference antenna
n_m	North relative position of m^{th} antenna with respect to reference antenna
u_m	Up relative position of m^{th} antenna with respect to reference antenna
d_m	Distance between the antenna elements of a rectangular array in x-direction
d_n	Distance between the antenna elements of a rectangular array in y-direction
$x_{m,n}(t)$	Signal received at $(m,n)^{th}$ antenna of a rectangular array
$s_k(t)$	k^{th} signal component received at $(m,n)^{th}$ antenna of a rectangular array
θ_k	Elevation angle of k^{th} signal component
ϕ_k	Azimuth angle of k^{th} signal component
θ_j	Elevation angle of j^{th} interference
ϕ_j	Azimuth angle of j^{th} interference
$\eta_{m,n}(t)$	Additive white noise component at $(m,n)^{th}$ antenna
$\mathbf{x}$	Received signal vector at the rectangular antenna array of size $MN \times 1$
$\boldsymbol{\eta}$	Additive white noise vector of size $MN \times 1$
$\mathbf{s}$	Signal vector received at the rectangular array with size $K \times 1$
$\mathbf{j}$	Electronic interference signal vector received at the rectangular array with size $J \times 1$
$\mathbf{A}$	Steering matrix of the K GNSS signals (LOS + NLOS) received at the rectangular array with size $MN \times K$
$\mathbf{B}$	Steering matrix of the J electronic interference signals received t the rectangular array with size $MN \times J$
$\mathbf{a}_k$	Steering vector of k^{th} signal component with size $MN \times 1$
$\mathbf{b}_j$	Steering vector of the j^{th} electronic interference signal with size $MN \times 1$
$\mathbf{w}_{DAS}$	Weight vector of the DAS beamformer
$\mathbf{R}_{xx}$	Covariance matrix of the incoming signal
$\mathbf{w}_{MPDR}$	Weight vector of the MPDR beamformer
$\mathbf{w}_{PM}$	Weight vector of power minimization
$\mathbf{q}$	Constraint vector of power minimization

$\mathbf{p}_u$	User position in ENU coordinate system
$\mathbf{p}_r^1\ \mathbf{p}_r^2\ \mathbf{p}_r^3\ \mathbf{p}_r^4$	Four corner positions of a reflector in ENU coordinate system
$\mathbf{p}_s^i$	Position of i^{th} satellite in ENU coordinate system
$\mathbf{p}_r^{r,i}$	Position of point of reflection in ENU coordinate system
$\mathbf{n}_{norm}$	Normal vector to the plane
$\Delta\tau_e$	Extra number of chips for the multipath signals
Δd_e	Extra distance travelled by the multipath signal
c	Speed of light
$\mathbf{v}_u$	User velocity vector
$\mathbf{v}_s^i$	Velocity vector of i^{th} satellite
$f_{d,los}^i$	Carrier Doppler of the LOS signal for the i^{th} satellite
$\mathbf{H}_{los}^i$	Unit vector of the LOS signal for i^{th} satellite
$f_{d,mp}^i$	Carrier Doppler of the multipath signal for the i^{th} satellite
$\mathbf{H}_{mp1}^i$	Unit vector from i^{th} satellite to reflector
$\mathbf{H}_{mp2}^i$	Unit vector from reflector to user for i^{th} satellite
n_c	Discrete time index representation
$y_{m,n}(n_c)$	Correlator output signal for the $(m,n)^{\text{th}}$ antenna element
$\eta_{m,n}(n_c)$	Noise component after the correlation for $(m,n)^{\text{th}}$ antenna element
$r_k(n_c)$	Correlator output of k^{th} signal component as observed at (1,1) antenna element
Δf_k	Frequency offset of k^{th} signal component as observed at (1,1) antenna element
$\Delta\varphi_k$	Phase offset of k^{th} signal component as observed at (1,1) antenna element
$\mathbf{R}_f$	Forward spatially smoothed covariance matrix
$\mathbf{R}_b$	Backward spatially smoothed covariance matrix
$\mathbf{R}_{fb}$	Forward-backward spatially smoothed covariance matrix
$\mathbf{w}_{MPDRSS}$	Weight vector of MPDRSS beamformer
ρ	Correlation coefficient between LOS and multipath signal
$\mathbf{C}$	Calibration matrix with size $MN \times MN$
$\mathbf{e}^B$	Unit vector pointing from user to satellite in body coordinate frame

Chapter One: INTRODUCTION

An overview of the effect of different interference sources on the operation of global navigation satellite systems and the use of antenna arrays to mitigate them are discussed. Subsequently, a literature review, objectives and outline of the thesis are provided.

1.1 GNSS and interference

GNSS receivers have become essential tools for navigation and timing, including personal navigation, fleet management, precise agriculture, automobiles, time reference, precise orbit determination of space vehicles, weather monitoring etc. However, these applications are vulnerable to a range of threats related to electronic interference sources. In particular, electronic interference and multipath are major technical challenges for the GNSS community.

1.1.1 Radio frequency interference (RFI)

Users on the earth surface receive GNSS signals with very low pre-correlation Signal to Noise Ratio (SNR), which makes them very sensitive to RFI. For instance, the received power level for the Global Positioning System (GPS) L1 Coarse/Acquisition (C/A) code signal is -158.5 dBW (GPS-ICD 2013), which is well below the thermal noise floor of a GPS receiver. It is well known that GNSS signals can be easily subject to interference from sources that transmit very low power in their respective frequency bands (e.g. Dovis 2015, Landry 1997). The interference can either deteriorate receiver performance or completely deny the GNSS service based on their spectral and power features (Dovis

2015, Misra & Enge 2001). Several examples of real cases of RF interference and their impact are given in Dovis (2015).

Interference signals affecting GNSS receivers can be classified as intentional or unintentional (Kaplan & Hegarty 2006). Intentional interference includes jamming and different levels of spoofing. Jamming refers to the intentional transmission of RF energy in the band of GNSS signals in order to block the receiver functionality. The level of threat associated with jammers cannot be disregarded, as jammers are easily available in portable formats and can be purchased at low costs, although illegally. In some cases, jamming is a preliminary step to spoofing, forcing the target receiver to lose the tracking of the real signal in order to re-acquire a stronger spoofing signal. Several studies have analyzed the spectral characteristics of the GNSS jammers and their impact on the receiver performance (e.g. Bauernfeind et al 2012). Jammers are severe threat for liability critical mass market applications. Spoofing is the transmission of GNSS like signals that are temporally and spectrally different than authentic GNSS signals. In the spoofing scenario, the victim receiver is forced to compute an erroneous navigation solution. Unintentional interference is due to communication systems and other RF transmitters with carrier frequencies close to GNSS frequency bands. The harmonics generated from the spurious emissions from these out of band systems collide with GNSS bandwidth resulting in unintentional interference. These unintentional interference worsens position accuracy due to introduced errors in the measurements and in some cases might force the signals to loose tracking. Potential sources of unintentional interference are aeronautical communication systems (such as Distance Measuring Equipment (DME), Tactical Air Navigation (TACAN)), satellite phones, mobile satellite service, VHF/UHF

communications, Digital Video Broadcasting – Terrestrial (DVB-T), air traffic control radars etc. Based on the frequency band occupied by interfering signals, they can also be classified as narrowband or wideband (Kaplan & Hegarty 2006). Narrowband interference occupies only a small portion of the desired bandwidth compared to the target GNSS band, whereas wideband interference occupies entire desired bandwidth. For example, Continuous Wave (CW) interference is treated as narrowband and Gaussian noise jammers as wideband.

1.1.2 Multipath interference

Multipath refers to the reception of GNSS satellite signals from more than one path due signal reflections from nearby objects including the ground. Ideally, the GNSS receiver antenna should receive only the direct line of sight (LOS) signal to obtain correct code and carrier phase measurements. However, in the case of multipath, the signal received by the antenna is a combination of direct and reflected signals. The reflected signals are usually having lower power and are delayed with respect to the direct signal. These reflected signals, when superimposed with the direct LOS signal, have a longer propagation time and can significantly distort amplitude and phase of the direct signal. The deformation in the correlation function due to multipath signals results in erroneous pseudorange measurements and in turn degraded position solutions. In dense multipath environments like urban canyons, it may be possible that LOS signals are completely blocked in which case the receiver receives only the reflected signals. Errors in code measurements due to multipath can range from a few tens of metres to hundreds of

metres. Unlike other error sources, multipath errors cannot be removed by differencing techniques as they decorrelate spatially very rapidly. Multipath also leads to incorrect ambiguity resolution, thereby affecting carrier phase positioning. If the pseudorange multipath error in becomes large, the initial position solution is biased and the ambiguity resolution search space will be enlarged resulting in longer ambiguity resolution time (Joosten et al 2002).

1.1.3 Interference countermeasures

The processing gain provided by GNSS receivers is not sufficient to combat all types of interference. This necessitates development of efficient interference mitigation techniques to guarantee the integrity of the navigation solution. Also, modern GNSS receivers support multiple constellations with multiple frequencies increasing the pass band bandwidth making them more susceptible to interference. Therefore, selecting a GNSS receiver with powerful interference mitigation techniques is an asset for the users. Tremendous amount of research has been conducted to mitigate both RFI and multipath at different stages of the receiver operations from antenna to navigation domain.

Ndili & Enge (1998) and Moelker (1998) investigated the use of Automatic Gain Control (AGC) and Analog to Digital Converter (ADC) outputs to detect and mitigate CW and pulsed interference. The effectiveness of different implementations of notch filters to mitigate various interference have been studied thoroughly (Montloin 2010, Giordanengo 2009). However, they impact the receiver performance by altering the correlation function and increasing the tracking jitter (Lin et al 2011, Borio et al 2008). Several methods have

been proposed based on C/N_0 monitoring to mitigate pulsed and CW interference (Thompson et al 2010, Balaei 2009). These methods are not efficient as degradation in C/N_0 could be due to environment as well. Kamel et al (2013) and Kim et al (2007) investigated performance of ultra-tight integration of GNSS and Inertial Navigation Systems (INS) under different interference scenarios.

Many correlators based techniques were developed to alleviate the code multipath problem such as Narrow Correlator (van Dierendonck et al 1992), Edge Correlator (Garlin et al 1996), Double Delta Correlator, Multipath Estimating Delay locked loop (MEDLL) (Van Nee et al 1994) to name a few. These methods are not effective for short range multipath. Also for techniques such as MEDLL and Synthetic Multicorrelators (Stöber et al 2011), it is difficult to estimate the number of reflected signals for a given environment. Apart from these techniques, several other technologies are investigated to detect and mitigate multipath, e.g. the use of 3D building models in urban canyons (Groves et al 2013) and GPS-INS integration (Soloviev et al 2011).

The techniques listed above for RFI and multipath mitigation use single antenna approaches in time and frequency domains and are limited to certain operating environments and interference scenarios. Especially, the techniques for RFI mitigation are effective against narrowband interference scenarios, the performance of these techniques significantly deteriorate in complex signal scenarios or scenarios with wideband interference (Cuntz et al 2016). Therefore, the need for robust interference mitigation techniques becomes essential. In that sense, spatial processing using multiple antennas could be one of the robust approach against different interference sources.

Antenna arrays, which use spatial domain processing, are well known in wireless communication applications and radar communications. The use of these techniques to GNSS domain started a decade ago. Even though these techniques are well studied in wireless communication systems, their application to GNSS differ from those in communications. In wireless communication systems, multipath signals are used to increase signal to noise ratio in order to reduce bit error rate. However, in GNSS, even though signal to noise can be increased, multipath causes bias in time delay estimation. In GNSS, the focus is to improve the time-delay estimation to provide reliable positioning. Also, the estimation of the carrier Doppler to derive user velocity is important in some applications such as GNSS-INS integration. In communication applications, carrier phase distortion is not an issue while it is of utmost importance for GNSS when using carrier phase measurements for high accuracy positioning; this unresolved issue is the major motivation of this thesis. The effectiveness of different beamforming techniques to alleviate GNSS vulnerabilities were studied in (Fernández-Prades et al 2016, Gupta et al 2016, Broumandan et al 2016, Cuntz et al 2016, Amin et al 2016, Arribas et al 2014). A detailed survey on the previous research on antenna arrays for GNSS and the associated challenges are listed in literature review section. Despite the complexity involved in antenna array based GNSS receivers, advances in technology provide the possibility of consumer grade systems in the near future. Kappen et al (2012) presented a low cost architecture concept for the multi-antenna receiver on the state of the art FPGA development platform. Apart from the receiver architecture, it is also important to emphasize the size of the antenna array. As mentioned in Gupta et al (2016), due to advances in antenna technology, size of the GNSS antenna arrays are becoming smaller

and with few antenna elements so that they can fit in existing systems constrained by physical requirements.

1.2 Motivation

As applications of antenna arrays in GNSS emerge, measurement accuracy and integrity requirements are becoming increasingly stringent. Apart from the size and complexity requirements, the major requirement is the availability and the accuracy of the code and carrier phase measurements to ensure integrity of the navigation solution. One of such applications could be the use of antenna arrays for high precision to combat both RFI and multipath. For example, in precision agriculture, it is required to provide reliable, quality solutions that optimize growers' productivity and efficiency. Also, GNSS can be used in constrcution equipments to automatically control operation of the equipment. In such applications, antenna array based GNSS receivers could be employed to provide better performance. Also, for these applications, higher grade antennas with good phase center stability can be used to construct arrays as cost is somewhat less of a concern. However, it is known that antenna array processing in the presence of interference induces measurement distortions. These phase distortions cause biases in the carrier and code phase measurements that are not acceptable for such applications. Therefore, it is necessary to investigate the application of antenna arrays for mitigating both electronic interference and multipath and analyze the accuracy and integrity of the code and carrier phase measurements. This motivates the investigation of different antenna processing techniques that can be used in GNSS applications to provide distortionless

measurements in the presence of interference and multipath signals. In order to perform this task, it is necessary to generate signals in a controlled environment which requires the development of multi-antenna software simulators and receivers.

1.3 Literature review

This section summarizes research work performed on space only processing approaches as applied to GNSS to deal with jamming and multipath signals.

1.3.1 GNSS software signal simulation tool

Simulation is a useful technique where one can reproduce the radio signals transmitted by the satellites to design and understand complex GNSS receiver operations in a controlled environment. Several approaches have been proposed to develop efficient GPS software signal simulators (e.g. Hu et al 2009, Julien et al 2004, Dong 2003, Burns et al 2002). These software simulators can generate signals for single antenna systems. However, the requirement here is to develop a multi-antenna GNSS signal simulator with options to add RFI and multipath. A novel method is proposed in this thesis to regenerate the signals from the collected Intermediate Frequency (IF) samples for the multi-antenna system. A number of multipath simulation methodologies have been listed by Nievinski et al (2014). One of the methods to simulate specular multipath signals is to use a ray-tracing approach, as discussed by Lau & Cross(2007) and Weiss et al (2007). This apporach has been used to simulate multipath signals in urban environments and study the carrier phase multipath effects. Simulator approach has been used in this research to generate multipath signals for the multi-antenna approach.

1.3.2 Antenna arrays in GNSS

A vast amount of research has been conducted to analyze the use of antenna array based technology to combat different interfering signals. The current state of the art interference mitigation technologies using antenna arrays, associated challenges and advanced array based GNSS receiver designs have been discussed by Gupta et al (2016), Fernández-Prades et al (2016), and Broumandan et al (2016).

1.3.2.1 Antenna array calibration

Antenna array calibration is the first step in implementing beamforming techniques that use signal Direction of Arrival (DOA) information. Due to antenna gain/phase mismatches and mutual coupling between antenna elements, the received signals from different antenna elements undergo additional phase shifts (Konovaltsev et al 2010, Kim et al 2004). The other factors affecting antenna gain and phase are antenna phase centre variations, RF front-end delays, perturbation in antenna element positions and uneven cable lengths (Daneshmand et al 2014, De Lorenzo et al 2012). Calibration is the process of estimating these additional gain and phase uncertainties. In GNSS applications, array calibration can be performed using actual GNSS signals as satellite positions are known precisely and the signals of various satellites from different directions are available. Different calibration methods using actual GNSS signals and associated challenges have been studied by Daneshmand et al (2014) and Backén et al (2008). In all these methods it is assumed that clean actual signals are available. However, there are chances of multipath being present in those datasets used for calibration which can induce significant gain and phase errors in the calibration parameters. Therefore, it is necessary to evaluate

the effect of multipath signals on calibration and propose a method to reduce the error in the calibration parameters estimation.

1.3.2.2 Interference suppression and measurement quality

Much of the work employing antenna arrays in GNSS has been focused on electronic interference mitigation (Fernández-Prades et al 2016, Arribas et al 2014, Sgammini et al 2012, Amin & Sun 2005, De Lorenzo et al 2005**)**. Fernández-Prades et al (2016) describes major beamforming and null steering techniques that have been applied in the GNSS domain. The performance of different null steering techniques was studied by Li et al (2011), Carrié et al (2005), Zoltowski & Gecan (1995). The most commonly used null steering technique is power inversion which tries to minimize the array output power. Power minimization methods with different constraints such as DOA and subspace have been studied. Arribas et al (2013) studied GPS signal acquisition performance by utilizing a power minimization algorithm for interference mitigation before despreading. Sgammini et al (2012) proposed a two stage blind adaptive beamformer based on orthogonal projections. Orthogonal projections are performed at the pre and post correlation stages to mitigate interference. However, projection based techniques do not guarantee a distortionless response which is important in GNSS applications. Fernández-Prades et al (2011) demonstrated Eigen beamforming, which requires noise power estimation and desired signal power and spatial signatures for interference mitigation in GNSS receivers. Sahmoudi (2007) studied increasing Signal to Interference plus Noise Ratio (SINR) in the presence of strong interference. The interference DOA is estimated and used as a constraint to obtain robust Capon beamforming, which can enhance acquisition and tracking performance of GPS receivers. The estimation of the interference DOA could be

challenging in some complex user scenarios. Lorenz & Boyd (2005) demonstrated performance of minimum variance beamformers for GNSS applications in the presence of uncertainty in array response. Amin & Sun (2005) proposed an interference suppression scheme using self-coherence properties of GNSS signals. These techniques assume that the interferers do not have the same periodic structure as that of GNSS signals.

Eventhough the techniques listed above are efficient to mitigate electronic interferences, the quality of the measurements is degraded due to signal phase distortions (Chuang 2014, Church et al 2007**,** De Lorenzo et al 2006). The degraded measurements lead to poor navigation solutions. These biases and distortions are not desirable for high-accuracy and high-precision applications as they adversely affect carrier phase measurements, thus challenging the ambiguity resolution process. The distortions in GNSS measurements caused by the antenna array processing have been studied previously; for instance, Chuang (2014) and Church (2009) demonstrated distortion in carrier phase measurements with actual data and demonstrated the dependency of distortion on satellites locations. Chuang (2013) observed code phase biases of the order of one to two metres using Monte-Carlo simulations in the presence of interference and mutual coupling. Kalyanaraman (2010) studied phase tracking loop performance for possible carrier phase distortions due to different array processing techiques such as minimun variance and Minimum Variance Distortionless Response (MVDR). It has been shown through simulations that minimum variance based beamformers suffer comparatively more phase distortion than a MVDR based technique. Kim et al (2004) studied GPS phase measurement distortions due phase centre variations of individual

antenna elements in an array. It has been shown that mutual coupling between antennas also causes phase distortion. Phase distortions around a few centimetres were observed and these are not tolerable for high precision applications. In addition, code phase measurement biases due to the phase delay and group delay of antenna elements were also observed. Eventhough the distortions in measurements were reported, thorough analysis of the tracking results, code and carrier phase measurments quality was not performed. The effect of array processing techniques on possible carrier phase cycle slips and navigation solution domain has not been fully explored. Therefore, it is necessary to evaluate the array based GNSS receiver performance under different interference scenarios.

A large amount of research articles has demonstrated the use of antenna arrays for GNSS multipath mitigation. Daneshmand (2013) demonstrated two stage beamforming to mitigate both electronic interference and multipath. Effectiveness of spatial smoothing, spatial filtering and antenna array motion have been demonstrated to mitigate both electronic interference and multipath through signal simulations. Rougerie et al (2012) proposed a method to estimate the multipath parameters such as delay, amplitude and frequency. However, in real world scenarios it is difficult to estimate these parameters for all the reflected signals and computation complexity increases with increase in the number of reflected signals. Fernádez-Prades et al (2011) studied the inherent capability of different Eigen beamforming techniques to mitigate multipath through simulations. Vicario et al (2010) analyzed robust beamforming techniques for Galileo ground stations and shown a reduction of tracking errors by 47%. A large planar array and a particular multipath scenario having reflections from less than 10˚ elevation satellites were

considered for the analysis. Sahmoudi et al (2007) used adaptive beamforming and high resolution direction finding methods to improve robustness against multipath and electronic interference. Seco-Granados et al (2005) used an ML estimator for the simple model of an equivalent zero mean Gaussian noise, which includes all of the undesired signals and the noise component. Even though ML estimators are very effective, they are computationally expensive and are generally not suited for real time applications. Amin et al (2005) used self-coherence properties of the GPS signal to mitigate electronic interference and multipath. As multipath signals are coherent with GNSS signals, this method fails to mitigate multipath and produces erroneous results (Morton et al 2004). Brown (2000) demonstrated estimation of direction, amplitude and delay of multipath signals through the Maximum Likelihood (ML) based technique. Seco-Granados & Rubio (1997) demonstrated the significance of using antenna arrays for electronic interference and multipath mitigation. A linearly constrained beamformer was used to set nulls in the direction of undesired signals while maintaining adequate antenna gain for Line of Sight (LOS) signals. The design of an appropriate beamformer reduces to the DOA estimation problem, which is challenging in environments where interference signals are coherent with the desired signals. Most of these techniques were developed or adopted to mitigate code phase multipath. However, performance of the GNSS array based receiver for time-delay estimation to compute pseudorange measurements under multipath environments has not been explored considerably. In addition, the performance of these techniques for carrier phase multipath has not been fully explored.

1.4 Objectives and contributions

The overall objective is to implement a multi-antenna GNSS receiver capable of high performance carrier phase tracking in the presence of interference and assess measurement and position performance under different interference scenarios using a practically realizable antenna array. Different spatial processing techniques to mitigate both electronic interference and multipath are explored. The problems involved in antenna array processing to provide distortionless measurements for high precision applications is the focus of this thesis. To this end, the following objectives are pursued:

a) Multi-antenna GNSS software signal simulator

   The first objective is to develop a multi-antenna GNSS software signal simulator to generate Intermediate Frequency (IF) samples. A new method to generate multi-antenna GNSS signals is proposed. This method uses IF samples collected either from a hardware GNSS simulator or from actual GNSS satellites. A ray tracing approach is used to generate the specular multipath signals. In most of the multipath simulations, the Doppler difference between LOS and multipath are not considered. However, in this software simulator, the Doppler difference between LOS and multipath signals are considered while generating the multipath signals. This merely depicts the real world scenario. The simulated signals are validated against hardware based GNSS simulators by comparing the carrier Doppler and navigation solution.

b) GNSS receiver under multipath interference

   For this objective, a practically realizable antenna array is considered for evaluating the performance of different spatial processing techniques to mitigate multipath. A specular multipath environment is considered. A multi-antenna GNSS receiver with

different beamforming techniques is developed. The performance of different beamforming techniques is compared against some of the state of the art correlator based techniques. The multi-antenna GNSS simulator is used to generate GPS signals under multipath environments and the code and carrier phase multipath mitigation are analyzed. An array with six antenna elements is assembled to collect actual GPS signals in multipath environments and the performance of the resulting array based GNSS receiver is evaluated for measurement and position quality.

c) Antenna array calibration in the presence of multipath signals

Antenna array calibration in multipath environments is evaluated. It has been shown that carrier phase errors due to multipath signals are periodic in nature with zero mean. This property is exploited to improve the estimation of calibration parameters. By observing the signals for several multipath periods and through averaging, the estimation of calibration parameters can be improved. The periodic nature of the carrier phase multipath errors is shown through simulated and actual GNSS signals. The proposed method to improve the calibration parameters is investigated with simulated and actual GNSS signals.

d) GNSS receiver under electronic interference

This part of the research will focus on code and carrier phase distortions induced by array processing techniques. The multi-antenna simulator is used to generate GPS signals under different interference scenarios. Actual GPS signals are collected in open-sky conditions and interference is added to the IF samples through a software script. The tracking performance with different spatial processing techniques is

analyzed focusing on carrier Doppler estimation and phase tracking performance. Later, carrier phase position performance is also evaluated.

In order to test the above mentioned objectives with actual signals, a number of trials were performed considering different array configurations and different antenna elements. Results from representative datasets are provided.

1.5 Contributions

Following are the contributions from this research:

a) Demonstration of the carrier phase based approach for high precision applications using antenna arrays in the presence of interference is the main contribution of this research. This is achieved by assessing performance of a multi-antenna GNSS receiver in terms of measurement accuracy in the presence of multipath and electronic interference. Using a practically realizable antenna array, it is shown that both code phase and carrier phase multipath errors can be reduced significantly after beamforming, a key finding for carrier phase applications. Reductions in multipath errors result in faster ambiguity resolution. It is also shown that a MPDR beamformer is able to provide fixed carrier phase position solutions (after resolving ambiguities) in the presence of electronic interference.

b) A method of simulating multi-antenna GNSS signals is proposed to achieve the above as it is a powerful tool to evaluate different beamforming techniques performance. The simulator provides options to simulate different interference sources including

electronic interference and multipath. Simulated multi-antenna signals can be used for high precision carrier phase positioning analysis.

c) The proposed method for reducing multipath errors in the array calibration process can be easily incorporated in the existing calibration algorithms. The method provides improved estimation of calibration parameters in various multipath environments.

1.6 Thesis outline

The remainder chapters of this thesis are detailed below.

Chapter 2 begins with an overview of different vulnerabilities and their impact on GNSS receiver performance. Different antenna array processing techniques used in this research are discussed. Various correlator based multipath mitigation techniques are briefly discussed. The performance metrics used to evaluate the results are then described. A discussion on the receiver architecture is provided.

Chapter 3 discusses the software signal simulation methodology. A new method for simulating the GNSS signals is introduced. An overview of the ray tracing approach to generate multipath signals is presented. The advantages of the software simulator developed are described. Comparison of the results with those of a hardware simulator is presented to validate the simulation methodology.

Chapter 4 presents the results of the array based GNSS receiver under multipath environments. Several Monte-Carlo simulation results for different beamforming methods are provided for the array structure considered in this research. The simulation scenario

and results with simulated signals are presented. The actual data collection setup is described and the corresponding results are demonstrated.

Chapter 5 investigates the antenna array calibration under multipath environments. The carrier phase errors in multipath environments are shown using both simulated and actual data. The method to reduce calibration parameter errors is discussed and the corresponding results with simulated and actual data are presented.

Chapter 6 characterizes the measurement distortions due to antenna array processing in electronic interference scenarios. Difference simulation scenarios are discussed and the results using those simulated data are presented. The test setup for collecting actual data is discussed and the measurement and navigation solution results using these data are provided.

Chapter 7 provides conclusions and recommendations for future work.

Chapter Two: BACKGROUND

2.1 GNSS overview

GNSS signals received by users on earth are buried under noise as they are transmitted from medium earth orbit satellites with nominal radius above 20,000 km. GNSS uses direct sequence spread spectrum modulation scheme (i) to implement multiple access (code division multiple access for all GNSS systems except GLONASS, which uses frequency division multiple access) (ii) to have anti-interference capability for narrow band interference sources (iii) to have precise ranging due to frequent phase inversion of the signals (Misra & Enge 2001).

2.1.1 GNSS signal structure

The legacy GPS signals at L1 frequency band uses carrier with a nominal frequency of 1575.42 MHz, a PRN code with 1.023 MHz chipping rate for civilian signals and data bits at 50 Hz rate. More complex systems with different signal structures were developed later to improve overall GNSS receiver performance in terms of signal tracking, improved multipath rejection, ranging precision and position accuracy. Other GNSS systems include European Galileo, Russian GLObalnaya NAvigatsionnaya Sputnikovaya Sistema (GLONASS), China's BeiDou Navigation Satellite System (BDS), India's Indian Regional Navigation Satellite System (IRNSS), also called NAVIC, and Quazi-Zenith Satellite System (QZSS) from Japan.

As this thesis focuses on GPS signals, the signal model and processing are discussed for these.

The received GPS signal from a particular satellite in the absence of interference at the input of the ADC after down conversion from RF to IF is given by

$$s_i(t) = \sqrt{2P_i}\, d_{p,i}(t-\tau_i)\, c_i(t-\tau_i)\cos\left(2\pi\left(f_{IF}+f_d^i\right)t+\varphi_i\right)+\eta_i(t) \quad (2\text{-}1)$$

where P_i is the received signal power, $d_{p,i}$ is the navigation data bit with values either +1 or -1, c_i is the spreading code, τ_i is the transit delay from the satellite to the user, f_{IF} is the IF carrier frequency, f_d^i is the carrier Doppler frequency, φ_i is the carrier phase of the incoming signal and η_i accounts for the additive white Gaussian noise.

The navigation data contains information about satellite orbital parameters, satellite health, satellite clock corrections and atmospheric error corrections. The spreading codes used in GPS L1 C/A are a class of gold codes with 1.023 MHz chipping frequency and 1023 code length. The repetition period of the C/A code is 1 ms. The C/A code exhibits line spectrum following a sinc shaped envelope with frequency spacing of 1 kHz. The carrier Doppler is mainly due to the relative motion between the satellite and the user as well as from the user clock drift.

Each GPS satellite transmits energy using directional antennas pointed towards Earth with transmit power of 27 W. Due to geometric spreading there is about 184.4 dB of signal power loss (Misra & Enge 2001) and up to 2 dB loss due to atmospheric effects (Spilker 1996). Due to these losses, the nominal received signal power in open sky environments is about -128.5 dBm (GPS ICD 2012). The received signal power also depends on the antenna being used and its gain pattern. For a typical antenna, the open sky received signal power varies from -123 dBm to -129 dBm (van Diggelen 2009) for high elevation satellites and several decibels lower for lower elevation satellites.

2.1.2 GNSS interference Signals

Any unwanted signal at the input of the receiver is treated as interference. Electronic interference can be considered as either interference occurring due to the radio frequency signals transmitted by other system/equipment or multipath interference which occurs due to the reflection/diffraction of the useful signals.

2.1.2.1 Electronic interference

In general, electronic interference can be classified as a function of the following different signal parameters (Kaplan & Hegarty 2006):

- Based on bandwidth occupied by the interference – narrowband (occupies only a small portion of the desired signal) or wideband (occupies most or all of the desired signal bandwidth).
- Unintentional interference (terrestrial communication signals and their harmonics) or intentional interference (civil jammer devices such as personal privacy devices and spoofing signals).
- Considering the signal structure and modulation type – continuous wave, chirp interference, amplitude modulation, frequency modulation, pulse modulation, phase modulation and matched spectrum.

More details on the classification and different types of the interference signals are given by Dovis (2015), De Bakker (2007) and Kaplan & Hegarty (2006). In this thesis, commonly used civil GPS jammers are considered such as Continuous Wave Interference (CWI), Bandlimited White Gaussian Noise (BWGN) and chirp signal jammers.

Continuous wave narrowband jammers

Continuous wave jammers can be modelled as a pure sinusoid with fixed frequency. These jammers contain a voltage controlled oscillator to generate the desired frequency. Personal privacy devices can generate such signals and they can be easily plugged into a vehicle. CW interference can be represented as

$$j_{cw}(t) = \sqrt{2P_{cw}}\cos\left(2\pi f_{cw}t + \varphi_{cw}\right) \tag{2-2}$$

where, P_{cw} is the power of the CW interference, f_{cw} is the interference frequency and φ_{cw} is the initial phase of the CW signal.

BWGN jammers

This type of jammers spread white noise across the whole frequency band of interest. These forms of wideband interference are difficult to mitigate using techniques such as notch filtering. Only advanced antenna technologies such as controlled reception pattern antennas can further improve other receiver enhancements against this threat.

Chirp signal jammers

These type of jammers can also be modelled as a pure sinusoid, however the frequency of the latter sweeps over a defined bandwidth. The bandwidth could occupy partial or entire desired signal bandwidth. As power is spread across the frequency range, these type of interference can be treated as wideband interference. The majority of in-car jammers transmit chirp signals with a bandwidth of 9.4 MHz to 44.9 MHz in the GPS L1 frequency band (Bauernfeind et al 2014). The sweep time will be usually tens of µs (Bauernfeind et al 2014). Chirp jammers are very effective in jamming the signal within

GNSS receivers. Chirp jammers use VCO with an input voltage of saw-tooth function. Mathematically, chirp signals can be modelled as

$$j_{chirp}(t) = \sqrt{2P_{chirp}} \cos\left(2\pi f_{chirp}(t)t + \varphi_{chirp}\right) \quad (2\text{-}3)$$

where P_{chirp} is the power of the interference which is usually constant, $f_{chirp}(t)$ is the interference frequency at time t and is a linear function of time and φ_{chirp} is the initial phase of the chirp signal. The instantaneous frequency $f_{chirp}(t)$ can be defined as

$$f_{chirp}(t) = f_{chirp_0} + k_{chirp}t \quad (2\text{-}4)$$

where f_{chirp_0} is the starting frequency and k_{chirp} is the chirp rate.

All in-car jammers are linear with a positive unidirectional or bidirectional sweep. In this research, chirp signals with one saw tooth function with unidirectional sweep are considered.

2.1.2.2 Multipath interference

Multipath occurs when a user receives a useful signal via two or more paths either through reflection or diffraction (Braasch 1996). The direct signal received from a satellite is known as a Line of Sight (LOS) signal and reflected signals are known as Non-Line of Sight (NLOS) signals. As paths travelled by NLOS signals are longer than LOS signals, they are always delayed relative to the latter. A composite signal formed from LOS and NLOS is received by the user and the measurements that are generated are erroneous. The NLOS signals can either sum up constructively or destructively with LOS causing amplification or attenuation of the signal. Multipath can occur either due to smooth reflecting surfaces (specular multipath) or rough reflecting surfaces (diffuse multipath). This is the dominant error source in single point and differential positioning systems. The

error caused by multipath depends on the relative delay between LOS and reflected signals, power of the NLOS signals, phase values of the NLOS signals with respect to the LOS one, number of NLOS signals received, receiver tracking architectures, GNSS signal type and chipping frequency (Kaplan & Hegarty 2006, Misra & Enge 2001). Multipath signals can be modelled similar to the desired signal as shown in Equation 2-1 with different values for power, code delay, carrier Doppler and carrier phase.

2.1.2.3 GNSS signal model in presence of interference

The received signal from a particular satellite *i* in the presence of multipath and electronic interference can be represented as

$$x(t) = \sum_{k=1}^{K} s_k^i(t) + \sum_{j=1}^{J} j_j(t) + \eta(t) \tag{2-5}$$

where, *K* represents the sum of LOS and multipath signals with *k*=1 representing the LOS signal, *J* is the number of interference sources, $\eta(t)$ is the AWGN component, and $j_j(t)$ represents either narrowband or wideband interference with power greater than the ambient noise.

2.2 GNSS receiver signal processing

In this section, the basic architecture of a GNSS receiver and effect of electronic and multipath interference on different blocks are discussed.

The generic architecture of a GNSS receiver is shown in Figure 2-1. It consists of an antenna to receive electromagnetic signals, a RF front-end to downconvert and digitize the signal, baseband signal processing stage to decode the information embedded in the

signals and the navigation processor to compute the navigation solution using the measurements from the baseband processor.

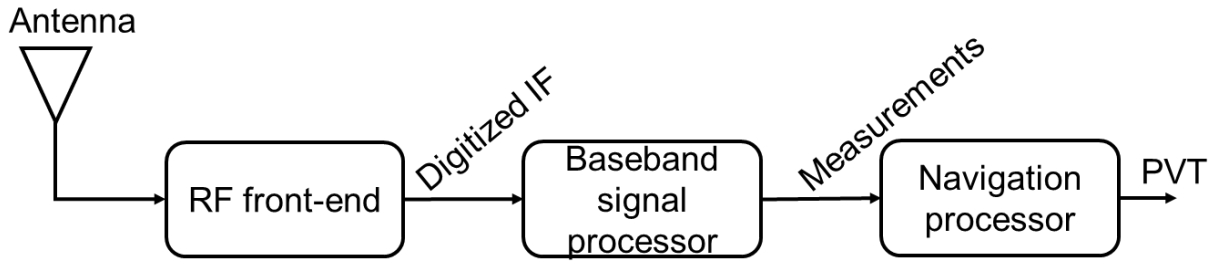

Figure 2-1: Generic GNSS receiver architecture

Operations performed by each of the above blocks and the effect of interference on each block are discussed briefly in the subsequent sections.

2.2.1 Antenna

The antenna is the first element in the GNSS receiver process as it receives the electromagnetic signals transmitted by satellites and converts them to electrical signals. The antenna, which acts as both spatial and frequency filter, has a major effect on the subsequent stages of the receiver operation (Rao 2013). As GNSS uses RHCP signals, most of the receivers use RHCP antennas. Circular polarization is preferred over linear polarization as linear polarized signals change polarization while travelling through the ionosphere due to the earth's magnetic field. Multipath signals with single reflection change their polarization to Left Hand Circular Polarization (LHCP) and they can be easily discriminated by the RHCP receiving antennas which depends on signals incident angles. Survey and geodetic applications require high accuracy antennas which are usually bulky and consume more power. Consumer applications such as handheld and automotive use small patch antennas which consume less power and are inexpensive. The main

characteristics of any antenna are its gain pattern, beamwidth and the phase centre stability. In most standard GNSS applications omnidirectional gain pattern is preferred. Usually, the gain will be maximum at the broadside (90° elevation) and has a roll-off of 10 to 20 dB towards horizon. The gain will be near zero below the horizon to attenuate ground reflected multipath signals. Beamwidth refers to the frequency band which is allowed to pass through the antenna. Usually commercial grade handheld antennas are single frequency, whereas survey grade antennas are broadband allowing multiple GNSS frequencies/multi-constellations to be observed. Another quality factor is the phase centre stability, which is important for high precision applications. Phase centre refers to the point where all the signals received from satellites are collected. The phase centre varies with the direction of the receiving signal. Most commercial applications not requiring cm level accuracy do not consider antenna phase centre stability. However, high precision receivers, such as those used for Real Time Kinematic (RTK) applications, a few mm of phase centre error can become significant.

Even though GNSS receivers are good at mitigating some of the interference sources due to advanced receiver signal processing techniques, it is necessary to keep unwanted signals out of the receiver as much as possible. In that sense, antennas can be designed carefully to reject out of band interference signals from unwanted signals such as cellular base stations, cellphones, radars etc. When these signals enter through the antenna, the Low Noise Amplifier (LNA) may be forced to operate in the nonlinear region and produce incorrect results. In this research, survey grade GPS L1 antennas are used with a precise phase centre (5 mm RMS) (Novatel 501 Datasheet, 1994).

2.2.2 RF front-end

RF front-end is the first functional block immediately after the antenna, which provides signal conditioning such as filtering, amplification and finally digitizing the incoming signal to be used further in the receiver signal chain. A typical receiver RF front-end block diagram is shown in Figure 2-2. The electrical signal from the antenna is amplified, filtered and down converted to the convenient IF signal. The typical elements in the RF front-end are LNA, filters, mixers, oscillator and ADC.

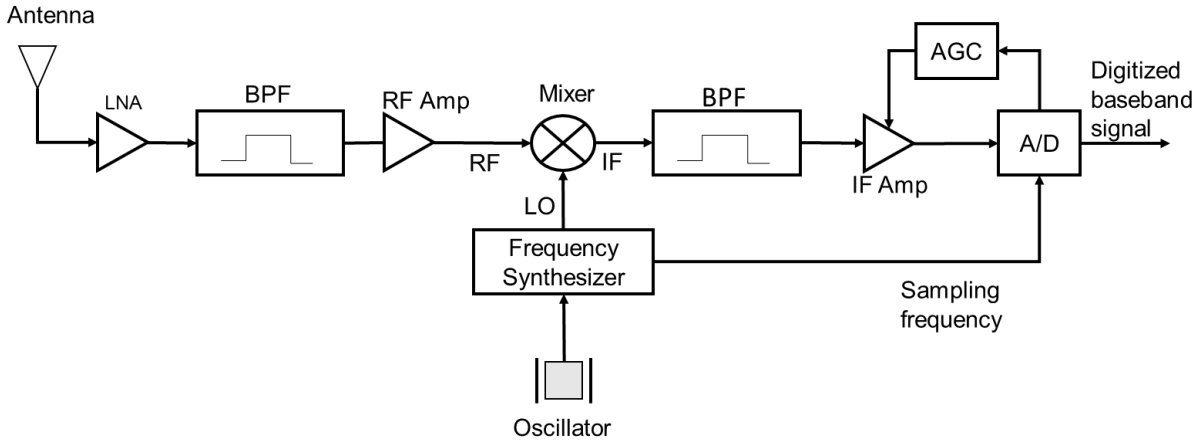

Figure 2-2: Block diagram of GNSS receiver RF front-end

The LNA is the first element immediately after the antenna which boosts the incoming RF signal. LNAs are placed very close to the antenna as it determines the overall noise figure of the receiver. The LNA is usually designed for high gain and low noise. Typically, LNAs used in GNSS receivers provide 20 dB of gain and have 3 dB of noise. Apart from the amplification provided by LNAs, power amplifiers are used in different stages of the front-end to provide nearly 100 dB gain for the incoming signal. This is to maintain the thermal noise level within the dynamic range of the ADC input.

The Band Pass Filter (BPF) before the mixer is used to remove the image frequencies. The BPF after the mixer is used to attenuate the out of band spurious signals and the unwanted signals from the mixing stage. The frond-end filter bandwidth determines the sampling frequency and also affects the code tracking performance by rounding off the correlator triangle and limiting the correlator chip spacing. The higher the bandwidth, the higher the performance at the cost of a higher number of samples to process, which increases the computational burden.

The role of the mixer is used to down convert the signal frequency from RF to IF, which is more easily managed by the rest of the receiver. This is accomplished by multiplying the incoming signal with a pure sinusoidal Local Oscillator (LO) signal generated from an oscillator through a frequency synthesizer. The IF signal contains all of the modulation that is present in the transmitted signal; only the carrier has been shifted in frequency. The gain of the IF signal is controlled by the AGC which accounts for cable losses and high power in the signal due to strong interference. In the presence of strong interference, AGC reduces the gain of the IF signal causing attenuation of the GNSS signals. The analog IF signal is converted to digital using ADC through a quantization process. A simple converter is the one-bit converter used in low cost receivers, which simply retains the sign of the input signal at the expense of slight performance loss (Misra & Enge 2001). The reference oscillator is a critical component in the receiver. It is used to generate the LO for the mixer, generate sampling frequency for the ADC operation and provide clock for the digital processing stages from correlator to PVT solution. Crystal based oscillators are common in typical GNSS receivers. Low cost commercial receivers use either a crystal oscillator (XO) or a temperature compensated crystal oscillator (TCXO). These

oscillators are sensitive to temperature and the frequency stability varies over time during the operation. Some geodetic quality receivers use high stability oscillators such as Oven Controlled Crystal Oscillator (OCXO) and atomic clocks. These oscillators are bulky and consume more power. Receivers equipped with such oscillators can produce carrier phase measurements with lower noise.

The proper functioning of the front-end can be disrupted by high levels of electronic interference. For example, pulsed interference can damage the LNA if its power exceeds the power specification of the front-end (Deshpande & Cannon 2004). A power limiter is usually placed before the LNA to prevent the damage from high power interference. In the presence of high power interference, amplifiers and filters start to work in their non-linear regions and degrade the performance. As mentioned earlier, in the absence of interference, AGC gain depends only on the thermal noise power as the signal is buried in noise. However, in the presence of high power in-band interference, the AGC gain is adjusted as per interference power. This leads to the suppression of the useful signal and even it may be lost and cannot be recovered. This situation usually happens with wide band interference whose bandwidth occupies the entire GNSS signal band. Even in the case of narrowband CW interference, AGC can suppress the input signal to avoid saturation attenuating GNSS signal. The statistics of the signal at the output of the ADC can be used to detect the presence of interference signal. For example, interference free signal distribution is Gaussian. But when CW is present, the distribution in the outermost bins will be higher. A statistical analysis of the ADC output allows one to detect the presence of interference even when high power interference drives AGC into saturation. In GPS, 90% of the power is present in the 2 MHz bandwidth centered on L1. In low cost

receivers where a low pseudorange accuracy is acceptable, antenna or the filters can be designed for a 2 MHz bandwidth around the centre frequency. Any interference falling outside the useful 2 MHz bandwidth can be eliminated at the front-end level.

2.2.3 Baseband signal processor

Baseband signal processing consists of two steps, namely acquisition and tracking. Acquisition detects the presence of satellite signals and finds coarse estimates of the signal parameters such as code delay and carrier Doppler. These estimates are used in the tracking stage to track the incoming signal in terms of code delay, carrier Doppler and carrier phase to produce corresponding measurements which are used by navigation processor.

2.2.3.1 Signal acquisition

A typical acquisition block consists of correlation, search and verification stages (Kaplan & Hegarty 2006). Correlation is basically a matched filter which performs two functions: carrier Doppler removal and code de-spreading. The acquisition search is a three dimensional search over different satellites, code delay and carrier Doppler. For each PRN, the incoming signal is correlated with different code and carrier replica signals generated based on the search space. For example, in the case of GPS L1 C/A code, since one code period is 1023 code chips long, and the search has to be done at intervals of ½ chip, there are 2046 possible values for the code phase to be examined. The possible Doppler shift for a static receiver is mainly determined by the speed of the satellite, between -4.2 kHz and + 4.2 kHz (van Diggelen 2009). The drift of the local oscillator must be added to this interval. The Doppler interval must be divided in steps;

the size of the steps depends largely on the integration time. With an integration time of 1 ms the corresponding Doppler resolution is 667 Hz, hence the Doppler interval is divided into 15 steps. The most common approach for performing a two-dimensional search is the FFT-based method (Tsui 2000). In order to detect the presence of satellite signal, the maximum correlation power obtained is compared against a threshold which is defined based on the desired probability of false alarm. If the maximum correlation power exceeds the threshold, the signal is detected and the coarse Doppler and code delay from the corresponding cell are passed to the tracking stage. The verification stage improves the reliability of the acquisition process by further testing the candidate cell.

Different search techniques can be used in the acquisition process, namely serial, parallel and hybrid. In a serial search, each bin is searched one-by-one. It is computationally simple but a time consuming process. The parallel search uses bunch of matched filters to search over the entire space. It is fast at the expense of computational load. A hybrid search is a balanced approach between serial and parallel.

In the presence of CWI, due to the harmonics generated by multiplying the locally generated carrier signal and incoming CWI, the acquisition search space in the Doppler domain becomes challenging (Dovis 2015). With the increase in the CWI power, the modulation effect by these harmonics become significant, increasing the probability of false alarm. In the case of BWGN interference, the noise floor is increased in the entire search area as noise is spread all over the GNSS filtered signal components. Due to an increase in the noise floor, the correlation peak will be masked and the acquisition process will fail.

2.2.3.2 Signal tracking

After the acquisition process detects the presence of different satellite signals present in the incoming signals along with their course estimates of delay and Doppler values, these estimates are passed to the tracking module where these estimates are refined and related changes are continuously tracked. In the traditional scalar tracking architecture, each satellite will have separate tracking channel independent of each other as shown in Figure 2-3.

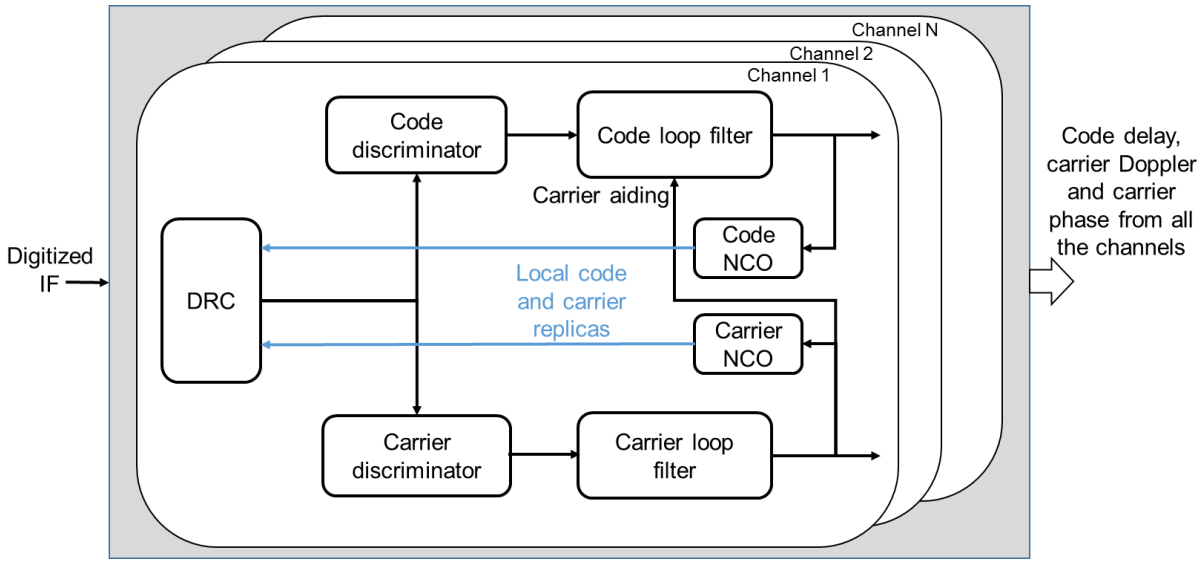

Figure 2-3: Block diagram of signal tracking loop module

The first step in the tracking stage is Doppler Removal and Correlation (DRC). The DRC performs three functions, namely (i) removing the carrier from the incoming signal by multiplying it with the locally generated carrier replica, (ii) correlating it with the locally generated code replica and (iii) performing Integration and Dump (I&D) on the correlation values. The integration and dump operation is carried out by the summation of the number of samples, which is determined by the coherent integration time. The coherent integration time depends on the state of bit synchronization. Before bit synchronization,

for GPS L1 C/A receiver, coherent integration time is set to 1 ms and after bit synchronization up to 20 ms. The in-phase and quadrature components from the integration and dump process are used in the tracking loops. A tracking loop consists of a discriminator to generate the error signal, loop filter to reduce noise from the discriminator outputs and a Numerically Controlled Oscillator (NCO) to generate code and carrier replica based on estimated Doppler and code phase.

Each channel has two tracking loops, one for the code and the other for the carrier. Each of the code and carrier tracking loop consists of its own discriminator, filter and NCO. The code tracking loop is commonly known as Delay Lock Loop (DLL). The carrier lock loop can be either Frequency Lock Loop (FLL) or Phase Lock Loop (PLL) (Kaplan & Hegarty 2006). Basically, DLL makes use of multiple DRC with different delays for each. In the basic DLL architecture three correlators, namely early, prompt and late, are used (Ward et al 2006) and the error between incoming and local signal is minimized by balancing early and late parts. The choice of the discriminator depends on the user requirements and the most commonly used DLL discriminators for GNSS applications are listed in Kaplan & Hegarty (2006). The FLL is used only to track the carrier frequency information, whereas the PLL is used to track both phase and frequency. In this research the PLL is used as carrier phase observations are required. Different PLL discriminators used in GNSS applications can be found in Kaplan & Hegarty (2006). The objective of the loop filter is to reduce the noise in the error signal in order to produce an accurate estimate of the incoming signal. The order of the loop filter depends on the signal dynamics (van Dierendonck 1996).

The tracking performance parameters used in this research are the Carrier-to-Noise (C/N_0) ratio and Phase Lock Indicator (PLI).

Carrier-to-noise ratio (C/N_0)

The carrier-to-noise ratio is a common measure of satellite signal power received at the receiver antenna. It is expressed as the ratio of carrier power to the noise power per unit bandwidth. Assuming the data bit boundary is known and the coherent integration time is 20 ms, the C/N_0 can be computed using the method described in van Dierendonck (1996) as

$$C/N_0 = 10\log 10\left(\frac{1}{T}\frac{\mu - 1}{20 - \mu}\right) \tag{2-6}$$

where 20 refers to the coherent integration time, T is 1 ms. μ represents the Narrow Band Power (NBP) to the Wide Band Power (WBP) of the prompt correlator output and is given by

$$\mu = \frac{NBP}{WBP} = \frac{\left(\sum_{t=1}^{T_c} I^i_{p,acc}\right)^2 + \left(\sum_{t=1}^{T_c} Q^i_{p,acc}\right)^2}{\left(\sum_{t=1}^{T_c} (I^i_{p,acc} + Q^i_{p,acc})\right)} \tag{2-7}$$

where $I^i_{p,acc}$ and $Q^i_{p,acc}$ are the 1 ms prompt correlator accumulated values of i^{th} satellite and T_c is 20, which represents the 20 ms coherent integration time.

Phase lock indicator (PLI)

Phase lock indicator is a useful parameter to evaluate the performance of carrier phase tracking (van Dierendonck 1996). PLI can be calculated at a given time epoch of the tracking loop update using the in-phase and quadrature phase correlation values as

$$PLI=\frac{\left(I_{p,acc}^{i}\right)^2-\left(Q_{p.acc}^{i}\right)^2}{\left(I_{p,acc}^{i}\right)^2+\left(Q_{p.acc}^{i}\right)^2} \quad (2\text{-}8)$$

Effect of electronic interference on signal tracking

Interference on the signal tracking has a direct impact on the quality of the measurements generated. Narrow band interference increases the variance of the correlator outputs modifying the shape of the s-curve of the code discriminator (Dovis 2015). This causes the bias in the generated pseudorange measurements. Narrow band interference also increases the variance of the carrier phase measurements. BWGN interference has a direct impact on the carrier phase discriminator output variance due to the increase in the thermal noise.

The effect of CWI and chirp signal on C/N_0 and PLI as compared to the interference free scenario is shown in Figure 2-4. The jamming to signal power of 30 dB is considered. CWI interference is assumed to be at an offset of 1 kHz from the IF frequency. Chirp interference bandwidth is assumed to be 10 MHz and sweep time of 12 us. Interference has been added after ten seconds for the receiver so that it can acquire the signal and track in PLL mode. In the presence of CWI and chirp, degradation in C/N_0 and PLI can be observed.

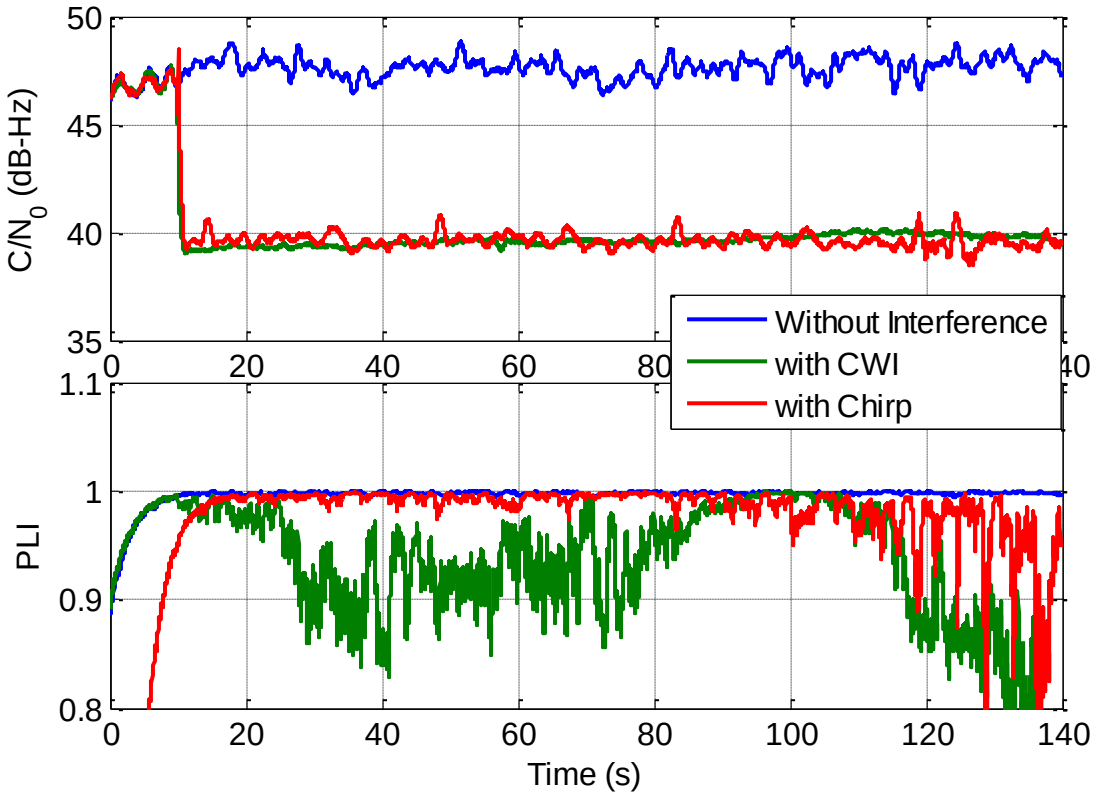

Figure 2-4: Effect of interference on C/N_0 and PLI

Effect of multipath on signal tracking

Code multipath results in bias in the pseudorange measurements and can be visualized using the correlation triangle as shown in Figure 2-5. Here, it is assumed that the NLOS signal is coming with a delay of 0.5 chips relative to LOS and with an amplitude attenuation of 0.75. The standard correlator spacing of 1 chip between early and late arms is considered. In GNSS receivers, measurements are generated corresponding to the prompt correlation value which is shifted as compared to the LOS due to shape of the composite signal. This error directly translates into a pseudorange bias and in turn affects the navigation solution.

Carrier phase multipath signals are sinusoidal in nature. Similar to code phase measurements, carrier phase measurements also become erroneous in the presence of

multipath. However, the maximum multipath error in carrier phase measurements can be up to quarter of wavelength of the GNSS signal (5 cm for GPS L1) (Misra & Enge 2001).

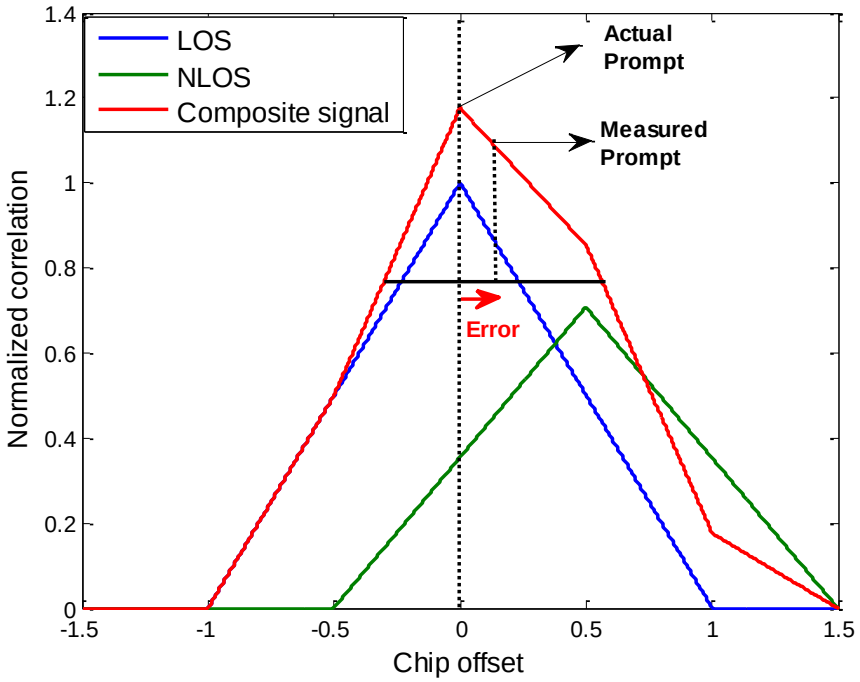

Figure 2-5: Illustration of code multipath error through correlation triangle

Correlator based techniques such as Narrow Correlator (van Dierendonck et al 1992), Multipath Estimating Delay Locked Loop (MEDLL) (Van Nee et al 1994), Edge Correlator (Garlin et al1996), High Resolution Correlator (HRC) (McGraw & Braasch 1999), etc., are well studied in GNSS applications. In this research the Narrow Correlator and double delta correlator in the form of strobe correlator are used as benchmark for performance comparison. Usually a correlator spacing of 0.1 chips is used to build up the discriminator function when using Narrow Correlators (Irsigler & Eissfeller 2003). With double delta correlators, code discriminators are formed by linear combination of two discriminator pairs instead of one.

The early-minus-late discriminator function for the Narrow Correlator can be expressed as

$$\Delta\tau_i = E_i - L_i \tag{2-9}$$

where E_i and L_i are the early and late parts of the correlation triangle for i^{th} satellite with 0.1 chip spacing between them.

The strobe correlator discriminator is implemented through a linear combination of two narrow correlators with two different correlator spacing and can be expressed as

$$\Delta\tau_i = \frac{\Delta d_2}{\Delta d_1}\left(E_{i,1} - L_{i,1}\right) - \left(E_{i,2} - L_{i,2}\right) \tag{2-10}$$

where $E_{i,1}, E_{i,1}$ are the early correlator points on the correlation triangle, $L_{i,1}$, $L_{i,2}$ are the late correlator points on correlation triangle, Δd_1 is the correlator spacing between $E_{i,1}$ and $L_{i,1}$ and Δd_2 is the spacing between $E_{i,2}$ and $L_{i,2}$. This correlator is effective for short delay multipath signals as compared to Narrow Correlator given by Equation 2-9.

2.2.4 Navigation processor

The objective of the navigation processor is to demodulate the navigation messages and compute the receiver position, velocity and time using the measurements from the tracking stages. There is an intermediate stage between the tracking and navigation processor, which converts tracking outputs into observations – pseudorange and carrier phase observations in terms of cycles and pseudorange rates. Satellite positions are computed from the orbital parameters decoded from the navigation message. Position is estimated using either the pseudorange observations (code phase based solution) or both

pseudorange and carrier phase observations. Pseudorange and/or carrier phase rates are used to estimate user velocity. The quality of the output solution depends on the errors in the observations such as satellite clock, ephemeris error, atmospheric errors, multipath error and receiver noise where multipath plays major role as other errors are not significant for code phase based solution. The carrier phase measurements are ambiguous. Different differencing techniques (single, double and triple difference) can be used to remove/reduce the common errors between the two users in order to improve the navigation solution. The most common navigation estimation filters used in stand-alone GNSS applications are least squares and Kalman filter.

2.3 Basics of antenna array processing

An antenna array is a system where signals from several spatially separated antennas are combined to achieve a modified reception pattern. The use of antenna array in a wireless system has several advantages such as increasing the signal-to-noise ratio, providing an ability to determine the direction of arrival of signals, acts as a spatial filter which allows desired signals to pass through without distortion and at the same time nullifying directional interference sources (Naidu 2012). In linear arrays, antenna elements are arranged in a linear fashion, which can provide modified pattern either in elevation or azimuth. In planar arrays such as circular or rectangular, antenna elements are arranged in a two-dimensional fashion, which can provide modified pattern in both azimuth and elevation. Apart from these shapes, antenna arrays could also be constructed in three dimensions. One such example is the spherical cap adaptive antenna array (Lambert et al 2009) where antenna elements are placed on a spherical surface.

These types of antenna are developed to overcome the poor low elevation resolution of the planar arrays.

In antenna array systems, one of the antennas is referred to as the reference antenna with respect to which signals received by other antenna elements are described. The signals received at different antenna elements can be considered as the delayed replicas of the signal received by the reference antenna. For narrowband systems, where the reciprocal of the maximum propagation delay across the array is greater than signal bandwidth (Van Trees 2002), the time delays across antenna elements can be approximated by phase shifts. The relative phase differences between different antenna elements can be expressed in terms of the vector wave number (Van Trees 2002), which is a function of direction of the signal source and wavelength of the signal. Consider an array with M antenna elements with arbitrary structure as shown in Figure 2-6.

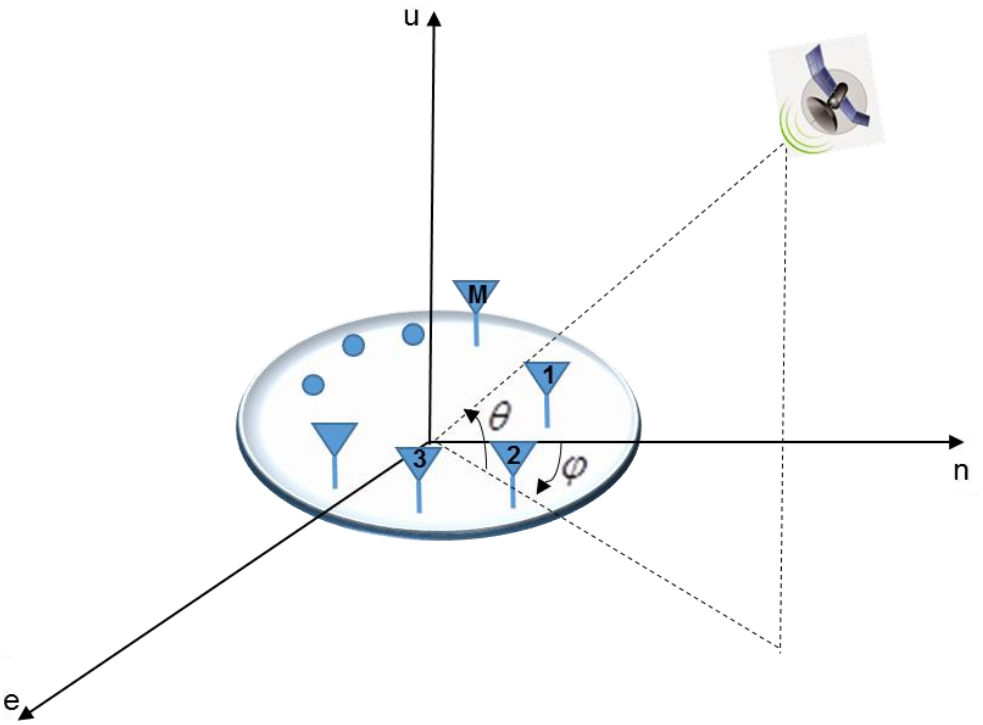

Figure 2-6: Illustration of an antenna array receiving single signal from a source at a specific elevation and azimuth

The vector wave number for a signal received from direction (θ,ϕ) can be expressed as (Van Trees 2002)

$$\mathbf{k} = \frac{2\pi}{\lambda}\left[\cos\theta\sin\phi \;\; \cos\theta\cos\phi \;\; \sin\theta\right]^T \tag{2-11}$$

where, θ and ϕ are the elevation and azimuth angles, and λ is the wavelength of the GNSS carrier signal. By knowing the relative positions of the antenna elements with respect to the reference antenna, the phase differences between the signals received from the antenna elements can be obtained. A phase difference can be expressed as a complex vector known as steering vector. For a *M*-element array, this vector can be represented as

$$\mathbf{a}(\theta,\phi) = \begin{bmatrix} 1 & a_2 & a_3 & ..... & a_M \end{bmatrix} \quad (2\text{-}12)$$
$$= \begin{bmatrix} 1 & \exp\{-j\mathbf{k}^T\mathbf{p}_2\} & \exp\{-j\mathbf{k}^T\mathbf{p}_3\} & ... & \exp\{-j\mathbf{k}^T\mathbf{p}_M\} \end{bmatrix}^T$$

where $\mathbf{p}_m = [e_m \; n_m \; u_m]$ is the relative position of the m^{th} antenna with respect to the reference antenna.

In array processing, signals from each antenna are combined to have constructive or destructive effects in specific direction. In order to do so, signals from each antenna are multiplied by a complex value, which will alter each antenna signal amplitude and phase before combining. These complex values are in general referred to as “Weights”. The weights are computed based on some optimization criterion (Van Tress 2002). Some of the optimization criteria used in this research are summarized in subsequent sections. The basic principle of any optimization criterion is to change the incoming signal’s phase received from each antenna such that the desired signals will have a constructive effect, whereas the undesired signals will have a destructive effect. For the array structure considered in Figure 2-6, the array combining can be illustrated as shown in Figure 2-7. The combined signal can be expressed as

$$y = \sum_{i=1}^{M} w_m s_m = \mathbf{w}^H \mathbf{x} \quad (2\text{-}13)$$

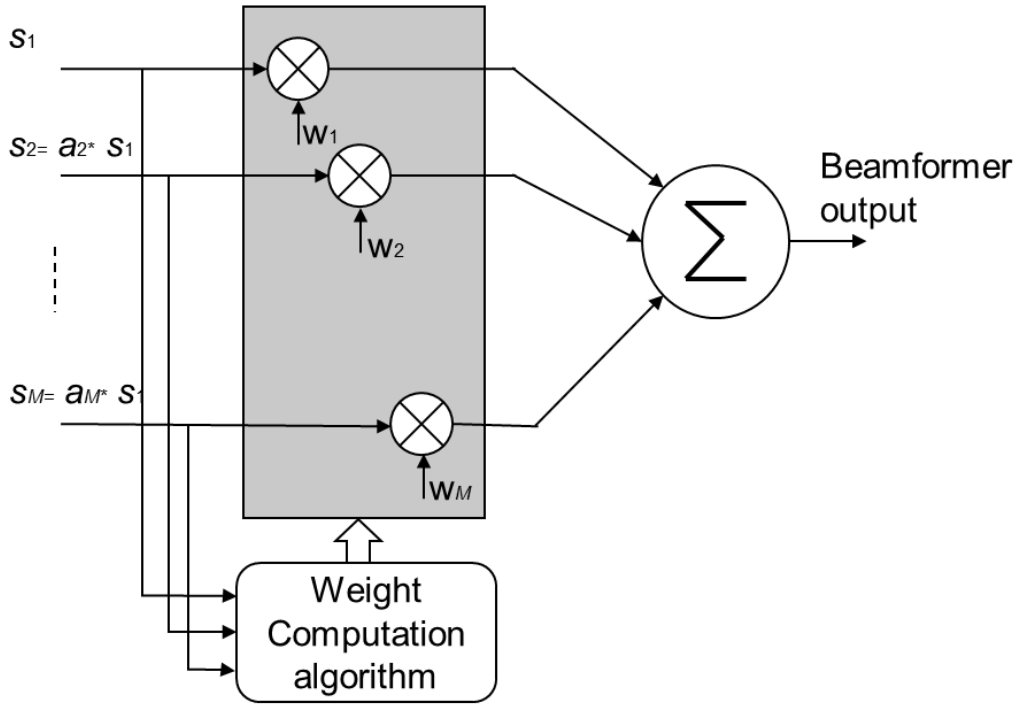

Figure 2-7: Basic antenna array processing scheme

The effective reception pattern after combining signals from individual antenna elements can be analyzed using the composite beampattern of the array, which refers to the response of the array to signals coming from different DOAs and can be represented as (Allen 2005)

$$BP(\theta,\varphi) = \mathbf{w}^H \mathbf{a}(\theta,\phi) \tag{2-14}$$

Several factors can affect the effective reception pattern of the antenna array such as

- Spacing between antenna elements
- Number of antenna elements
- Weight control algorithm
- Individual antenna element radiation pattern
- Structure of the array

- Mutual coupling between antenna elements

By increasing the number of antenna elements, the side lobes and the number of degrees of freedom can be improved. Degrees of freedom refer to the number of beams and nulls that can be obtained with an antenna array. For any array processing algorithms, optimal spacing between the antenna elements is chosen as $\frac{\lambda}{2}$ (Van Trees 2002). Increasing the spacing more than that optimal spacing results in undesired grating lobes, which refers to the side lobes with similar gain as that of the main lobe. It is also assumed that the radiation pattern of individual antenna elements is similar to each other. However, in practical applications, the radiation pattern of each antenna may be different and can affect the overall reception pattern. The other major factor that can affect the reception pattern is the mutual coupling between the antenna elements. Mutual coupling refers to the electromagnetic interaction between the antenna elements, which affects the radiation pattern of individual elements and in turn the overall array pattern.

Antenna signals can be combined spatially and/or temporally to enhance the desired signal or to suppress interference. Methods which use only spatial degrees of freedom are commonly known as Space Only Processing (SOP). The methods that use both spatial as well as temporal/frequency domain are known as Space Time Processing (STP)/Space Frequency Processing (SFP) (Gupta et al 2016). In this research only spatial processing is considered.

The weights can be fixed or can be changed adaptively based on the changing environment. If the weights are fixed, then the reception pattern will be fixed which is commonly known as Fixed Reception Pattern Antenna (FRPA). In Controlled Reception

Pattern Antenna (CRPA), weights are computed adaptively to change the reception pattern. In this thesis, block adaptation (Van Veen & Buckley 1988) is used. In this method, statistics estimated from the temporal block of incoming data are used in the weight computation algorithm.

2.4 Antenna array processing in GNSS

Considering recent advances in the antenna and GNSS receiver technologies, antenna array based GNSS receivers are increasingly being considered. Examples of proof of concept prototypes can be found in Gupta et al (2016), Fernández-Prades et al (2016), Broumandan et al (2016), Cuntz et al (2016), Arribas et al (2014). The following section details some of the possible architectures of array based GNSS receivers.

2.4.1 Array based GNSS receiver architectures

Array processing in GNSS can be used before the receiver at the IF sample level or within the receiver. The most commonly deployed system is single output nulling antenna (Fernandez-Prades et al 2016), which provides a single output that can be fed to the conventional single antenna receiver. Such a system is generally used to sense the presence of interference signals and place nulls in the interference directions. In other systems, array processing is performed within the receiver in the baseband processing stage either before or after correlation (Cuntz et al 2016, Broumandan et al 2016). These systems can use either null steering or beamforming techniques. Null steering approaches are generally performed before the correlation process to mitigate the interference before the tracking stage. In beam steering approaches, multiple beams are

formed, each corresponding to a particular satellite, which can be performed either before or after the correlation process (Fernandez-Prades et al 2016). As correlation and dump process and beamforming are liner operations, performance of both pre-correlation beamforming and post-correlation beamforming should be similar (De Lorenzo 2007). The only difference is that pre-correlation beamforming occurs at sampling frequency (usually in MHz) whereas post-correlation beamforming occurs at the integration and dump frequency (usually in kHz).

2.4.2 Multi-antenna GNSS signal model

In this research, a rectangular array is used. Consider the case of a GNSS receiver equipped with an *M*×*N* element uniform rectangular array. The elements are lying in the x-y plane and are equally spaced by d_m in the x-direction and d_n in the y-direction as shown in Figure 2-8.

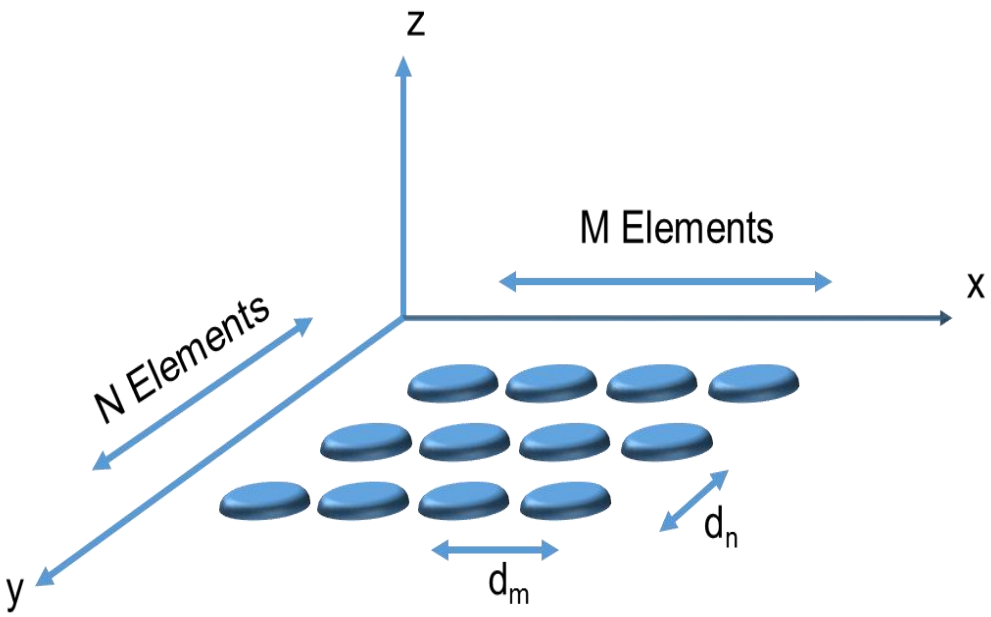

Figure 2-8: Rectangular array structure with *M*×*N* elements

For the sake of simplicity, signals from only one satellite are considered in the model and the index *i* is not omitted in the expressions. After down-conversion and sampling, the digitized signal received at the (*m, n*)[th] antenna element can be expressed as

$$x_{m,n}(t) = \sum_{k=1}^{K} s_k(t) e^{i\frac{2\pi}{\lambda}\left[(m-1)d_m \sin(\theta_k)\sin(\phi_k)+(n-1)d_n \sin(\theta_k)\cos(\phi_k)\right]} + \sum_{j=1}^{J} j_j(t) e^{i\frac{2\pi}{\lambda}\left[(m-1)d_m \sin(\theta_j)\sin(\phi_j)+(n-1)d_n \sin(\theta_j)\cos(\phi_j)\right]} + \eta_{m,n}(t) \quad (2\text{-}15)$$

where $s_k(t)$ is the k^{th} the signal component where k=1 refers to the LOS and k=2:K refers to NLOS signals, $j_j(t)$ is the j^{th} electronic interference, λ refers to the wavelength of the signal, (θ_k, ϕ_k) is the elevation and azimuth angle of the corresponding LOS or NLOS signal, (θ_j, ϕ_j) is the elevation and azimuth angle of the electronic interference signal, K is the number of LOS and multipath signals, J is the number of electronic interference signals, and $\eta_{m,n}(t)$ is the additive spatially white noise of the (*m, n*)[th] antenna element. The impinged signals from all the antenna elements can be represented in the matrix form as

$$\mathbf{x} = \mathbf{As} + \mathbf{Bj} + \boldsymbol{\eta} \quad (2\text{-}16)$$

where $\mathbf{x}$ is the MN×1 received signal vector and $\boldsymbol{\eta}$ is the MN×1 noise vector, $\mathbf{s}$ is the K×1 signal vector with LOS and NLOS signals, $\mathbf{j}$ is the J×1 signal vector with electronic interference signals; these vectors are given by

$$\mathbf{x} = \left[x_{1,1}(t), x_{2,1}(t), \ldots x_{M,1}(t), x_{1,2}(t), \ldots x_{M,N}(t)\right]^T \quad (2\text{-}17)$$

$$\mathbf{s} = \left[s_1(t), s_2(t), \ldots s_K(t) \right]^T \tag{2-18}$$

$$\mathbf{j} = \left[j_1(t), j_2(t), \ldots j_K(t) \right]^T \tag{2-19}$$

$$\boldsymbol{\eta} = \left[\eta_{1,1}(n_c), \eta_{2,1}(n_c), \ldots \eta_{M,1}(n_c), \eta_{1,2}(n_c), \ldots \eta_{M,N}(n_c) \right]^T \tag{2-20}$$

The steering matrices $\mathbf{A}$ and $\mathbf{B}$ are of dimensions $MN \times K$ and $MN \times J$ respectively and are given by

$$\mathbf{A} = \left[\mathbf{a}_1, \mathbf{a}_2, \ldots\ldots \mathbf{a}_K \right] \tag{2-21}$$

$$\mathbf{B} = \left[\mathbf{b}_1, \mathbf{b}_2, \ldots\ldots \mathbf{b}_J \right] \tag{2-22}$$

where $\mathbf{a}_k$ is the $MN \times 1$ steering vector of the k^{th} signal component coming from direction (θ_k, ϕ_k), and where $\mathbf{b}_j$ is the $MN \times 1$ steering vector of the j^{th} electronic interference signal coming from direction (θ_j, ϕ_j). Both $\mathbf{a}_k$ and $\mathbf{b}_j$ have the similar structure, so here only $\mathbf{a}_k$ is defined which is given by

$$\mathbf{a}_k = \left[\mathbf{c}_k^T, \gamma_k \mathbf{c}_k^T, \ldots\ldots, \gamma_k^{(N-1)} \mathbf{c}_k^T \right]^T \tag{2-23}$$

$$\mathbf{c}_k = \left[1, \beta_k, \ldots\ldots \beta_k^{(M-1)} \right]^T$$

$$\gamma_k = e^{j\frac{2\pi}{\lambda} d_n \sin(\theta_k)\cos(\phi_k)}$$

$$\beta_k = e^{j\frac{2\pi}{\lambda} d_m \sin(\theta_k)\sin(\phi_k)}$$

2.4.3 Spatial processing techniques

In any antenna array application, beamforming techniques can make use of either calibrated or non-calibrated array. Beamforming techniques that do not consider a calibrated array are referred to as blind beamforming techniques. Even though blind beamforming techniques are easy to implement, they may degrade the performance of

the GNSS receiver by unintentionally nullifying the desired signal. Therefore, beamforming techniques which exploit the satellite signal directions are preferable. Numerous beamforming and null steering techniques exist and a detailed analysis of most of these techniques can be found in Van Trees (2002). The techniques used here, namely Delay And Sum (DAS) beamformer, Power Minimization (PM) and Minimum Power Distortionless Response (MPDR) beamformer, are discussed below.

2.4.3.1 DAS beamformer

The DAS beamformer relies only on the spatial information of the LOS signal (Van Trees 2002). This beamformer does not guarantee a distortionless response as it just points the main beam in the direction of the LOS signal and does not consider any other constraints to preserve the desired shape of correlation peaks. The optimum weights for the DAS beamformer can be obtained as

$$\mathbf{w}_{DAS} = \frac{1}{MN}\mathbf{a}_1 \tag{2-24}$$

where MN is the total number of antenna elements in the array and $\mathbf{a}_1$ is the steering vector of the LOS signal.

2.4.3.2 MPDR Beamformer

The MPDR beamformer is a distortionless beamformer that minimizes total output power by constraining unity gain in the direction of the desired signal (Van Trees 2002). This beamformer relies on the covariance matrix of the received signal, which is normally computed by temporal averaging of the spatial samples. The covariance matrix of the received signal can be obtained as

$$\mathbf{R}_{xx} = \frac{1}{K_T}\sum_{k=1}^{K_T}\mathbf{x}\mathbf{x}^H \tag{2-25}$$

where K_T is the number of temporal snap-shots.

The optimum weight vector for the MPDR beamformer is (Van Trees 2002)

$$\mathbf{w}_{MPDR} = \frac{\mathbf{R}_{xx}^{-1}\mathbf{a}_1}{\mathbf{a}_1^H\mathbf{R}_{xx}^{-1}\mathbf{a}_1} \tag{2-26}$$

2.4.3.3 Power minimization

This blind beamforming algorithm does not consider the direction of arrival of the desired signals in the optimization criterion. As compared to the MPDR beamformer where separate beamformer is required for each satellite, this approach requires only one beamforming block to nullify the interference sources and can be performed before the correlation process. The optimum weight vector is given by

$$\mathbf{w}_{PM} = \frac{\mathbf{R}_{xx}^{-1}\mathbf{q}}{\mathbf{q}^H\mathbf{R}_{xx}^{-1}\mathbf{q}} \tag{2-27}$$

where $\mathbf{q}$ is the constraint vector given by

$$\mathbf{q} = \begin{bmatrix}1 & 0 & 0 \ldots 0\end{bmatrix}^T \tag{2-28}$$

2.4.3.4 Effect of signal correlation on optimum beamformers

The performance of the beamformer degrades in the presence of multipath signals resulting in LOS signal cancellation (Widrow et al 1982) and fails to mitigate multipath (Reddy et al 1987). The other problem with multipath signals is the rank deficiency of the cross covariance matrix due to which Eigen based methods fail to perform properly. A number of techniques have been proposed in the literature to deal with signal coherency

problem. Some of the well known preprocessing techniques (Van Trees 2002) are discussed in the following sub-sections.

Spatial smoothing

Spatial smoothing has been used to deal with coherent signals for spectral estimation (Shan et al 1985). It is a pre-processing scheme which partitions the total array of sensors into several subarrays and then generates an average of the subarray output covariance matrices. In this research, spatail smoothing is used and more details on this technique can be found in Chapter 4.

Spatial filtering

Spatial filtering is a process of removing a signal component from the incoming signals based on the directional information. This method was studied in detail to avoid the performance degradation of the Eigen vector beamformer in the presence of interference and high sensor noise (Citron & Kailath 1984). Widrow et al (1982) demonstrated signal cancellation when the desired signal and interference are correlated by considering sinusoidal signals of the same frequency. In order to deal with signal cancellation, spatial filtering could be employed. In GNSS applications, the desired satellite signal direction could be obtained beforehand. With the knowledge of the steering vector of the desired signal, signals from all the antennas can be aligned in phase and by taking the difference between the signals from consecutive antenna elements, the desired signal can be removed from the incoming one. Assuming one desired and one multipath signal, after

removing the desired signal only multipath component will remain in the incoming signal along with noise.

Moving antenna array

To deal with the signal cancellation phenomenon, spatial dithering techniques have been used (Widrow et al 1982). Spatial dithering was achieved by physically moving the array in directions orthogonal to the desired direction. Because of the mechanical motion, signals from the desired direction are undistorted where as from other directions are modulated. This allows the optimum beamformer to remove the undesired signals without cancelling desired signal. The antenna array motion was further studied and analyzed for DOA estimation in multipath environments (Haber & Zoltowski 1986). The basic idea with a moving antenna array is to induce different Doppler values for desired and multipath signals so by averaging over several differential Doppler cycles, signal correlation can be reduced. In the case of GNSS, a moving antenna array can introduce a few Hz of Doppler difference between desired and multipath signals depending on user velocity. The Doppler difference increases with an increase in velocity at which the array is moving. Thus for a dynamic GNSS user, it is possible to achieve desired decorrelation depending on the antenna velocity. Hence, optimum beamformers could be employed to mitigate multipath effects.

2.5 Summary

In this chapter, GNSS signal structure and associated vulnerabilities followed by an overview of different GNSS receiver signal processing blocks were discussed. The effects

of electronic and multipath interference on different stages of the receiver were described. A review of array processing, array based GNSS receivers, signal models and spatial processing techniques used in research was then presented.

Chapter Three: MULTI-ANTENNA GNSS SIGNAL SIMULATOR

3.1 Introduction

As mentioned in Chapter 1 & 2, antenna array processing is very effective against different kinds of interference. It is necessary to test and validate the effectiveness of different array processing techniques in different interference scenarios. One way to evaluate performance is to use field data. However, this may lead to uncertainties due to unknown factors and transmission of interference signals would be an issue. Another way is to generate signals in a controlled environment either through software or combination of hardware and software. In this chapter a software testbed is developed using GNSS signals simulated in a controlled environment. Simulating GNSS signals has many advantages, namely (i) error sources such as atmosphere, multipath and interference can be modelled and controlled through software, (ii) the user trajectory can be defined, (iii) for a given GNSS constellation, the signal can be simulated in different scenarios for repeatability tests, and (iv) the simulator can be modified easily with different features.

This software simulator generates signals for several antennas simultaneously. A novel method is proposed to generate the signals with an option to add different interference sources. This multi-antenna simulation tool will be useful in characterizing various antenna array processing techniques in terms of calibration methods, measurement and position distortions in subsequent chapters. It generates GPS satellite signals for different antenna elements for a given array configuration and interference scenarios. The methodology and the software implementation of the simulator are described in detail

below. The quality of the simulated signals is tested under different user scenarios and the results are provided.

3.2 Simulator architecture and methodology

The basic blocks of the multi-antenna GPS signal simulator are shown in Figure 3-1. The architecture resembles that of a software GNSS receiver with modifications in the tracking module. The signal model defined in Equation 2-15 is used to simulate the multi-antenna signals.

Input to the simulator consists of IF samples (digital baseband samples) from a hardware GNSS simulator using a data acquisition system. The Spirent GNSS simulator and National Instrument's data acquisition system is used. The simulation is controlled using two option files, namely the GNSS signal option file and interference signal option file. The GNSS option file defines parameters related to the digital baseband samples such as sampling frequency, ADC resolution, visible satellites and number of channels to be simulated and the antenna array structure. This also defines acquisition and tracking control parameters such as the acquisition search space, tracking loop bandwidth and its order. The interference option file is related to interference signals to be simulated, namely multipath and electronic interference. For multipath interference, it defines parameters such as the number of reflectors and their coordinates, the number of multipath signals to be simulated and multipath attenuation. For electronic interference, it defines parameters such as frequency, bandwidth, interference power and interference directions.

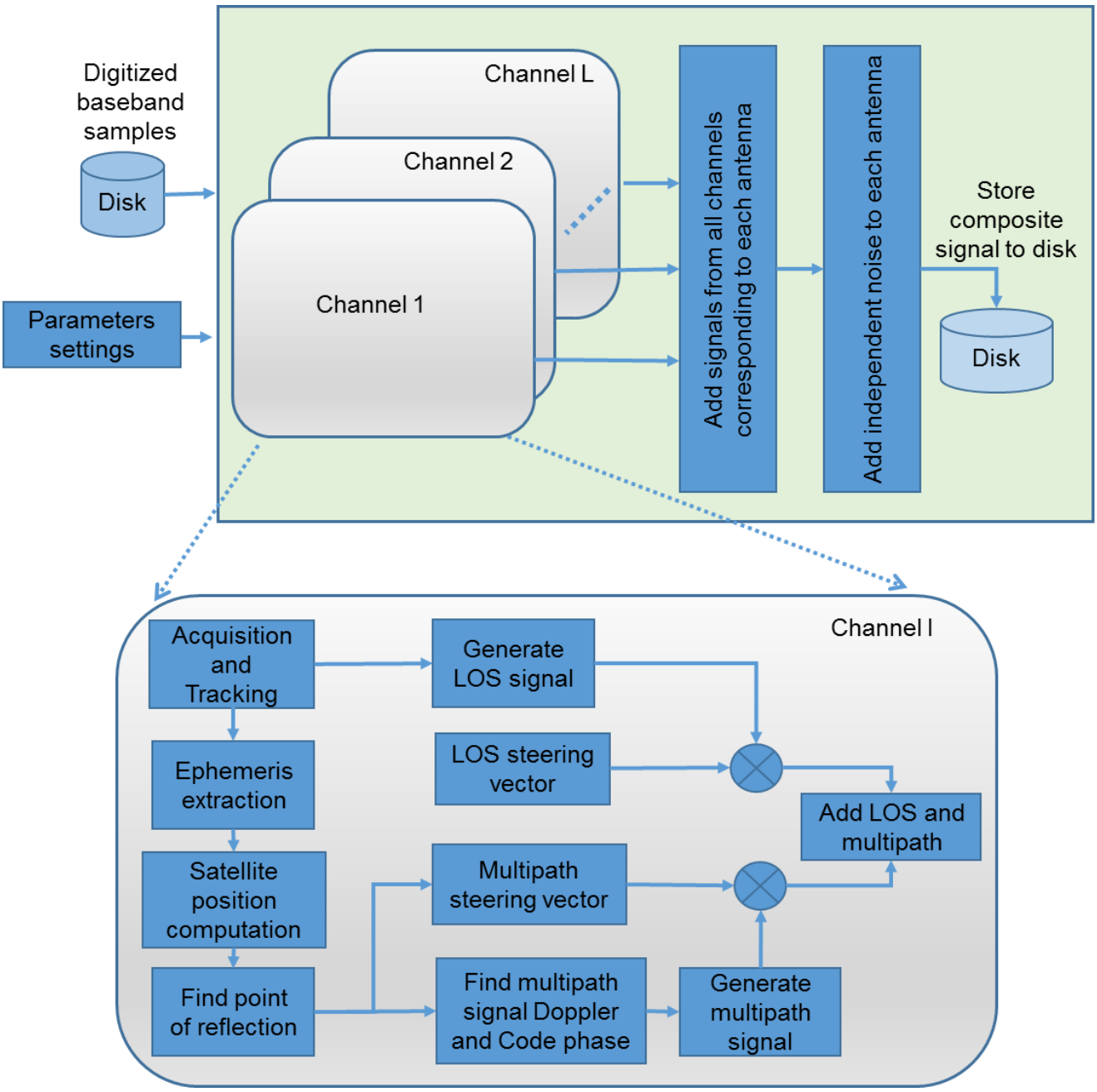

Figure 3-1: Multi-antenna signal simulator architecture

The parameters which can be controlled through option files are listed in Table 3-1.

Table 3-1: Simulator controllable parameters

Parameters	Description
Digital baseband samples	Binary data file collected using data acquisition system
Sampling frequency	Defines the sampling frequency used for collecting digital baseband samples
Data type	Data type of the digital samples e.g. integer 8 or integer 16
Tracking loop settings	Defines PLL and DLL tracking loop bandwidth and order
Antenna array configuration	Defines number of array elements and their relative position in East-North-Up (ENU) coordinate format
Calibration matrix	Defines the calibration matrix elements – useful in testing different calibration methods
Reflector geometry	Defines four corners of reflectors in ENU format
Multipath attenuation	Defines attenuation factor of multipath signals for different satellites
Interference frequency	Defines frequency of the CWI
Interference bandwidth	Defines the bandwidth of the chip interference and BLWN
Interference DOA	Defines direction of arrival of interference signals
User reference position	This is the reference position corresponding to user trajectory if the user is static; this position can be a fixed position defined in geodetic coordinates. If the user is moving, the corresponding motion file generated from the hardware simulator can be provided.

All visible satellites listed in the option file are acquired and tracked using the IF samples. During the initial tracking state, satellites are tracked in PLL with higher bandwidth and loop order without assisting DLL. Later, based on the PLI, the tracking state is switched to PLL assisted DLL mode. The replica signals generated during this tracking stage are

used to generate multi-antenna signals. The replica signal consists of the C/A code replica, the carrier replica and the navigation data bits. The code replica corresponds to the prompt code replica generated from the code tracking loop. The summation of all the replica signals from all the tracked satellites plus noise corresponds to a single antenna signal.

The quality of the simulated signals mainly depends on the tracking loop settings of the software simulator. In the carrier phase tracking loop (PLL), thermal noise is treated as the only source of error as other source of errors such as dynamic stress, oscillator phase noise may be transient or negligible (Kaplan & Hegarty 2006). The thermal noise jitter for a PLL discriminator depends on integration time, C/N_0 and carrier loop noise bandwidth. For the GPS C/A code with 20 ms integration time, 1-sigma thermal noise is below 5° for carrier loop noise bandwidths up to 20 Hz (Kaplan & Hegarty 2006). This is well within the 1-sigma rule threshold (<15°). In this simulator, a two-quadrant arctangent PLL discriminator is used with a carrier noise bandwidth of 15 Hz, integration time of 20 ms and C/N_0 above 45 dB-Hz. This ensures that the tracking error is minimal for the accurate generation of carrier replica signals. In the absence of multipath, major errors in the code tracking loop (DLL) are thermal noise jitter and dynamic stress (Kaplan & Hegarty 2006). The DLL jitter depends on the filter noise bandwidth, integration time, C/N_0 and correlator spacing (which depends on front-end bandwidth). Lower loop bandwidth results in lower jitter, which can be achieved by carrier aiding to effectively removes the code dynamics. Reducing correlator spacing also reduces the tracking jitter. The simulator described herein uses PLL-assisted DLL with non-coherent early-late power discriminator with 0.1 Hz noise bandwidth and correlator spacing of 0.1 chips between early and late parts.

3.2.1 Multi-antenna signal simulation

Upon successful tracking followed by data bit boundary detection, ephemeris data is decoded and satellite positions and velocities are computed. Using satellite positions and user positions from the option file, satellite azimuth and elevation are computed. Using the antenna array configuration defined in the option file and satellite LOS signal directions, LOS steering vectors are computed for all satellites. The replica signals from each satellite are multiplied with corresponding steering vectors to generate multi-antenna signals. The signals from all the satellites are added corresponding to each of the antenna. Later, independent white Gaussian noise is added to each antenna signal to have desired C/N_0 for the simulated signals.

3.2.2 Interference signal simulation

Electronic interference signals are generated using the models described in Section 2.1. The focus of this section is to discuss multipath signal simulation methodology, which is done using a ray-tracing approach. Based on the reflector positions and the satellite positions, a point of reflection for the multipath signals is computed. Later, reflection points are tested to lie within the boundary of the reflector surface to identify them as valid reflection points. Once a valid reflection point is obtained, the extra distance travelled by the multipath signals is converted to the number of code chips and the code phase, which is then added to LOS prompt code to generate C/A code corresponding to a multipath signal. Due to reflection, Doppler observed by the multipath signal will be different from that of the LOS signal. The computation of multipath Doppler values is discussed in subsequent sections. The attenuation factors of multipath signals for different satellites

are defined in the multipath option file. Using the Doppler information, replica code and the attenuation factor, multipath signals are generated for each visible satellite. Using the point of reflection and known user position, the multipath signal DOAs are computed and the corresponding steering vectors are generated. The multi-antenna multipath signals thus generated for a particular satellite are then added to the corresponding LOS multi-antenna replica signals. The combined LOS and multipath signals from all satellites are added together to generate composite GNSS signals.

Multipath Simulation Model

A typical simulated multipath scenario is illustrated in Figure 3-2. The user antenna receives direct a LOS signal from a satellite and a reflected signal shown in red. The following assumptions are made for the multipath model used in the simulation (Lau et al 2007):

- Since multipath signals arriving at a user after multiple reflections are usually weak. Therefore, for this simulation only single reflection is considered.
- The reflector is a plane rectangular smooth surface.
- The reflections are specular in nature.
- Only one NLOS signal is considered.

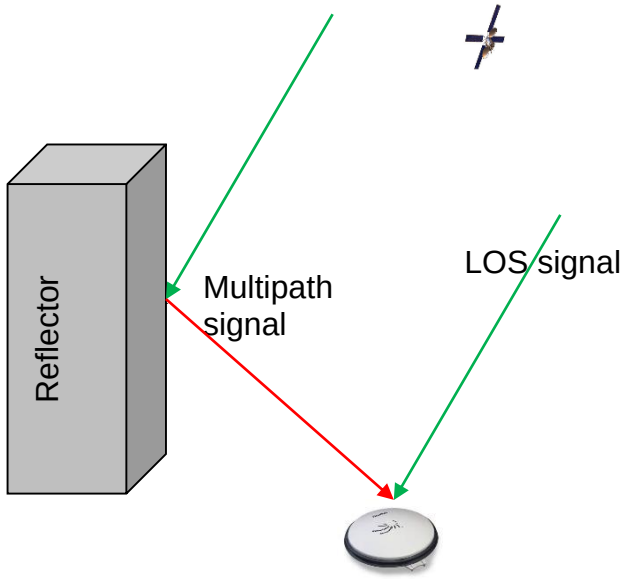

Figure 3-2: Illustration of LOS and multipath signals

The algorithm for finding the point of reflection, code phase delay and Doppler corresponding to the multipath signals are now discussed.

Finding point of reflection

In this function, a ray-tracing method is used to find this point (Lau et al 2007). The first step is to find it on the plane formed using the coordinates of the reflector, which is referred to as the reflector plane. For this, one needs to find the angle of incidence from the satellite on the plane and the angle of reflection. Instead of this, one can find the image of the antenna or the user position with respect to the plane. A vector is constructed from the satellite position to the image of the user position. The intersection of this vector with the reflector plane gives the reflection point. Once the reflection point is obtained, bound checks can be performed to verify whether the point lies on the reflector surface. The mathematical equations to find the point of reflection are as follows:

Let $\mathbf{p}_u$ – user position in East-North-Up (ENU) coordinate system

$\mathbf{p}_r^1, \mathbf{p}_r^2, \mathbf{p}_r^3, \mathbf{p}_r^4$ – Four corners of the reflector in ENU coordinate system

$\mathbf{p}_s^i$ – i^{th} satellite position

$\mathbf{p}_r^{r,i}$ – Reflection point on the plane that is to be estimated.

The steps involved for finding the point of reflection and validating whether it is a valid reflection are as follows

- Find the image of the user position with respect to the reflector:

  In order to find the image of the user position, the closest point on the plane from the user position is required and is obtained as

$$\mathbf{p}_r^m = \mathbf{p}_u + t_{const1}\mathbf{n}_{norm} \tag{3-1}$$

  where, $\mathbf{n}_{norm}$ is the normal vector to the plane which is the cross product between the two vectors formed using reflector corner points and t_{const1} is the real number obtained as

$$t_{const1} = \frac{\left(\mathbf{p}_r^1 - \mathbf{p}_u\right).\mathbf{n}_{norm}}{\mathbf{n}_{norm}.\mathbf{n}_{norm}} \tag{3-2}$$

  Here, '.' represents the dot product between two vectors. The image of the user positon is obtained as

$$\mathbf{p}_r^u = \mathbf{p}_u + 2\left(\mathbf{p}_r^m - \mathbf{p}_u\right) \tag{3-3}$$

- Check whether the reflection can occur from the given satellite for this reflector:

  Find the range distance from the satellite to both user position and image of the user position. If the distance from satellite to the user position is more than the distance

from satellite to image of the user position, then reflection is not valid. This is the case when the reflector blocks the LOS signal to the user. Reflection happens if both user and satellite are on one side of the reflector.

- Find the intersection between the line joining user image position and satellite and the plane formed by the reflector:

  The point of reflection is obtained as

$$\mathbf{p}_r^{r,i} = \mathbf{p}_s^i + t_{const2}\left(\mathbf{p}_r^u - \mathbf{p}_s^i\right) \tag{3-4}$$

  The real parameter t_{const2} is computed as

$$t_{const2} = \frac{\left(\mathbf{p}_r^1 - \mathbf{p}_u\right).\mathbf{n}_{norm}}{\left(\mathbf{p}_r^u - \mathbf{p}_s^i\right).\mathbf{n}_{norm}} \tag{3-5}$$

- Validate the reflection point:

  Check whether the reflection point is within the minimum and maximum bounds of the corner coordinates.

The reflection observed for one of the satellites is shown in Figure 3-3. The blue line is the vector joining reflection point and satellite. The green line is the reflection from reflector to the user position.

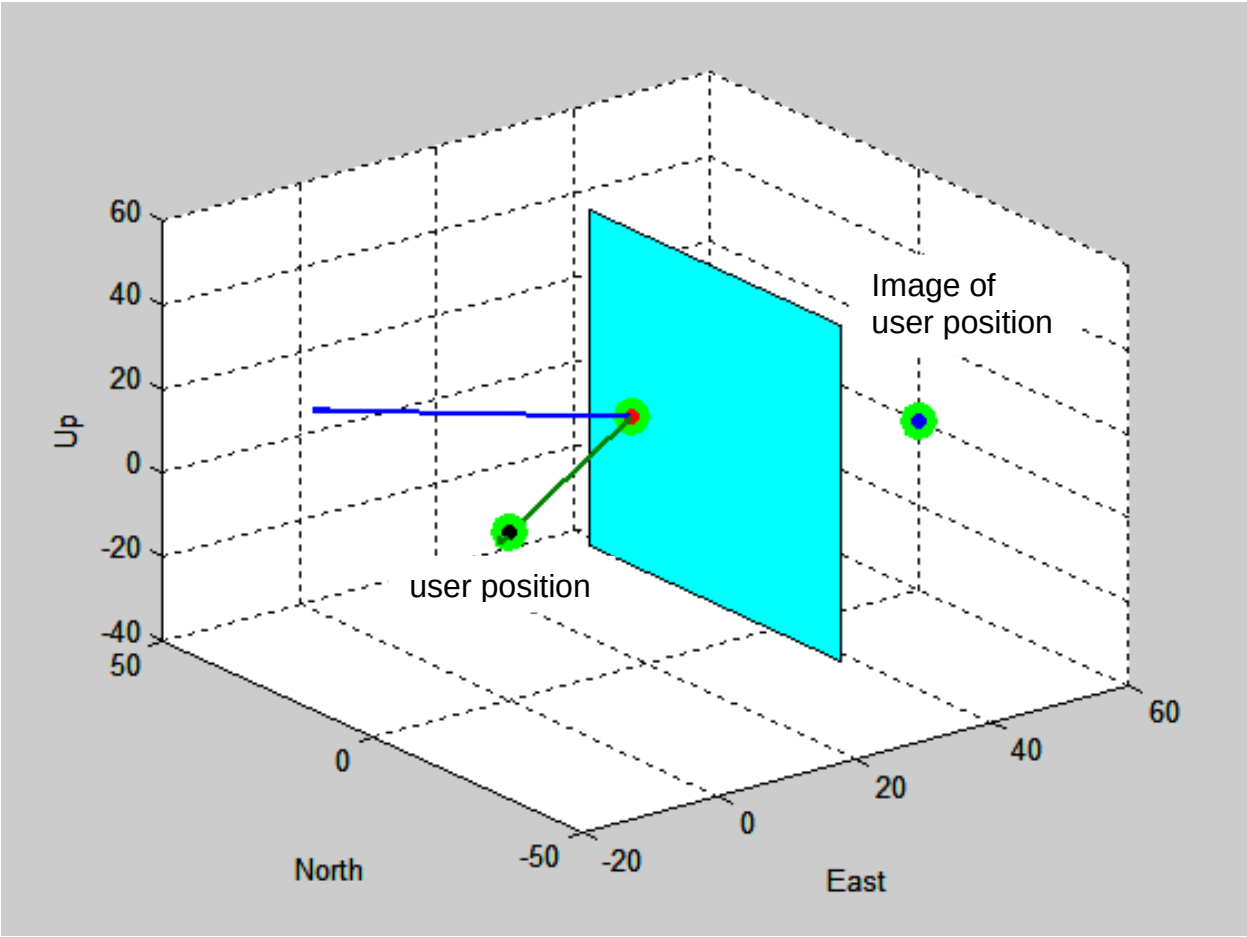

Figure 3-3: Illustration of point of reflection for a rectangular reflector

Once the reflection point is obtained, the Doppler difference between the LOS and multipath signal and the extra code delay and carrier phase corresponding to the extra distance travelled are computed.

Computing multipath code chip

The LOS signal distance is computed by using the satellite and user position through the range equation. If the i^{th} satellite position coordinates in Earth Centered Earth Fixed (ECEF) system are denoted as $(p^i_{sx}, p^i_{sy}, p^i_{sz})$ and the user position coordinates as (p_{ux}, p_{uy}, p_{uz}),

$$\rho_{los} = \sqrt{\left(p^i_{sx} - p_{ux}\right)^2 + \left(p^i_{sy} - p_{uy}\right)^2 + \left(p^i_{sz} - p_{uz}\right)^2} \tag{3-6}$$

Similarly, using the image of the user position (p^u_{rx} , p^u_{ry} , p^u_{rz}) with respect to the reflector, the multipath signal distance can be computed as

$$\rho_{mp} = \sqrt{\left(p^i_{sx} - p^u_{rx}\right)^2 + \left(p^i_{sy} - p^u_{ry}\right)^2 + \left(p^i_{sz} - p^u_{rz}\right)^2} \tag{3-7}$$

By taking the difference between LOS and multipath signal distances, the extra distance travelled by a multipath signal is computed.

$$\rho_e = \rho_{mp} - \rho_{los} \tag{3-8}$$

The extra distance travelled can be transformed into the number of chips by using the following relation:

$$\tau_e = \rho_e * \frac{1023000}{c} \tag{3-9}$$

Computing multipath Doppler

The Doppler frequency is the change in the signal frequency from satellite to the user. As Doppler is due to the relative motion between the satellite and the user, these parameters are related using the following equation:

$$f^i_d = \frac{\left(\mathbf{v}^i_s - \mathbf{v}_u\right)\mathbf{H}^i}{\lambda} \tag{3-10}$$

where $\mathbf{V}^i_s$ is the i^{th} satellite velocity vector, $\mathbf{v}_u$ is user velocity vector, $\mathbf{H}^i$ is unit vector from satellite *i* to user and λ is the signal wavelength.

For the case of a LOS signal, Equation 3-10 can be written as

$$f^i_{\mathrm{d},los} = \frac{\left(\mathbf{v}^j_s - \mathbf{v}_u\right)\mathbf{H}^i_{los}}{\lambda} \tag{3-11}$$

where $\mathbf{H}^i_{los}$ is the unit vector for the LOS signal.

Similarly, the multipath signal Doppler can be computed as

$$f^i_{d,mp} = \frac{\left(\mathbf{v}^j_s - \mathbf{v}_r\right)\mathbf{H}^i_{mp1}}{\lambda} - \frac{\mathbf{v}_u\mathbf{H}^i_{mp2}}{\lambda} \tag{3-12}$$

where $\mathbf{v}_r$ is the reflector velocity vector, $\mathbf{H}^i_{mp1}$ is the unit vector from satellite to reflector and $\mathbf{H}^i_{mp2}$ is the unit vector from reflector to user.

The difference between the LOS and multipath signal Doppler is computed using Equation 3-11 and Equation 3-12 and added to the carrier signal generated for LOS during tracking to obtain the carrier signal corresponding to multipath.

3.3 Simulator validation

A static user scenario with good GPS satellite visibility is chosen for simulations. Input IF samples are collected from the hardware simulator through the data acquisition unit. A MATLAB™ based GPS software receiver is used for the analysis. The receiver software was modified in the process to have multi-antenna functionality with different array processing techniques.

The signals simulated are validated under three categories:

- Single antenna signal validation – analysis of carrier Doppler accuracy, measurement and position accuracies.

- Multi-antenna signal validation – analysis in terms of array gain after combining signals from all antennas.
- Interference simulation – analysis in terms of interference mitigation using array processing approach.

The sky plot of the visible satellites as a function of azimuth and elevation are shown in Figure 3-4.

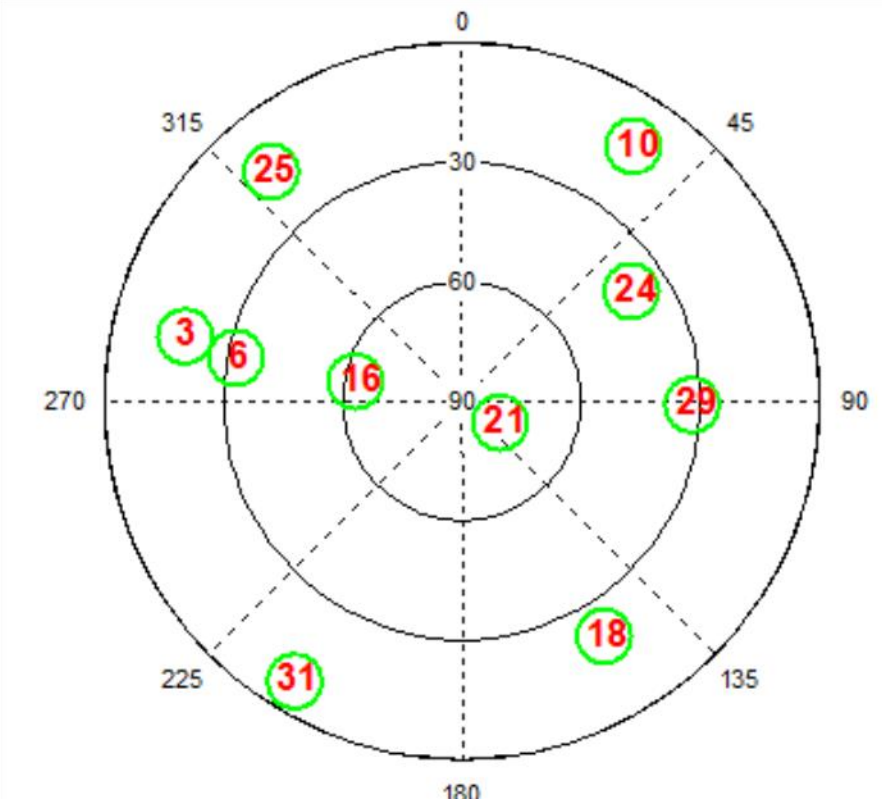

Figure 3-4: Sky plot of the visible satellites considered for validation of the simulator

3.3.1 Single antenna simulator validation

As the simulator uses IF samples collected from a hardware simulator to simulate the signals, the quality of the simulated signals can be compared with that of the input IF samples. This can be done by using the software receiver measurement results and comparing simulated and input signal samples.

Tracking domain analysis

In the tracking domain, the major parameter to be verified is the carrier Doppler. Therefore, the Doppler outputs from the software receiver are compared with both inputs and outputs of the software simulator. Here, a second order PLL with a 15 Hz bandwidth is used along with 20 ms coherent integration. Carrier Doppler values for one of the PRN (PRN 21) are shown in Figure 3-5(a). It can be observed that Doppler values of the input and output overlap with standard deviations of 0.4 Hz for both. In order to further verify, Doppler differences of input and output IF samples for various PRNs are computed and shown in Figure 3-5(b). It can be observed that the mean values of the differences are near zero, indicating that the software simulator performance is comparable with the hardware simulator. The mean and standard deviations of Doppler differences between hard and software simulated signals for various PRNs are provided in Table 3-2.

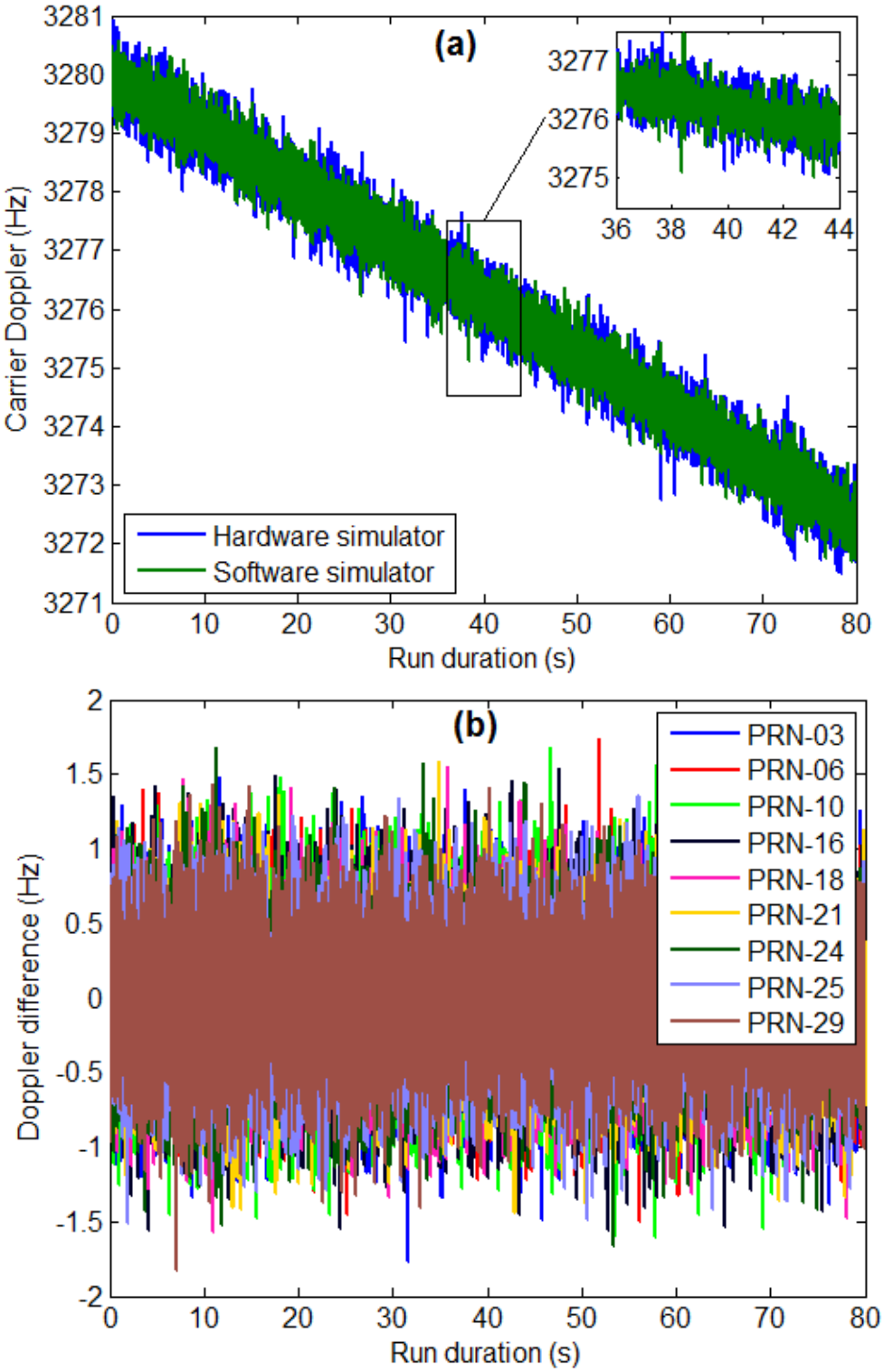

Figure 3-5 : (a) Carrier Doppler values from PRN 21 (b) Doppler differences for each PRN between hardware and software simulators

Table 3-2: Doppler errors between hardware and software simulators

PRN	Doppler differences between hardware and software simulator	
	Mean (Hz)	Standard deviation (Hz)
PRN 3	0.0	0.4
PRN 6	0.0	0.3
PRN 10	0.0	0.4
PRN 16	0.0	0.4
PRN 18	0.0	0.5
PRN 21	0.0	0.4
PRN 24	0.0	0.3
PRN 25	0.0	0.4
PRN 29	0.0	0.3

Measurement domain analysis

Measurement domain analysis is performed by analyzing the differences between the measurements generated by the hardware and software simulator IF samples. Pseudorange and carrier phase measurement differences for different PRNs are shown in Figure 3-6. The means of the differences for both pseudorange and carrier phase measurements are near zero. This validation is important to analyze the measurement distortions caused by different array processing techniques. As measurements obtained from the software simulated IF samples are not biased, possible biases in the measurements after array processing techniques can be determined precisely. The

standard deviations of the pseudorange measurements are observed to be 8 cm and those of carrier phase measurements about 1 mm as shown in Table 3-3.

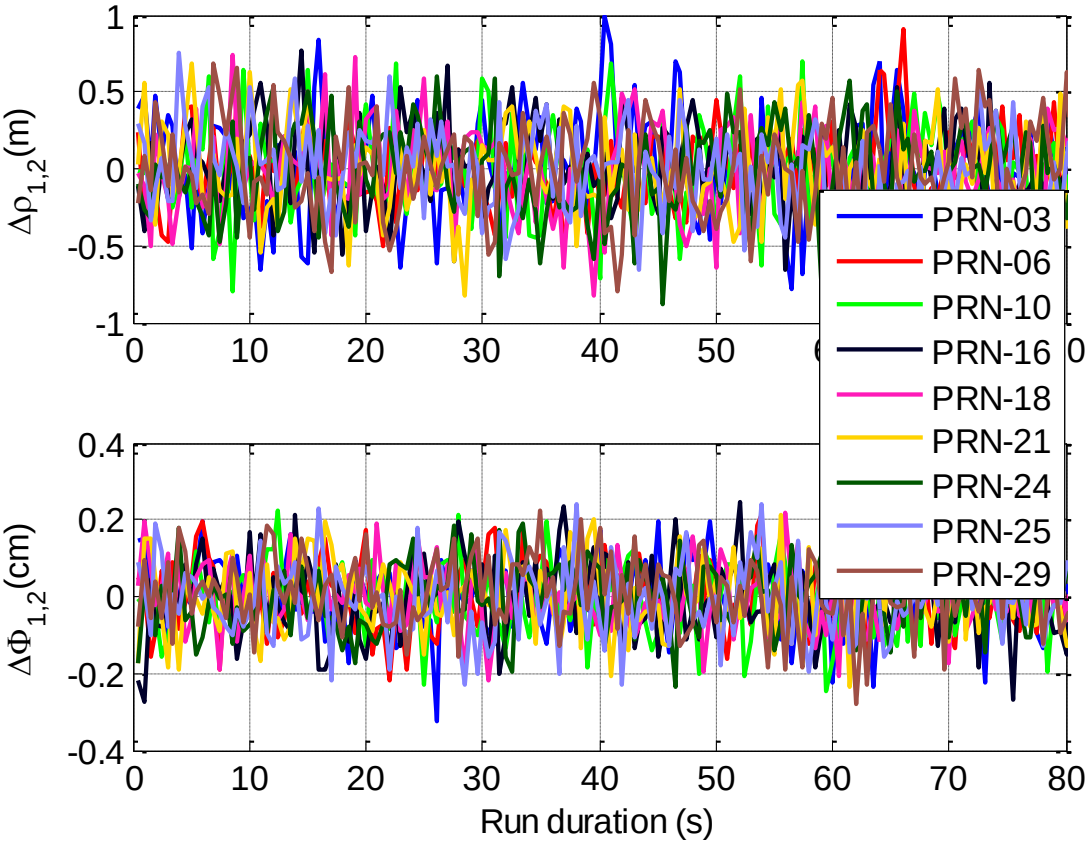

Figure 3-6: Differences between measurements generated from hardware and software simulator IF samples

Table 3-3: Differences between the measurements generated from hardware and software simulator IF samples

PRN	Pseudorange error (cm)		Carrier phase error (mm)	
	Mean	Standard deviation	Mean	Standard deviation
PRN 3	0.0	7.8	0.0	0.9
PRN 6	0.0	7.4	0.0	0.8
PRN 10	0.0	7.6	0.0	1.0
PRN 16	0.0	7.3	0.0	1.0
PRN 18	0.0	7.2	0.0	0.8
PRN 21	0.0	7.5	0.0	0.9
PRN 24	0.0	7.4	0.0	0.9
PRN 25	0.0	7.5	0.0	0.9
PRN 29	0.0	7.1	0.0	0.9

Position domain analysis

Position domain analysis is performed using code phase and carrier phase position solutions. The software receiver provides code phase based position solutions which can be compared with the known user position used in the simulations. Position errors in terms of northing, easting and height using pseudorange measurements are shown in Figure 3-7(a). Means of the position errors are near zero. Position errors using carrier phase measurements are shown in Figure 3-7(b). Carrier phase based position solutions are computed with the open source RTKLib software (Takasu 2007). RTKLib requires measurements from base and remote stations to compute position solution. Base station measurements are generated using a Novatel Propak receiver. Input for the Novatel

receiver is from the hardware simulator using the same user scenario that is being used in the software simulator. The remote station measurements are from the software receiver using the software simulated IF samples. As this acts as zero baseline, the position errors obtained should only be due to measurement noise. It can be observed from Figure 3-7(b) that the means are near zero (after integer ambiguity resolution) and the standard deviations are also minimal. These results are important for the measurement distortion analysis using array processing techniques.

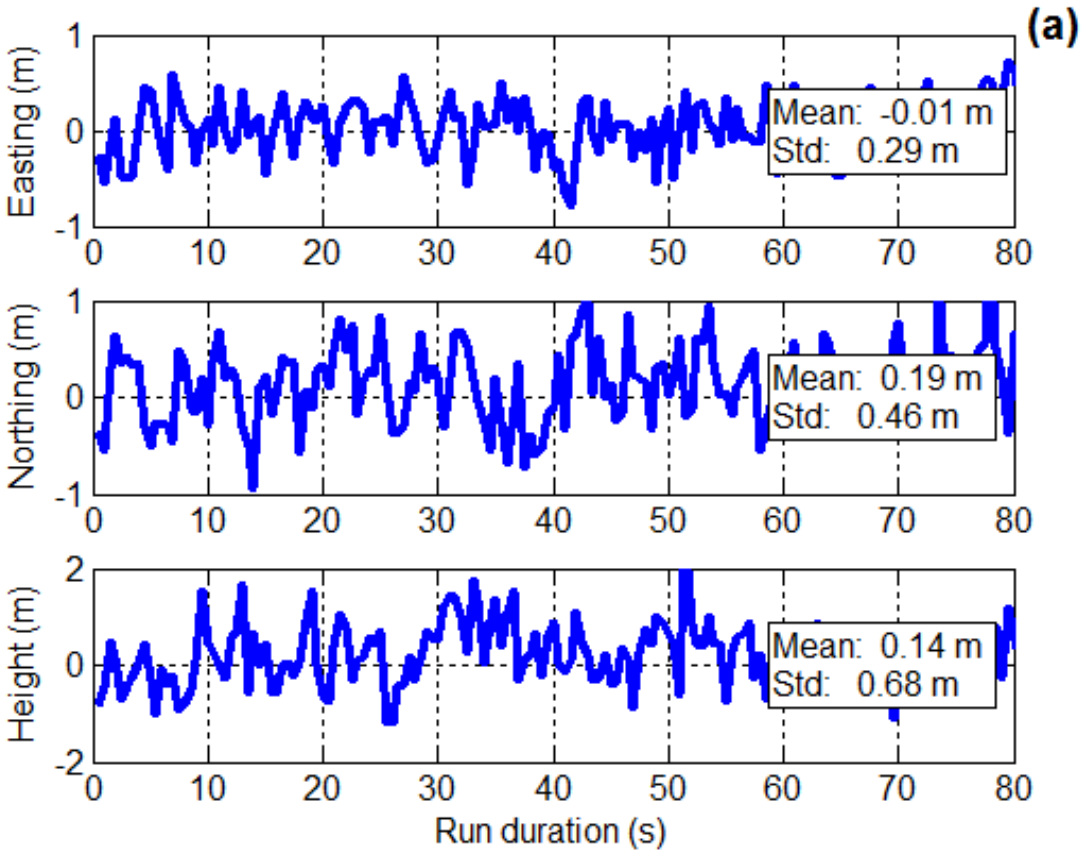

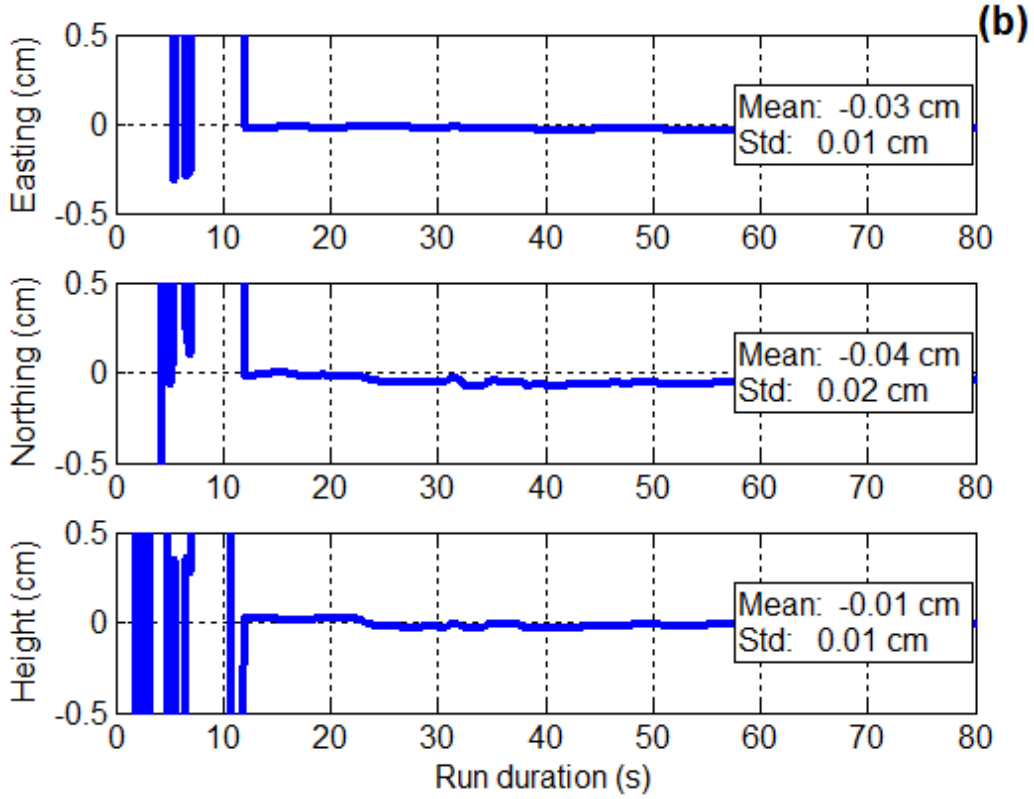

Figure 3-7: Position errors from (a) code phase based position solutions (b) carrier phase based position solutions

3.3.2 Multi-antenna simulator validation

Multi-antenna simulator performance was validated by performing beamforming and comparing the C/N_0 values before and after. Signals were simulated for a 3x2 rectangular array of six antenna elements. The simulated signals were combined using the DAS beamformer. Initially the reference antenna signal (from one of the array antenna elements) was tracked for 10 seconds without beamforming after which beamforming was performed. This is to show the improvement in C/N_0 before and after beamforming. C/N_0 values for different satellites before and after beamforming are shown in Figure 3-8. It can be observed that a gain of nearly 8 dB was observed for all satellites. As six satellites are

used, a gain of 10*log10(6) =7.7 dB is expected and the measured gain is of the same magnitude. This validates the simulation of multi-antenna signals.

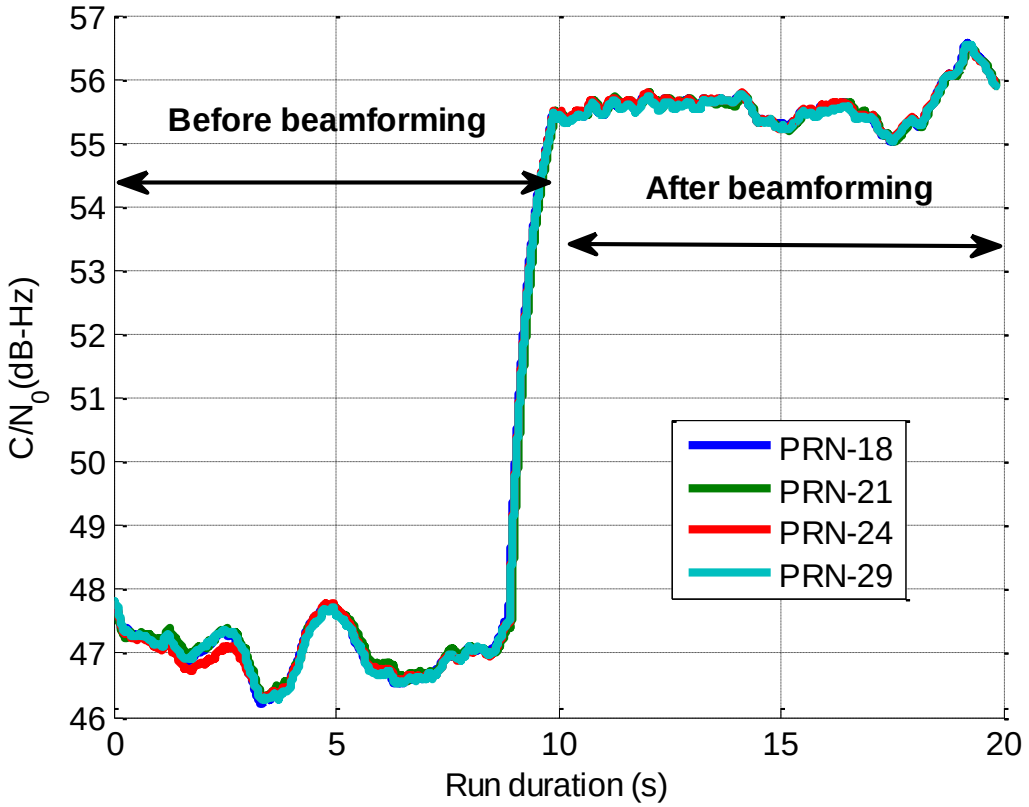

Figure 3-8: C/N$_0$ gain before and after beamforming

3.3.3 Interference simulation validation

In this section, multipath interference is validated. It was discussed in Section 2.1 that multipath produces constructive and destructive effects on the signal and that these can be observed through C/N$_0$ variations. For the static user scenario, a reflector was placed at a distance of 30 m from the user. It was assumed that only single reflection exists and LOS is stronger than multipath signal. Relative multipath signal power is assumed to be 0.75. Reflector was placed such that PRN 10 which is at lower elevation experienced

multipath. PRN 21, which is at higher elevation, is not affected by multipath. It is assumed that all satellites have same C/N_0 values irrespective of their elevation. C/N_0 variations of PRN 10 and PRN 21 are shown in Figure 3-9. Periodic variations can be observed in PRN 10 C/N_0 values. As the user is static, the periodicity is of the order of seconds.

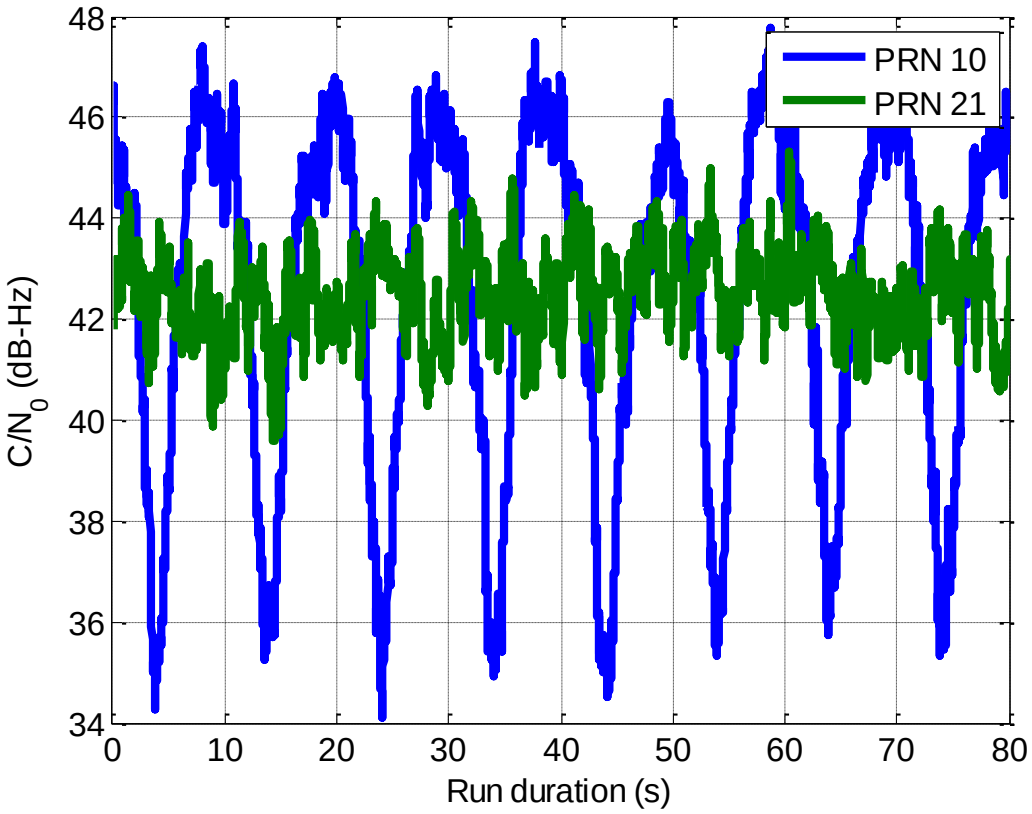

Figure 3-9: C/N_0 variations with (PRN 10) and without (PRN 21) multipath

3.4 Summary

This chapter described a novel method of simulating multi-antenna GNSS signals. Software architecture and methodology of multipath signals simulation were described. The functionality of the simulator as validated through various tests in terms of signal quality, multi-antenna signals and multipath signal generation. The simulator is validated

using single antenna hardware simulated data as well as actual data. This simulator will now be used in the next chapters for measurement analysis using different array processing techniques.

Chapter Four: GNSS ANTENNA ARRAY RECEIVER PERFORMANCE UNDER MULTIPATH INTERFERENCE

The focus of this chapter is to investigate the performance of array processing techniques to mitigate short-range multipath signals. As GNSS signals are below the noise level before the correlation process, spatial processing to mitigate multipath signals is mostly performed after the de-spreading process (i.e., correlation and Doppler removal) (Arribas et al 2012, Chen et al 2012). First, the inherent capability of DAS and MPDR beamformers to mitigate multipath are studied without any preprocessing to decorrelate the LOS and multipath signals. Then, a preprocessing technique called ***spatial smoothing*** is used to decorrelate the signals. This process consists of two stages; in the first stage, spatial smoothing is used to decorrelate LOS and multipath signals while in the second stage, spatially smoothed signals are combined using the MPDR beamformer. Measurement and position results from simulated and actual GPS signals are provided.

4.1 Signal and system model

Consider the case of a GNSS receiver equipped with an *M*×*N* element uniform rectangular array as descried in Section 2.4.2. The signals impinging on the antenna array are the desired signals, multipath and noise. For simplicity, signals from one satellite are considered below. After down-conversion and sampling, the digitized signal received at the $(m,n)^{\text{th}}$ antenna element can be expressed as

$$x_{m,n}(n_t) = \sum_{k=1}^{K} s_k(n_t)\, e^{j\frac{2\pi}{\lambda}\left[(m-1)d_m \sin(\theta_k)\sin(\phi_k)+(n-1)d_n \sin(\theta_k)\cos(\phi_k)\right]} + v_{mn}(n_t) \tag{4-1}$$

where $s_k(n_t)$ is the k^{th} signal component as observed at antenna element, k=1 refers to the desired signal and k=2:K refer to multipath signals, λ is the signal wavelength, (θ_k, ϕ_k) are the elevation and azimuth angle of the k^{th} component, $v_{m,n}(n_t)$ is the additive spatially white noise of the $(m,n)^{th}$ antenna element and n_t represents the discrete time index.

Multipath mitigation is performed after the de-spreading process. Hence, the signal model after the correlation process is considered here. Let the correlator output signal for the $(m,n)^{th}$ antenna element be expressed as

$$y_{m,n}(n_c) = \sum_{k=1}^{K} r_k(n_c) e^{j\frac{2\pi}{\lambda}\left[(m-1)d_m \sin(\theta_k)\sin(\phi_k)+(n-1)d_n \sin(\theta_k)\cos(\phi_k)\right]} + \eta_{m,n}(n_c) \quad (4\text{-}2)$$

where n_c represents the time index after correlation, $\eta_{m,n}(n_c)$ is the white noise component, $r_k(n_c)$ shows the correlator output of the k^{th} signal component as observed at the (1,1) antenna element, which is given by

$$r_k(n_c) = \alpha_k e^{j2\pi\Delta f_k n_c T_c + j\Delta\varphi_k} \quad (4\text{-}3)$$

where α_k is the attenuation factor, Δf_k represents the frequency offset and $\Delta\varphi_k$ is the phase shift; T_c is the coherent integration time.

The correlator output from all the antenna elements can be represented in matrix form as

$$\mathbf{y} = \mathbf{A}\mathbf{r} + \boldsymbol{\eta} \quad (4\text{-}4)$$

where $\mathbf{y}$ is the MN×1 correlator output vector, $\mathbf{A}$ is the steering matrix, $\boldsymbol{\eta}$ is MN×1 noise vector, $\mathbf{r}$ is Kx1 correlator output vector; these vectors can be written as

$$\mathbf{y} = \left[y_{1,1}(n_c), y_{2,1}(n_c), \ldots y_{M,1}(n_c), y_{1,2}(n_c), \ldots y_{M,N}(n_c) \right]^T \tag{4-5}$$

$$\boldsymbol{\eta} = \left[\eta_{1,1}(n_c), \eta_{2,1}(n_c), \ldots \eta_{M,1}(n_c), \eta_{1,2}(n_c), \ldots \eta_{M,N}(n_c) \right]^T \tag{4-6}$$

$$\mathbf{r} = \left[r_1(n_c), r_2(n_c), \ldots r_K(n_c) \right]^T \tag{4-7}$$

The steering matrix **A** is of dimension $MN \times K$ and is given by

$$\mathbf{A} = \left[\mathbf{a}_1, \mathbf{a}_2, \ldots\ldots \mathbf{a}_K \right] \tag{4-8}$$

where $\mathbf{a}_k$ is the $MN \times 1$ steering vector of the k^{th} signal component coming from direction (θ_k, ϕ_k), which is given by

$$\begin{aligned} \mathbf{a}_k &= \left[\mathbf{c}_k^T, \gamma_k \mathbf{c}_k^T, \ldots\ldots, \gamma_k^{(N-1)} \mathbf{c}_k^T \right]^T \\ \mathbf{c}_k &= \left[1, \beta_k, \ldots\ldots \beta_k^{(M-1)} \right]^T \\ \gamma_k &= e^{j \frac{2\pi}{\lambda} d_n \sin(\theta_k) \cos(\phi_k)} \\ \beta_k &= e^{j \frac{2\pi}{\lambda} d_m \sin(\theta_k) \sin(\phi_k)} \end{aligned} \tag{4-9}$$

4.2 Effect of multipath signals on beamforming

DAS and MPDR beamformers with and without spatial smoothing are considered here. The effect of correlation between LOS and multipath signals on beamformers is discussed and different numerical simulations are performed to evaluate the performance of these beamforming techniques to mitigate multipath signals for GNSS applications. The main difference between GNSS and other systems is that the measurement quality is of most importance beside the signal strength improvement. Any type of filtering that distorts the

measurement quality affects the performance of a GNSS receiver. Hence, special care should be devoted into beamforming design and implementation.

The correlation between LOS and multipath signals has an adverse effect on the beamformer's performance (Widrow et al 1982, Reddy et al 1987, Daneshmand et al 2013). As the covariance matrix is obtained by temporal averaging, the temporal cross correlation between the desired and the multipath signals is very high since their phase relation stays fairly constant during the averaging time. Therefore, the system considers the sum of the desired and multipath signals as one wave and computes weights to minimize the total output power. However, as desired and multipath signals are treated as one wave, the weights will have a destructive effect on the desired signal and in the process of mitigating multipath, the desired signal will also be cancelled (Widrow et al 1982). In addition, the beamformer fails to form deep nulls in the direction of multipath (Chen et al 2012). If the phase relation between the desired signal and multipath can be randomized, then the coherence between the signals will be reduced. This can be achieved by receiving antenna array signals from different spatial locations, which can be performed either via moving the array (Daneshmand et al 2013) or through spatial smoothing techniques (Reddy et al 1987). In the case of a static GNSS receiver, spatial smoothing can be applied to decorrelate the signals. In this method, antenna elements are grouped into a smaller number of overlapping subarrays (Van Trees 2002, Reddy et al 1987). The basic requirement for spatial smoothing is that the steering vector should have a Vandermonde structure as in the case of linear and rectangular arrays (Van Trees 2002). The Vandermonde structure refers to the progressive linear phase shift of the signals across the antenna elements in an array. The covariance matrices from all the

subarrays are then averaged to form the spatially smoothed covariance matrix. The subarray concept emulates antenna array motion where signals received by different subarrays correspond to different spatial points. In this case, the phase relation between LOS and multipath is different for different subarrays and averaging the spatial covariance matrix over several subarrays reduces the correlation between the LOS and multipath signals. Along with forward smoothing, complex conjugated backward smoothing can be performed to improve the decorrelation as well as increase the antenna aperture (Reddy et al 1987).

4.2.1 MPDR Beamformer with Spatial Smoothing (MPDRSS)

Consider an $M \times N$ array divided into overlapping subarrays of size $\{M_s, N_s\}$. Assume P subarrays in the x-direction and Q in the y-direction. Let $\mathbf{R}_{fpq}$ be the covariance matrix of the $[p,q]^{th}$ forward subarray. The forward spatially smoothed covariance matrix is the sample means of all the forward subarray covariance matrices and can be computed as

$$\mathbf{R}_f = \frac{1}{PQ}\sum_{p=1}^{P}\sum_{q=1}^{Q}\mathbf{R}_{fpq} \tag{4-10}$$

Similarly, if $\mathbf{R}_b$ is the backward spatially smoothed covariance matrix, then the forward-backward spatially averaged covariance matrix is given by

$$\mathbf{R}_{fb} = \frac{\mathbf{R}_f + \mathbf{R}_b}{2} \tag{4-11}$$

The optimum weight vector for the MPDR beamformer with spatial smoothing is (Van Trees 2002)

$$\mathbf{w}_{MPDRSS} = \frac{\mathbf{R}_{fb}^{-1}\mathbf{a}_{11}}{\mathbf{a}_{11}^{H}\mathbf{R}_{fb}^{-1}\mathbf{a}_{11}} \tag{4-12}$$

where $\mathbf{a}_{11}$ is the steering vector of the LOS signal for the first subarray.

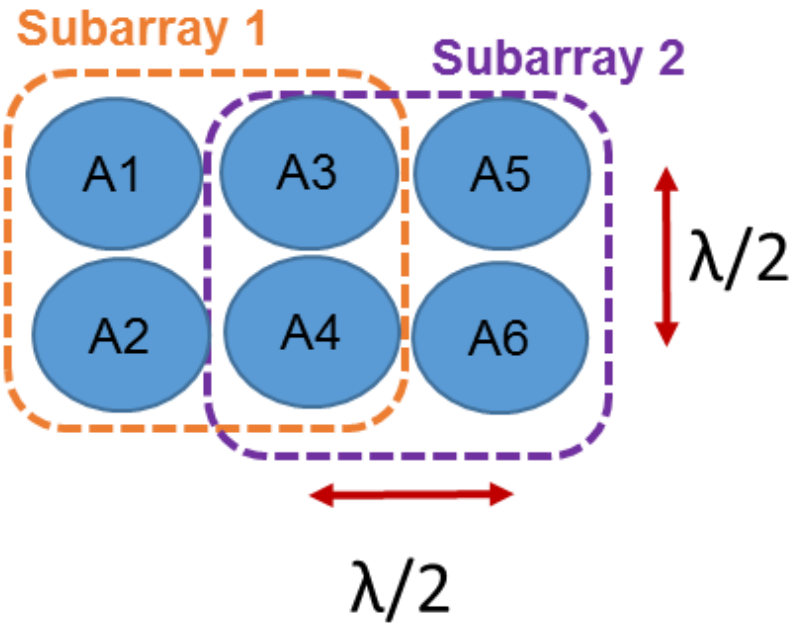

Figure 4-1: Subarray architecture for a 3x2 URA

Beamformer's performance depends on a number of factors such as the number of antenna elements, array configuration and incoming signal direction of arrival to name a few. The size and the number of antenna elements are some of the limitations for practical applications in terms of cost and system complexity. Hence, investigation of the performance of an antenna array based GNSS receiver with a limited number of antenna elements while still being able to perform spatial smoothing is important. Consider a URA with six antenna elements (M=3, N=2). The subarray formation for the spatial smoothing is shown in Figure 4-1. Due to the limited number of elements in the array only two subarrays (P = 2, Q = 1) are constructed with size {J=2, L=2}. The decorrelation obtained

by spatial smoothing and in turn the performance of the beamformer are analyzed in the following sections.

4.3 Numerical Simulations

This section presents numerical simulation results for the array structure shown in Figure 4-1 with inter-element spacing of 9.5 cm. The performance of the beamforming techniques in the presence of multipath signals is evaluated using the Signal-to-Multipath Ratio (SMR) (Arribas et al 2014) metric. SMR refers to the ratio between the LOS power and multipath power at the output of the beamformer and is expressed in dB. The pre-beamformer SMR is assumed to be 0 dB. Here, it is assumed that multipath is coming from (15˚, 175˚) and the LOS signal azimuth is (50˚). Beamformer performance for different correlation coefficients of the LOS and multipath signals for different LOS signal elevations is assessed. For the two signals case, r_1 (LOS) and r_2 (multipath), the covariance matrix can be represented as

$$\mathbf{R}_{yy} = \mathbf{A}\mathbf{R}_s\mathbf{A}^H + \sigma_\eta^2\mathbf{I} \tag{4-13}$$

where $\mathbf{R}_s$ is the source covariance matrix and σ_η^2 is the noise variance. The source covariance can be defined as

$$\mathbf{R}_s = \begin{bmatrix} \sigma_{r1}^2 & \sigma_{r1}\sigma_{r2}\rho \\ \sigma_{r1}\sigma_{r2}\rho & \sigma_{r2}^2 \end{bmatrix} \tag{4-14}$$

where σ_{r1}^2 is the variance of the source signal, σ_{r2}^2 is the variance of the multipath signal and ρ is the correlation coefficient between the LOS and multipath, defined as

$$\rho = \frac{E\left[r_1 r_2^H\right]}{\sqrt{E\left[r_1 r_1^H\right]}\sqrt{E\left[r_2 r_2^H\right]}} \tag{4-15}$$

The power of both LOS and multipath is set to 10 ($\sigma_{r1}^2 = \sigma_{r2}^2 = 10$) and the noise variance is assumed to be 1. The elevation of the LOS signal is swept from 0˚ to 90˚ for different magnitudes of the correlation coefficient between the signals and the SMR performance of both MPDR and MPDRSS is shown in Figure 4-2. The MPDR performance is the same for different LOS signal elevations for a given correlation coefficient. For very low correlation coefficients, which is the case when LOS and multipath signals are uncorrelated to each other, the MPDR beamformer yields a SMR up to 40 dB. However, as correlation increases, beamformer performance decreases and results in low SMR values. As seen in Figure 4-2, when the correlation coefficient magnitude is above 0.6, the SMR is nearly 0 dB. The performance of MPDRSS is better than MPDR for higher elevation satellites when signals are correlated to each other. This is due to the fact that the angular separation of the LOS from multipath signals is higher and spatial smoothing is able to provide better decorrelation. As can be seen in Figure 4-2, SMR up to 10 dB can be achieved using MPDRSS for higher elevation satellites even when signals are highly correlated. Since the decorrelation achieved by the spatial smoothing process is a function of the DOA of the incoming signals and the number of antenna elements, the MPDRSS beamformer performance is different for different signals impinging on the array from different directions. However, it was observed that for the rectangular array considered, MPDRSS beamformer performance improves with an increase in the elevation angle of the LOS signal, given that the multipath signal is coming from low elevation.

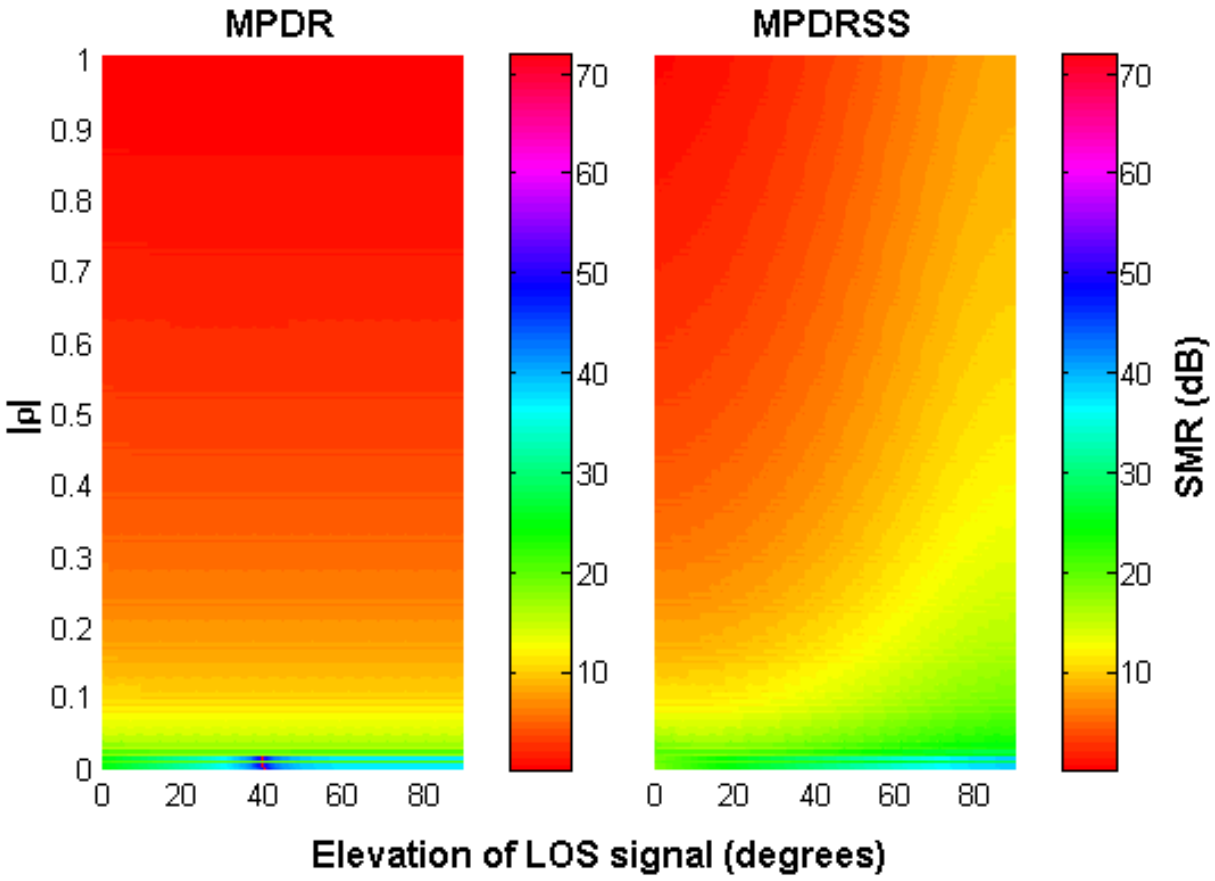

Figure 4-2: Output SMR performance with MPDR and MPDRSS with multipath coming from (15˚, 175˚) and LOS azimuth (50˚) for different magnitudes of the correlation coefficient. [Indicates improvement in SMR for higher elevation satellites using MPDRSS as compared to MPDR as correlation between signal increases].

The beampatterns for the DAS, MPDR and MPDRSS beamformers for different correlation coefficients for a higher elevation satellite with multipath from low elevation are shown in Figure 4-3. Here, it is assumed that the LOS signal is coming from (75˚, 50˚) and multipath from (15˚, 175˚). As the DAS beamformer does not rely on the statistics of the received signal, the performance will be same for any correlation between LOS and multipath signals. However, MPDR performance only improves when the correlation between LOS

and multipath is very low. MPDRSS provides better attenuation of the multipath signals. Even when signals are highly correlated, MPDRSS can attenuate multipath by up to 10 dB. Based on the LOS signal directions and correlation between LOS and multipath signals, the DAS beamformer performance could be similar to that of MPDR and MPDRSS. In some cases, it might be better than MPDR as correlation can degrade the performance of the latter.

The beampatterns for the DAS, MPDR and MPDRSS beamformers for different correlation coefficients for a lower elevation satellite with multipath from low elevation are shown Figure 4-4. It is assumed that the LOS signal is coming from (20˚, 50˚) and multipath from (15˚, 175˚). It can be observed that multipath attenuation for a lower elevation satellite is lower as compared to that of the higher elevation satellite case for the same correlation coefficient with both MPDR and MPDRSS.

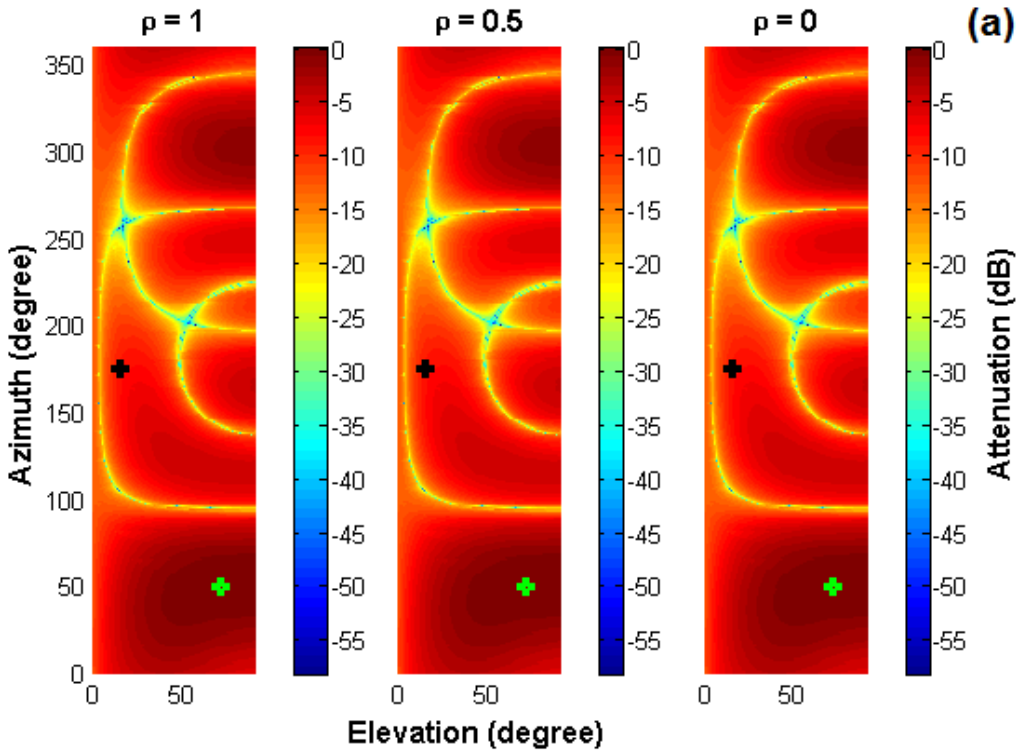
(a)
ρ = 1
ρ = 0.5
ρ = 0
Azimuth (degree)
Elevation (degree)
Attenuation (dB)
0
50
100
150
200
250
300
350
0
-5
-10
-15
-20
-25
-30
-35
-40
-45
-50
-55

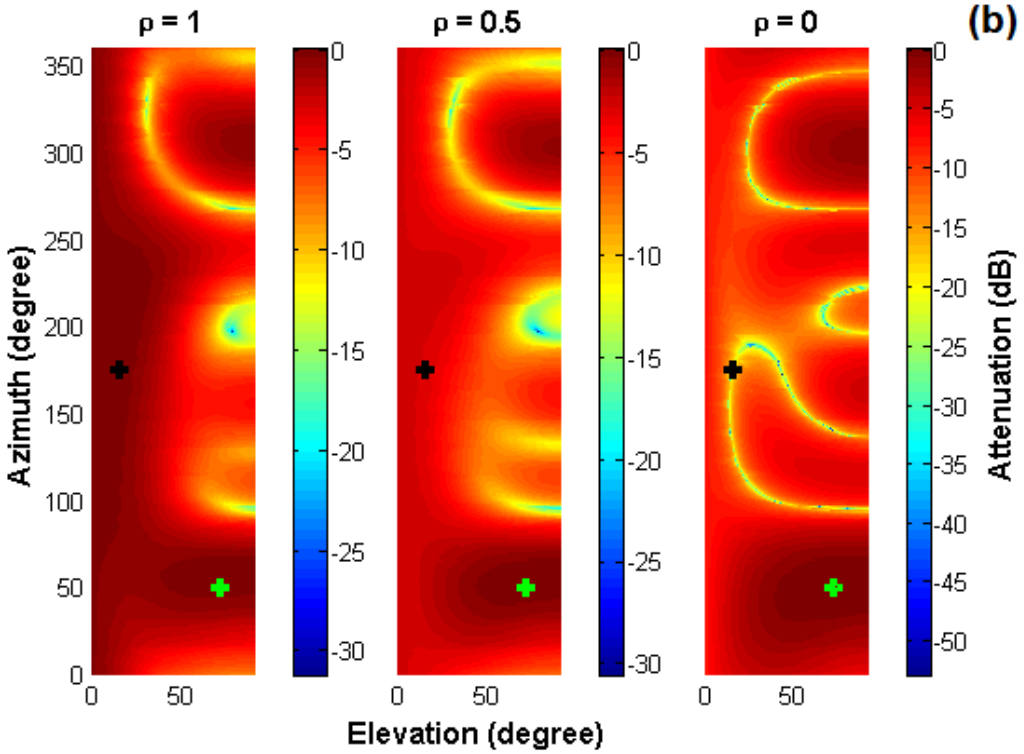
(b)
ρ = 1
ρ = 0.5
ρ = 0
Azimuth (degree)
Elevation (degree)
Attenuation (dB)
0
50
100
150
200
250
300
350
0
-5
-10
-15
-20
-25
-30
-35
-40
-45
-50

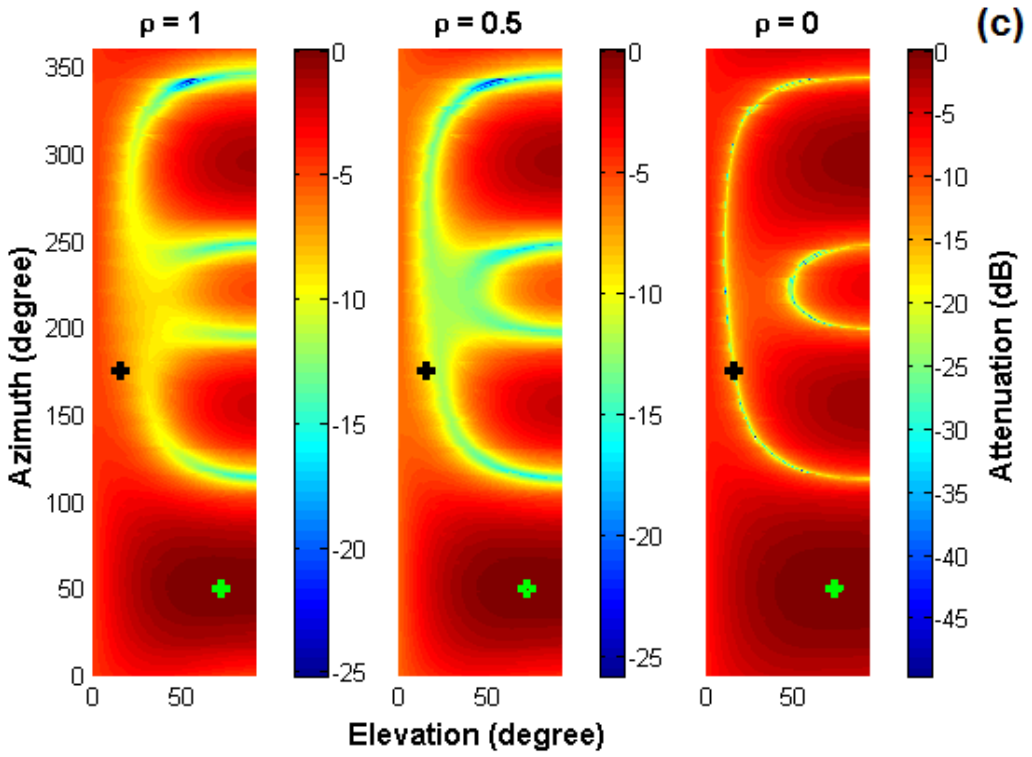

Figure 4-3 :Beampatterns with LOS (70˚, 50˚) and multipath (15˚, 175˚)

(a) Conventional beamformer (b) MPDR beamformer (c) MPDR beamformer with spatial smoothing

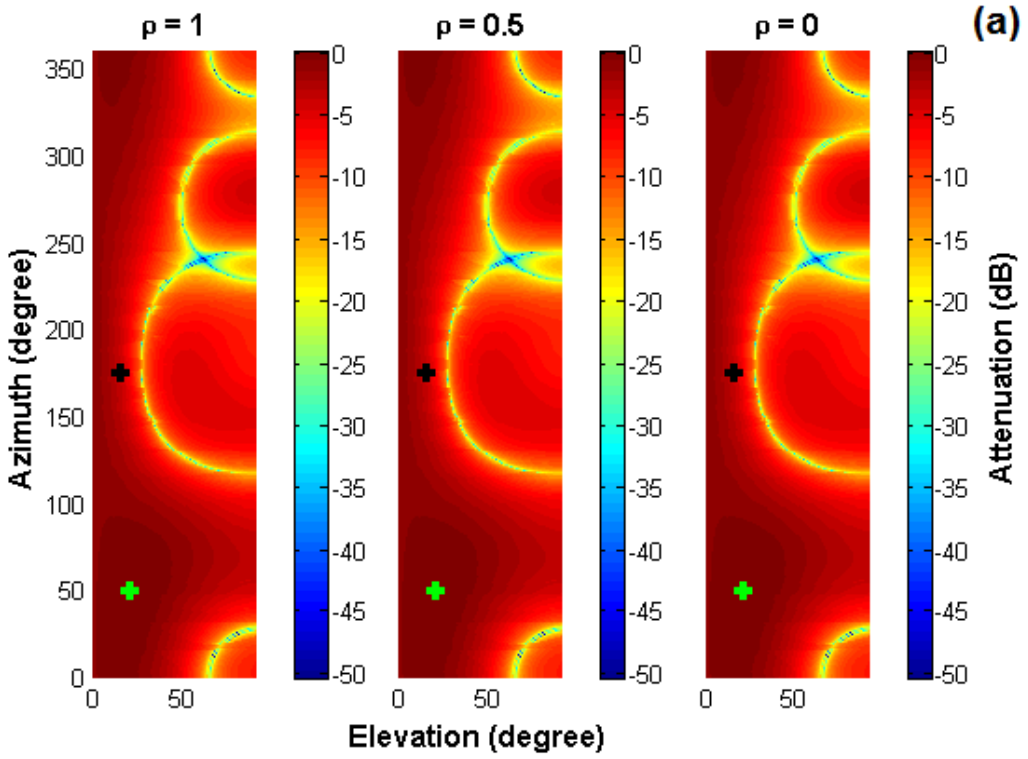
(a)
ρ = 1
ρ = 0.5
ρ = 0
Azimuth (degree)
Elevation (degree)
Attenuation (dB)
0
50
100
150
200
250
300
350
0
-5
-10
-15
-20
-25
-30
-35
-40
-45
-50

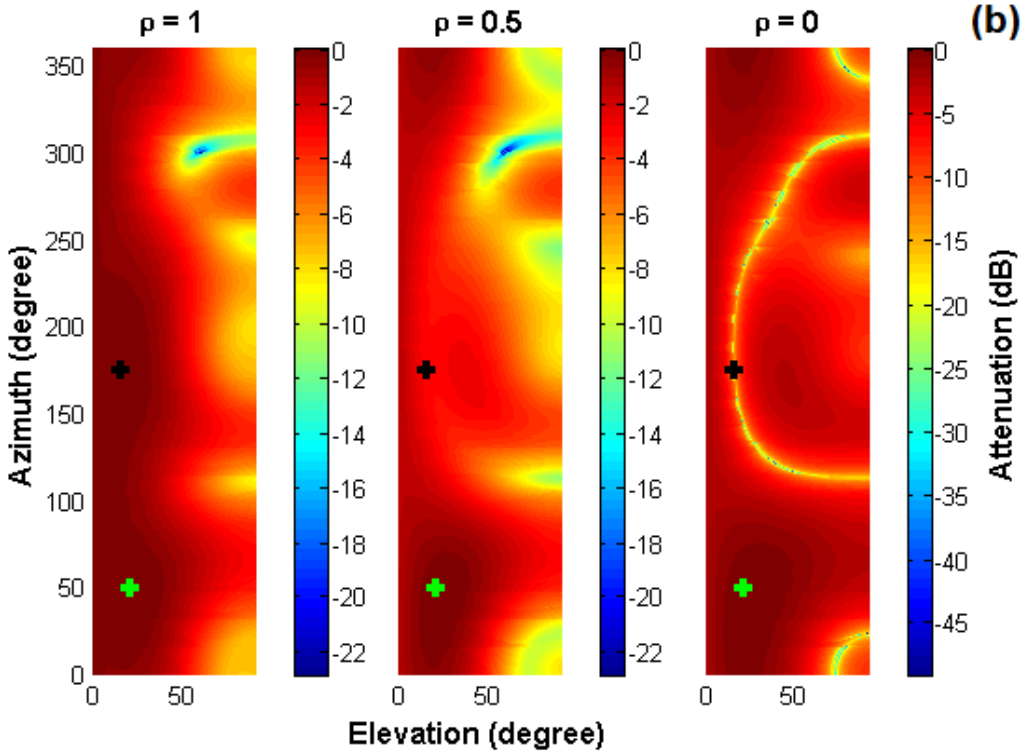
(b)
ρ = 1
ρ = 0.5
ρ = 0
Azimuth (degree)
Elevation (degree)
Attenuation (dB)
0
50
100
150
200
250
300
350
0
-2
-4
-6
-8
-10
-12
-14
-16
-18
-20
-22
-5
-10
-15
-20
-25
-30
-35
-40
-45

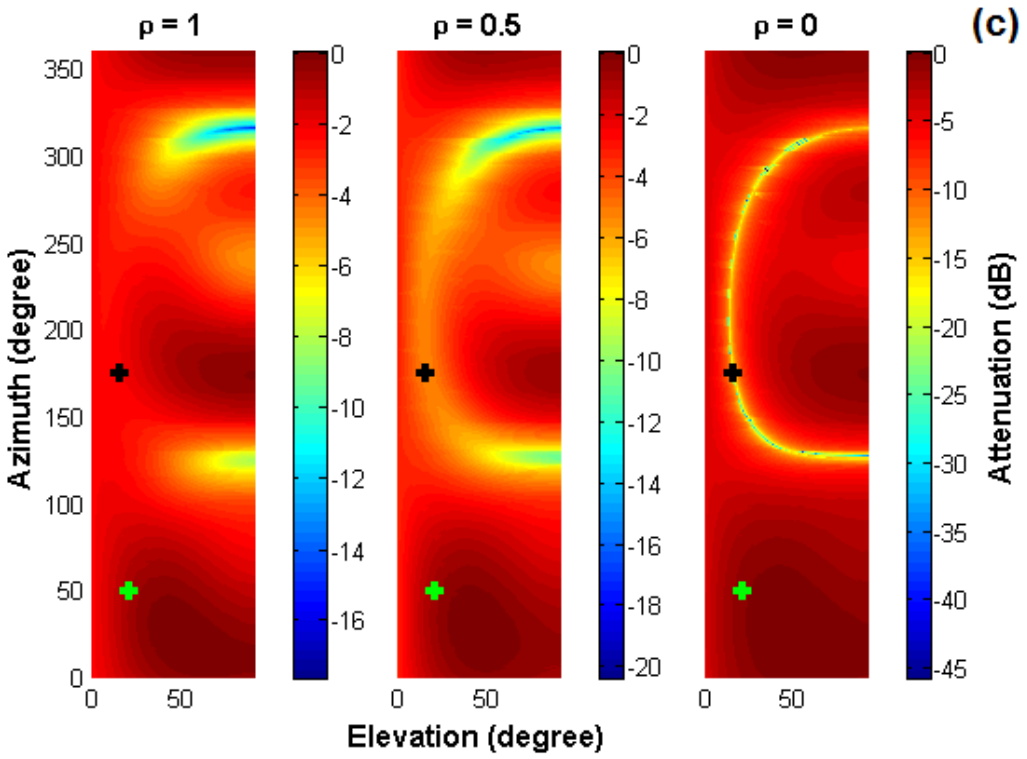

Figure 4-4: Beampatterns with LOS (20˚, 50˚) and multipath (15˚, 175˚)
(a) Conventional beamformer (b) MPDR beamformer (c) MPDR beamformer with spatial smoothing

4.4 Multi-antenna GPS Receiver

The acquisition and tracking of a single channel GPS receiver were modified for multi-antenna receiver functionalities. The navigation solution of an open source MATLAB™ based GPS software receiver (Borre et al 2007) was incorporated with the multi-antenna software receiver developed by the author. The basic blocks of the multi-antenna receiver are shown in Figure 4-5. One of the antenna elements in the array acts as the reference antenna. Satellite signals are acquired and tracked using the digital samples of the reference antenna. The Doppler and code delays obtained are used to de-spread the signals from other antennas so that relative phase values between the antenna elements

are maintained. After Doppler and code removal from the digital samples corresponding to each antenna, the prompt correlator values are used to compute the optimum weights using the MPDR beamformer. In order to capture the statistics of the incoming signals, prompt correlation values collected over 1 s are used to compute the covariance matrix of the MPDR beamformer. Thus its weights are updated every second. The DAS beamformer does not use the statistics of the prompt correlation values as it relies only on the satellite DOA. Weights for the DAS beamformer are also updated every second to capture the variations in DOA of the LOS signal. The weights computed are used to combine 1 ms, early, prompt and late correlator values of the six antennas. The combined correlator parts, namely early-prompt-late, are used by the tracking loops to generate the code and carrier replica signals.

Performance of beamforming techniques are compared with narrow correlator with 0.1 chip spacing between early and late parts and with Double Delta (DD) correlators. For the multi-antenna receiver architectures, narrow correlator with 0.1 chip spacing between early and late parts is used. Normalized non-coherent early minus late envelope code discriminator is used in all the cases. A first order DLL with bandwidth of 0.1 Hz is used in the PLL-assisted DLL mode. The C/N_0 is computed using narrowband power and wideband power as described in (Dierendonck 1996). The least squares method is used to compute the position solution with pseudorange measurements.

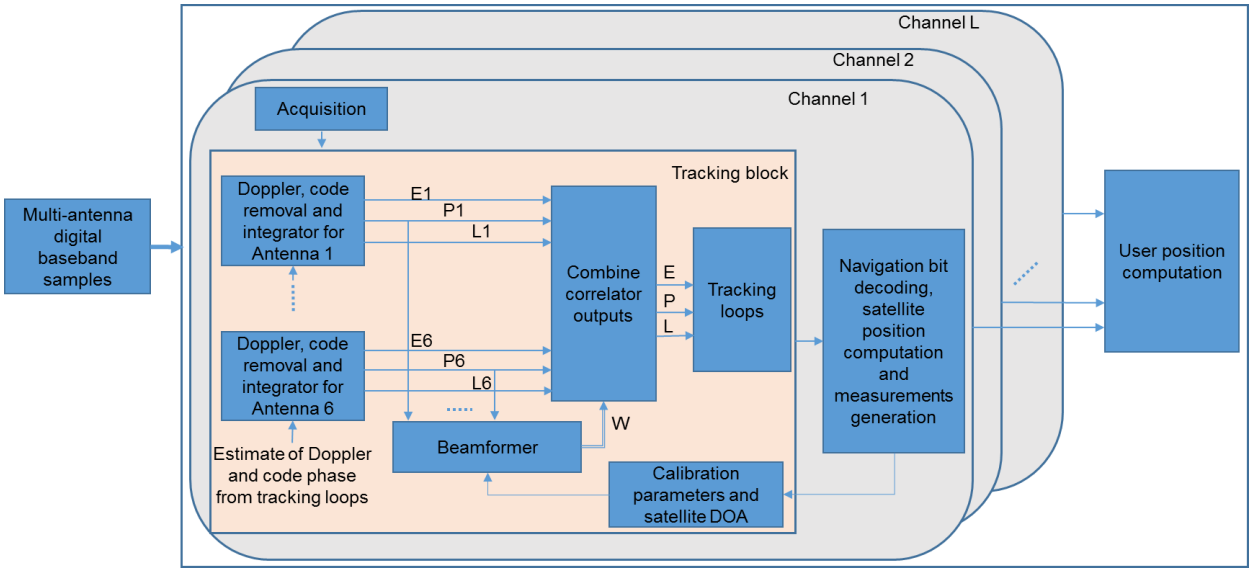

Figure 4-5: Multi-antenna GNSS receiver architecture

4.5 Simulation results

This section describes the multi-antenna GPS signal simulation scenario and the corresponding results for different beamforming techniques. A GPS receiver equipped with a rectangular array as shown in Figure 4-1 is considered for the simulations. A static user scenario was generated using the hardware simulator; atmospheric, satellite clock and multipath errors were disabled. The GPS signal from the hardware simulator was sampled at 20 MHz using the data acquisition system, which is input to the multi-antenna GPS signal simulator. To simulate multipath signals, four rectangular shaped reflectors with dimensions of 30 m x 50 m were considered. The reflectors were placed at a 30 m distance from the user in all the four directions. The reason for selecting reflectors in all the four directions is to simulate multipath for most of the low elevation satellites. Only specular multipath with single reflection was considered. A multipath attenuation factor of 0.75 was considered for each of the multipath signals. The DOAs of different satellites

used in the simulation are given in Table 4-1. Based on the ray tracing method, PRN 16 and PRN 21 do not have any multipath.

Table 4-1: Satellite DOAs used in simulations

PRN	6	10	16	18	21	24	25	29	31
Azimuth(degrees)	281	34	280	149	119	57	320	91	211
Elevation(degrees)	32	13	63	21	79	39	15	32	8

The performance of the beamformer was evaluated by analyzing the improvement in C/N_0 and multipath error reduction before and after beamforming. The multi-antenna software receiver was run in five different modes to generate C/N_0 and pseudorange observations as described in Table 4-2.

The received signal in Mode 1 is not affected by multipath and hence can be considered as a reference clean data for pseudorange error analysis. The pseudorange errors are computed by taking the differences between the pseudorange values obtained in Mode 1, which is the reference scenario, with those of Mode 2 to 5. The C/N_0 values and pseudorange errors for various modes in the case of PRN 6 are shown in Figure 4-6. Periodic variations can be observed in the C/N_0 values of Mode 2 due to the presence of multipath signals. Similar C/N_0 fluctuations were also observed in other similar measurements (Ray et al 1999). After beamforming with the six antennas (Mode 3 to 5), the C/N_0 variations are reduced and improvements occur. The C/N_0 values improve by 8 dB in Mode 3 and 4 and 6.5 dB in mode 5 as compared to Mode 1. The reason that C/N_0 values in Mode 5 are lower than those of Mode 3 and 4 is because a lower number of antennas is used during beamforming due to spatial smoothing process. Similarly,

pseudorange errors after beamforming, which are correlated to C/N_0 variations, are significantly reduced, indicating mitigation of the multipath signal using all the three beamforming techniques.

Table 4-2: Receiver software execution configurations

Mode	Configuration
Mode 1	LOS scenario is assumed. Reference antenna tracks all observable signals. (Narrow correlator is considered)
Mode 2	LOS and multipath scenario is assumed. Reference antenna tracks all observable signals. (Narrow correlator is considered)
Mode 3	LOS and multipath scenario is assumed. Multi-antenna receiver tracks all observable satellites utilizing DAS beamformer.
Mode 4	LOS and multipath scenario is assumed. Multi-antenna receiver tracks all observable satellites utilizing MPDR beamformer.
Mode 5	LOS and multipath scenario is assumed. Multi-antenna receiver tracks all observable satellites utilizing MPDRSS beamformer with spatial smoothing process.

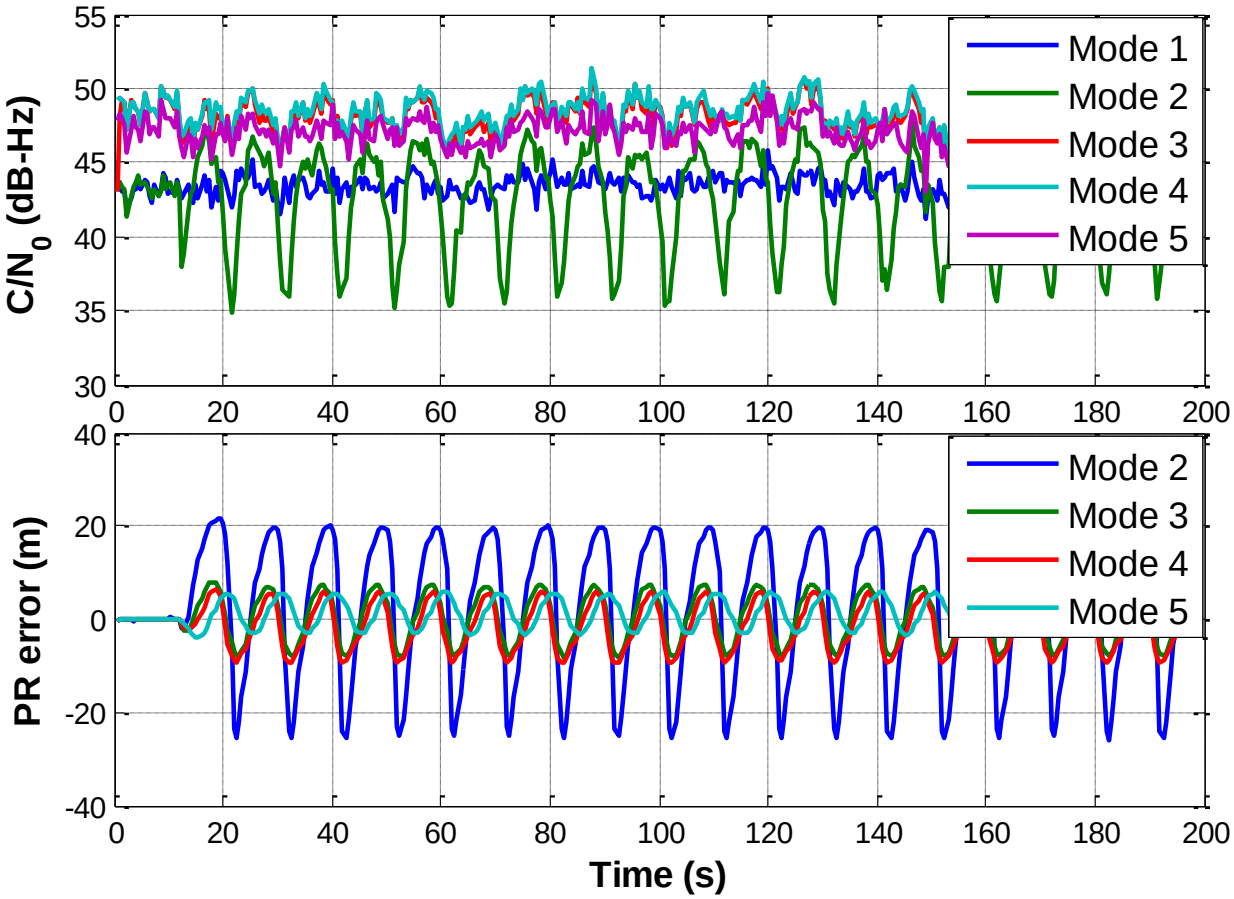

Figure 4-6: C/N_0 values and pseudorange errors for PRN 6

Comparisons of C/N_0 and pseudorange RMS errors for all of the PRNs before and after beamforming are shown in Figure 4-7. It is observed that the average C/N_0 gain for all the satellites is the same for each beamformer. The gain obtained using the MPDR beamformer with spatial smoothing is lower than that of the other two due to the lower number of elements used in the beamforming process. The pseudorange error reduction is different for different PRNs. The MPDR beamformer with spatial smoothing provides better attenuation of multipath signals than the other two. For all three beamformers, it can be observed that, for very low elevation satellites (< 15˚) such as PRN 10, 25 and 31, the pseudorange error reduction is minimal compared to that of satellites located at a

higher elevation. This occurs because the signals decorrelation depends on the angle of arrival of the LOS and multipath signals. Since decorrelation has a direct impact on the performance of beamformer, the attenuation of the multipath signals by the beamformer also depends on the direction of arrival of the signals. Considering Figure 4-7b, DAS and MPDR beamformers can reduce multipath errors by 2 to 8 m, whereas the MPDRSS beamformer can reduce up to 13 m. The MPDRSS multipath reduction performance is much better than other techniques for all PRNs.

It can also be observed in Figure 4-7 that for lower elevation satellites, the double delta correlator performance is better than array processing techniques. However, for higher elevation satellites (> 20˚), the double delta correlator and MPDRSS performance is similar. In this research, beamforming techniques are implemented using narrow correlators. However, beamforming techniques can be implemented with any correlator architecture, including double delta. Even though the double delta correlator is not considered here in the beamforming, multipath mitigation performance in this case should improve after beamforming, compared to the single antenna approach. The multi-antenna receiver architecture considered here can be extended to incorporate other correlators.

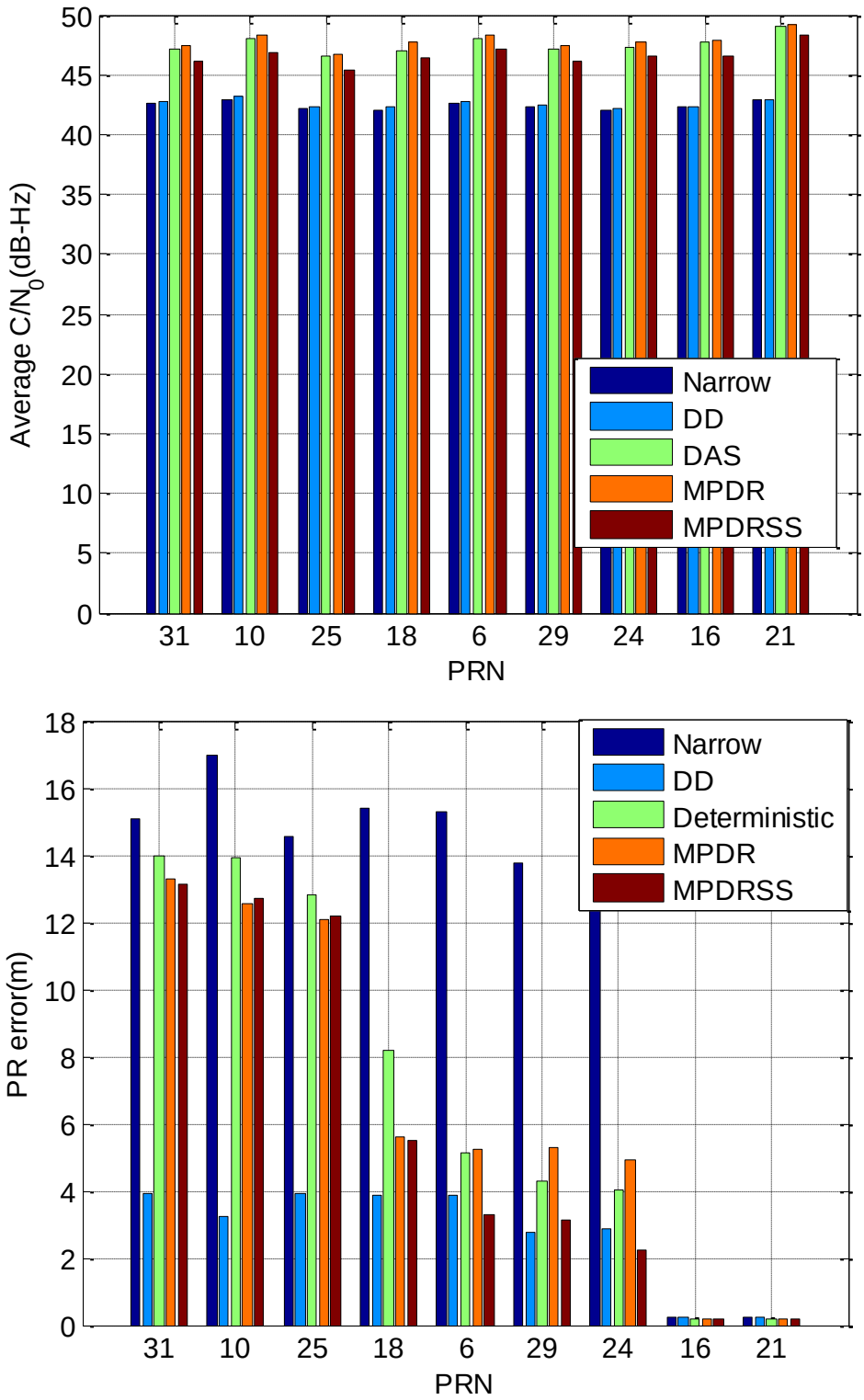

Figure 4-7: C/N$_0$ and pseudorange error performance comparison before and after beamforming

Performance values of beamforming techniques for carrier phase multipath mitigation are shown in Figure 4-8. “Before beamforming” refers to the tracking results obtained using baseband samples from the reference antenna (using narrow correlator). Array processing techniques are able to mitigate carrier phase multipath and greater reductions are observed for higher elevation satellites. For very low elevation satellites, the carrier phase measurements are further distorted by the array processing techniques which could be due to the higher correlation between LOS and multipath. However, for higher elevation satellites, carrier phase multipath can be significantly reduced.

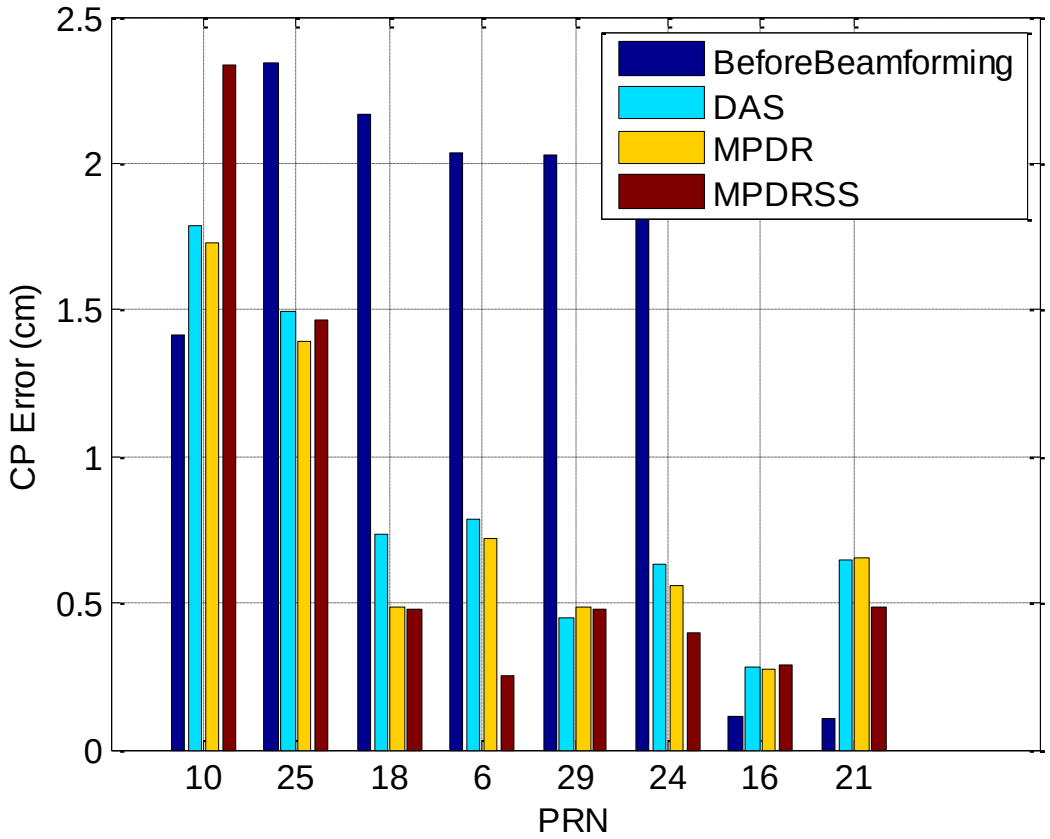

Figure 4-8: Carrier phase multipath error before and after beamforming

4.6 Field-test results

GPS data was collected in moderate specular multipath conditions. The location was chosen such that both LOS and multipath signals were observable with LOS being stronger than multipath signals. The setup, shown in Figure 4-9, consisted of six NovAtel 501 antennas (Novatel GPS Antenna Model 501) arranged in a rectangular fashion. These antennas have a diameter of 11.4 cm. Due to this physical limitation, the distance between antenna elements in the array configuration cannot be smaller than 11.4 cm. The array was mounted on a wooden platform on one end of the platform and a Novatel SPAN^{TM} LCI inertial system on the other end to provide platform attitude. Signals from the antenna array were collected using a Fraunhofer multiple RF front-end, which can collect digital samples from all the antennas simultaneously. The location of the data collection and the corresponding sky plot are shown in Figure 4-9. The glass building on the east side of the location acts as a specular reflector to generate multipath signals for the low elevation satellites visible in the west direction. Most of the satellites on the east side of data collection point were blocked by the building.

In order to perform array calibration, another data set was collected in open sky conditions with minimal multipath effect. The tracking architecture described in Figure 4-5 excluding the beamforming process was used to obtain the prompt correlation values to perform calibration. Carrier and code were tracked by the reference antenna and the replica signals generated from reference antenna were passed to the carrier and code tracking loops of the other antennas. The Doppler and code replica signals obtained after tracking the reference antenna signal were used to track other antenna signals to obtain relative signal amplitude and phase between different antennas. The prompt correlator values of

all the antennas were used to construct the steering vector, which is referred to as the measured steering vector. Based on the known attitude of the array and DOA of the satellite, the true steering vector was computed. A least squares based calibration method (Backén et al 2008) was used to compute the calibration matrix. As the number of visible satellites were larger than the number of antenna elements, very low elevation satellites were excluded from the calibration to avoid calibration errors due to multipath.

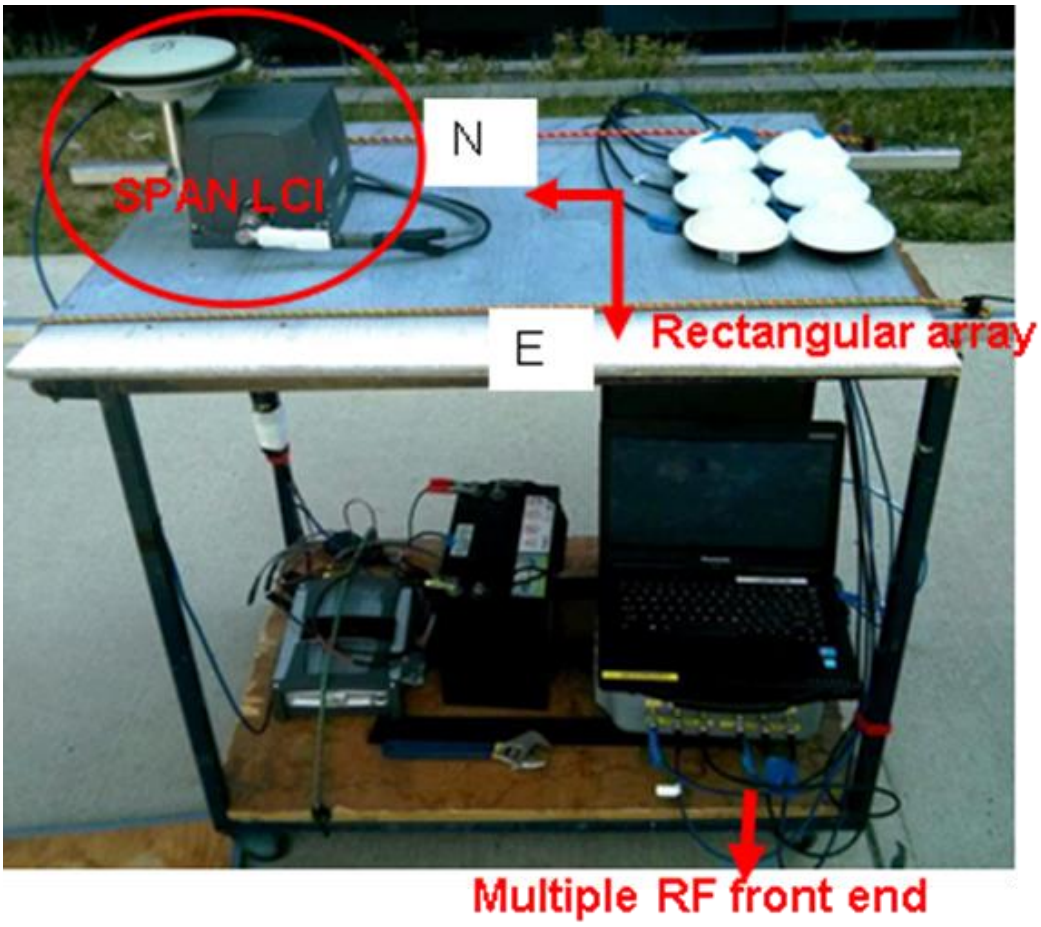

(a)

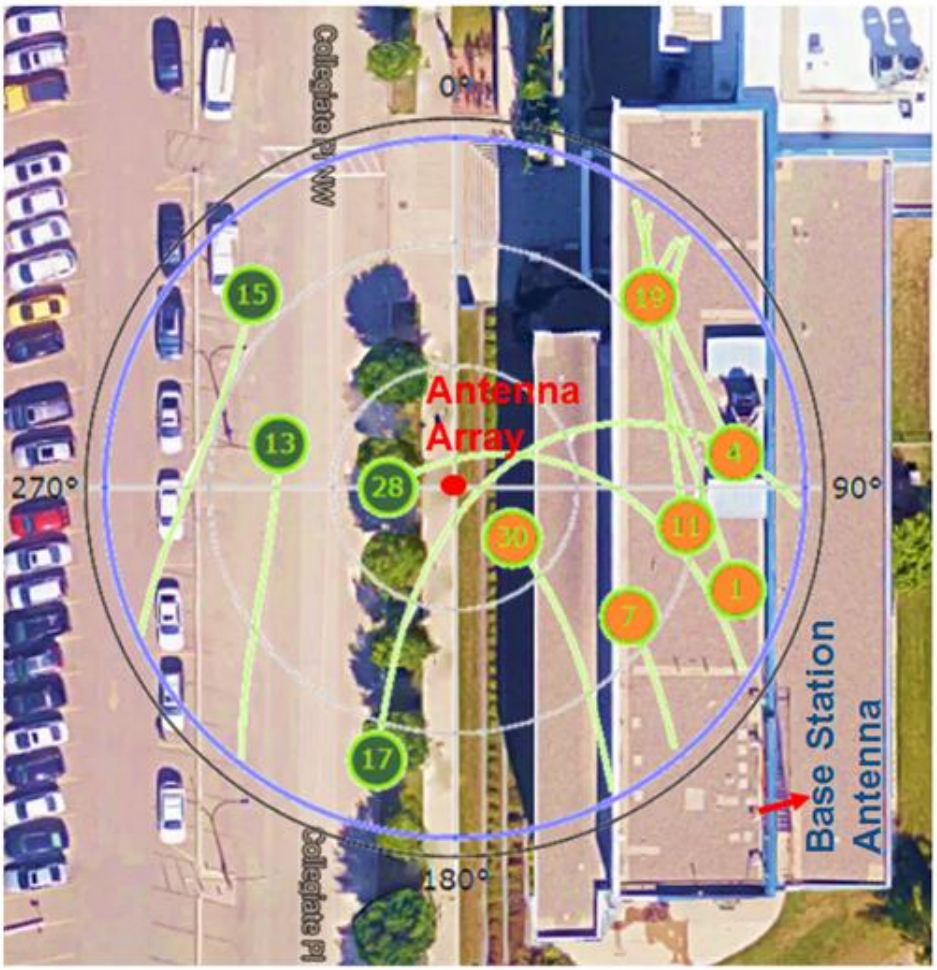

(b)

Figure 4-9: (a) Field data collection setup showing antenna array and data collection system and (b) Location of data collection with sky plot

Analysis results of Figure 4-10 show that some of the satellite signals were perturbed by multipath signals. An independent variation of C/N_0 values from different antenna elements confirms the existence of multipath (Brown 2000). The C/N_0 values obtained using GSNRx^{TM} for PRN 28 and 17 for different antenna elements are shown in Figure 4-10; PRN 28 is at a high elevation and PRN 17 at a low elevation. The rapid C/N_0 variations of PRN 28 at all the antennas are comparable to each other and are due to noise. PRN

17, which is affected by multipath, shows different C/N_0 periodic variations, indicating reception of different multipath signal phases at different antenna elements. For PRN28, the mean C/N_0 value is different for different antennas. These differences are due to the gain patterns of different antenna elements and will be corrected in the calibration process.

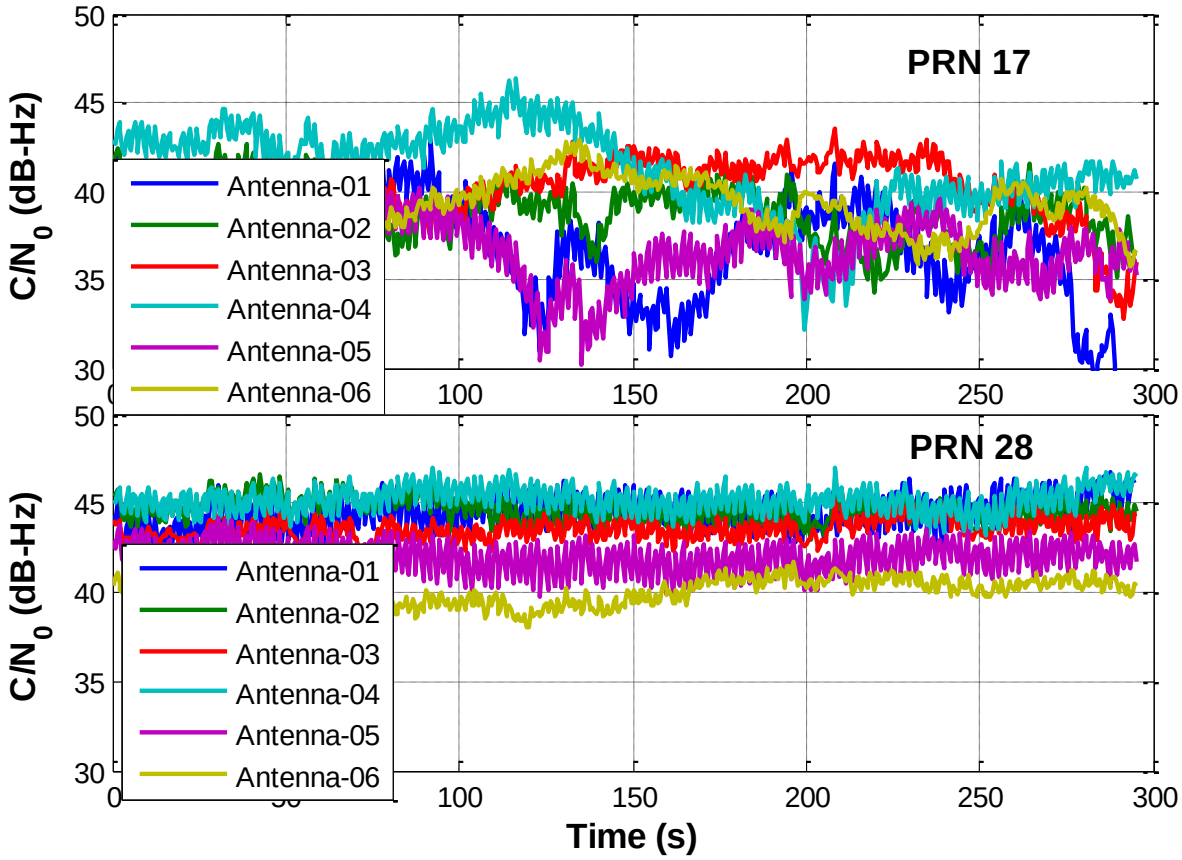

Figure 4-10: C/N_0 variations of PRN 17 and PRN 28 for different antenna array elements

The second analysis performed shows the improvement in C/N_0 values and pseudorange error reduction after the beamforming process. A modified multi-antenna software receiver was used for this analysis. The C/N_0 values before and after beamforming were computed for different PRNs and the results are shown in Figure 4-11a. "C/N_0 before

beamforming" refers to the C/N_0 values computed from the reference antenna signal using narrow correlator. Considering PRN 17, which is affected by multipath, the variations are reduced after combining signals from all antenna elements through beamforming and 4 to 8 dB improvement is obtained. All three beamformers are able to reduce C/N_0 variations.

To evaluate the pseudorange multipath error reduction, a closely spaced base station with known position was used. A NovAtel Propak receiver was used to collect data at the base station. By using the ephemeris information and the user position, the true range could be computed for each PRN. The pseudorange is the sum of true range and other errors such as ionospheric, tropospheric and satellite clock errors, multipath and measurement noise. Assuming no significant multipath errors are affecting the base station, differences between pseudorange and true range provide combined measurement errors as seen by the base station antenna. Similarly, the approximate remote receiver position can be obtained using SPAN^{TM} LCI unit with an accuracy of few centimetres. Here, "remote receiver" refers to the referece antenna of the antenna array. Using the approximate antenna position and ephemeris information, the true range can be obtained. By taking the difference between pseudorange and the true range, the combined measurement errors as seen by the remote station can also be obtained. As the base station and remote receiver were nearby, the differences between the pseudorange measurements cancel out all the errors except multipath, user clock biases and measurement noise. Pseudorange measurement noise was computed previously using zero-baseline testing and its standard deviation was 4 cm for both GSNRx and Novatel receivers. Therefore, by taking the differences between base and remote

receiver, the measurement noise of pseudorange will increase by up to 6 cm. However, compared to the magnitude of multipath errors at the few metre level, it can be neglected. As user clock biases are common for all the PRNs, performing double difference between PRNs should remove them. To perform double differencing, PRN 28, which is not affected significantly by multipath, was used as the reference satellite. The multipath errors for PRN 13,15 and 17 before and after beamforming are shown in Figure 4-11b. Consider data between 80 and 100 seconds for analysis; the C/N_0 degradation for antenna 1 (reference antenna) is significant in this time interval and a similar degradation can be observed with pseudorange errors. The beamformer is able to mitigate multipath and the RMS pseudorange error has decreased from 20 m to 0.8 m after beamforming using all the three beamformers. The RMS pseudorange error for PRN 17 considering the entire data set has decreased from 9 m to 0.9 m after beamforming. The RMS pseudornage errors for different PRNs for different beamforming techniques are shown in Table 4-3. Beamformer performance is different for different PRNs. This is due to different satellite DOAs and multipath signals as mentioned in the numerical simulation section.

Performance of field test results is more realistic than that of simulation. Considering PRN17 which is affected by multipath, the performance of the DAS beamformer depends only on the LOS signal's DOA. If the multipath signal direction coincides with one of the beampattern's nulls obtained from the DAS beamformer, it can significantly reduce the multipath effects. This was observed with PRN 17 in which case the DAS beamformer was able to reduce multipath error by 8 m. Similar performance of MPDR and MPDRSS are likely due to the sufficient decorrelation between the LOS and multipath signals over one second integration considered to compute the covariance matrix. Also, as shown in

Figure 3, for lower elevation satellites with sufficient decorrelation between LOS and multipath signals, performance indicators of the MPDR and MPDRSS beamformer are similar.

Table 4-3: RMS pseudorange errors before and after beamforming

PRN	RMS pseudorange errors (m)			
	Before beamforming (narrow correlator)	DAS	MPDR	MPDRSS
PRN 13	4.2	1.9	1.0	0.9
PRN 15	2.1	1.3	1.3	1.8
PRN 17	8.9	0.9	1.2	1.2

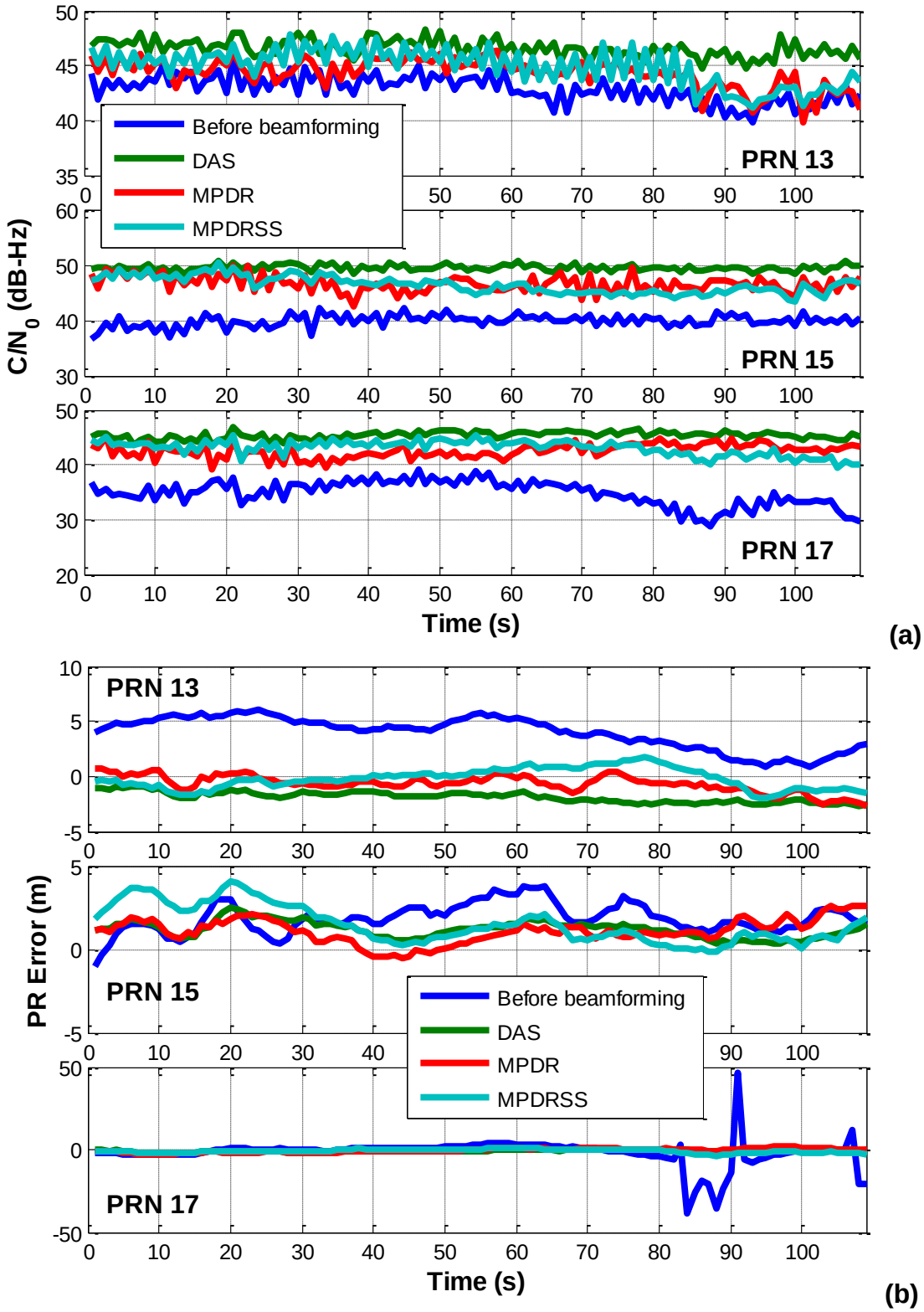

Figure 4-11: (a) C/N$_0$ and (b) Pseudorange errors before and after beamforming

The third analysis is performed to show the position improvement before and after beamforming. The least squares method was used to compute the position from pseudorange measurements. Four observable satellites, shown in green circles in Figure 4-9b, were used. Position solutions computed using pseudorange measurements generated from the reference antenna are referred to as the position solutions before beamforming. Similarly, position solutions computed using the pseudorange measurements after beamforming are referred to as the position solutions after beamforming. The reference position of the antenna array was computed using the outputs of the SPAN^{TM} LCI unit, which provides ultra-tight GNSS-INS solutions with accuracy of the order of few decimetres or better. Using the reference antenna array position, position errors before and after beamforming were computed and are shown in Figure 4-12. As only four satellites were visible, Position Dilution of Precision (PDOP) is of the order of 10. As shown after beamforming, the position errors are significantly reduced. The RMS position errors before and after beamforming are provided in Table 4-4.

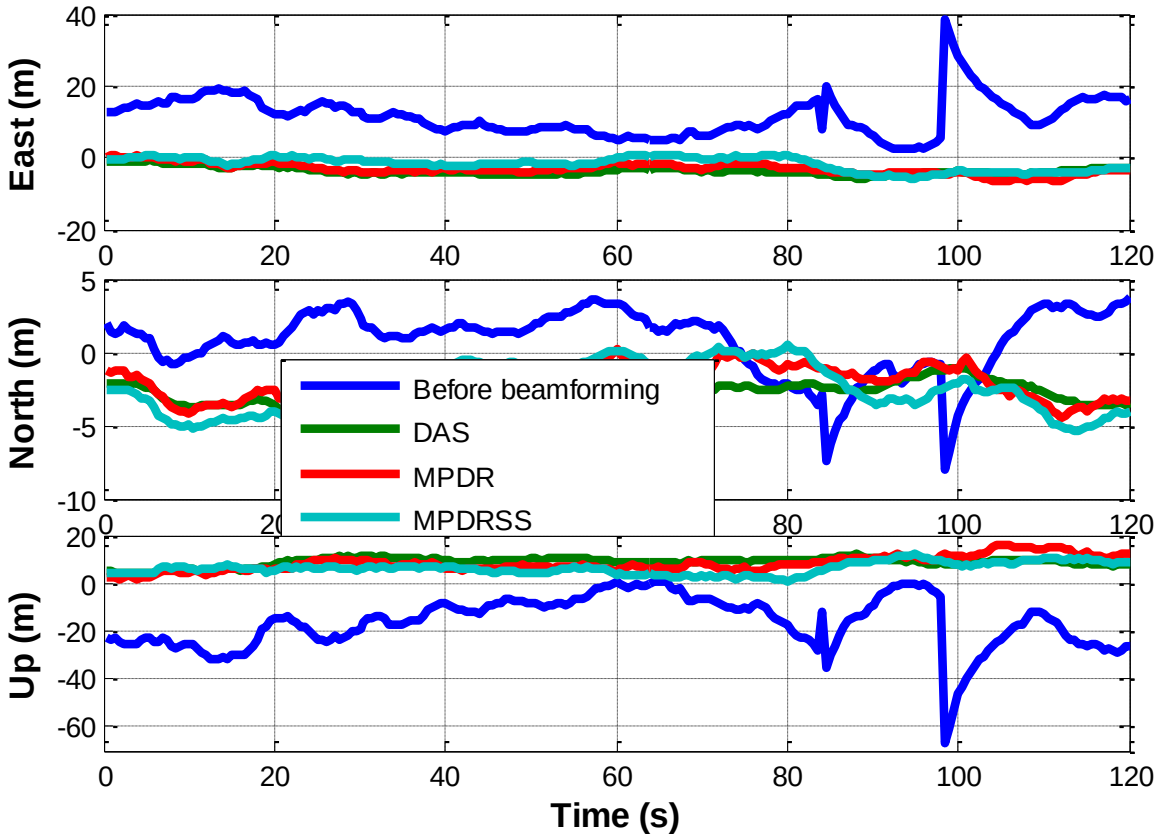

Figure 4-12: Position errors before and after beamforming

Table 4-4: RMS position errors before and after beamforming

RMS Position Errors	East (m)	North (m)	Up (m)
Before beamforming (narrow correlator)	12.7	2.2	19.5
DAS	3.8	3.5	9.0
MPDR	3.5	2.9	8.8
MPDRSS	3.5	2.9	8.8

4.7 Summary

In this chapter, multipath mitigation performance of different beamforming techniques namely DAS, MPDR and MPDRSS was evaluated and compared with single antenna techniques. The numerical simulation results show that the performance of MPDR and MPDRSS beamformers improves as the correlation between LOS and multipath signals decreases. It was observed that, for a rectangular array with six antenna elements, the MPDRSS beamformer provides better multipath mitigation for higher elevation satellites. Using the simulated GPS signals, pseudorange errors can be reduced by tens of metres in high multipath environments, thereby improving position accuracy. It was observed that the MPDRSS beamformer performs better than the MPDR and DAS beamformer. With actual GPS L1 signals collected in a moderate specular multipath scenario, a reduction of 10 m in RMS pseudorange error was observed for satellites affected by multipath signals. Pseudorange error reduction was reflected in the position solutions, with easting errors reduced by 8 m and height errors reduced by 10 m, based on the data set utilized. Finally, it was shown that a six-antenna rectangular array is effective to mitigate short-range multipath signals and provide an improved navigation solution, based on the data used in the analysis. Extensive testing would be required to confirm the magnitude of these enhancements in different environments.

Chapter Five: GNSS ANTENNA ARRAY CALIBRATION IN MULTIPATH ENVIRONMENTS

5.1 Introduction

Antenna array calibration is the first step towards implementation of any beamforming or null steering technique that uses signal DOA. Due to antenna gain/phase mismatches and mutual coupling, the signals received from different antenna elements undergo additional phase shifts (Konovaltsev et al 2010). The other factors, which affect the gain/phase characteristics of the antenna elements are antenna phase centre variations, RF front-end delays, perturbation of antenna element positions and uneven cable lengths (Daneshmand et al 2014, Anantharamu et al 2012, De Lorenzo et al 2011). The calibration process estimates these additional gain and phase uncertainties.

Traditional calibration techniques are conducted in anechoic chambers where signals are transmitted from known predefined directions. This process requires dedicated and expensive test setups. In GNSS applications, array calibration can be performed using live signals as satellite positions are known precisely and signals from different directions are available. Array calibration using live signals and associated challenges are discussed in Daneshmand et al (2014) and Backén et al (2008). For calibration using live signals, it is assumed that received signals are not affected by multipath components. However, the possibility of having multipath signals in the calibration dataset exists. Calibration process is a challenging problem in multipath scenario, which can introduce significant gain and phase errors in the calibration parameters. These are estimated using the relative gain and phase measurements between the antenna elements. As multipath

distorts these relative gain and phase measurements, the estimated calibration parameters will be erroneous. Several techniques based on maximum likelihood estimation have been analyzed for sensor array calibration in multipath environments for non-GNSS applications (e.g. Bu-hong 2004, Leshem et al 2000). However, these methods are not applicable to GNSS due to their implementation complexity and practicability.

The effect of multipath on carrier phase measurements was studied by Ray et al (1999) and it was demonstrated that it is periodic in nature with zero mean in specular multipath environments. The periodicity of multipath depends on the frequency differences between direct and multipath signals. The received phase and frequency of a multipath signal are highly dependent on the location of the reflector (Ray et al 1999). The zero mean periodic characteristic of carrier phase multipath can be exploited to reduce its effect on the calibration process. By observing signals from different antenna elements over the multipath period, one can average out the error. The carrier phase multipath error is correlated to carrier-to-noise ratio (C/N_0) variations and its period is the time interval from one C/N_0 null to the next one. By observing C/N_0 variations, one can determine the number of samples required for averaging in order to decrease the effect.

The performance of array calibration is analyzed herein using simulated and live GPS signals. The multi-antenna GNSS signal simulator described in Chapter 3 is used to generate GPS signals affected by multipath. The simulated signals are processed using the multi-antenna GPS software receiver described earlier to generate correlation values, which are then used in the calibration algorithm. Simulation results are validated using actual GNSS signals collected in specular multipath conditions using a multi-channel RF

front-end. The effect of averaging carrier phase measurements over several multipath cycles is demonstrated through reduction in DOA estimation errors.

5.2 Methodology

This section discusses the signal and system model and multi-antenna signal processing method to compute calibration parameters.

5.2.1 Signal and system model

For an *M*×*N* antenna array, the complex baseband signal vector consisting of measured phases and amplitudes at different antennas from i^{th} satellite can be represented as

$$\mathbf{x}_i = \mathbf{C}\mathbf{a}_i \tag{5-1}$$

where $\mathbf{x}_i$ is a *MN*×1 vector. The matrix $\mathbf{C}$ is the calibration matrix with size *MN*×*MN* containing phase and gain uncertainties across the antenna elements and mutual coupling. The steering vector of the satellite signal is denoted as $\mathbf{a}$ with *MN*×1 dimension and is given by

$$\mathbf{a}_i = \begin{bmatrix} e^{j\frac{2\pi}{\lambda}(\mathbf{e}_i^B)^T \mathbf{p}_{11}} \\ e^{j\frac{2\pi}{\lambda}(\mathbf{e}_i^B)^T \mathbf{p}_{12}} \\ \cdots \\ e^{j\frac{2\pi}{\lambda}(\mathbf{e}_i^B)^T \mathbf{p}_{MN}} \end{bmatrix} \tag{5-2}$$

where λ is the wavelength of the signal, $\mathbf{p}_{mn}$ is the *(m,n)*th antenna element position in the body coordinate frame and is a 3×1 vector. $\mathbf{e}_i^B$ is a 3×1 unit vector pointing to the i^{th} satellite in the body coordinate frame. A least squares approach can be used to estimate the calibration matrix by observing signals from satellites coming from different directions.

Let L be the number of satellites from which relative gain and phase measurements are available. It is assumed that $L > MN$. Assume that from all satellite measurements can be represented by the MNxL matrix as

$$\mathbf{X} = \left[\mathbf{x}_1 \;\; \mathbf{x}_2 \;\; ... \;\; \mathbf{x}_L\right] \tag{5-3}$$

Equation 5-1 can be written as

$$\mathbf{X} = \mathbf{CA} \tag{5-4}$$

where $\mathbf{A}$ is the steering vector matrix from all the satellites and is given by

$$\mathbf{A} = \left[\mathbf{a}_1 \;\; \mathbf{a}_2 \;\; ... \;\; \mathbf{a}_L\right] \tag{5-5}$$

The least squares solution of $\mathbf{C}$ is

$$\mathbf{C} = \mathbf{X}\mathbf{A}^H\left(\mathbf{A}\mathbf{A}^H\right)^{-1} \tag{5-6}$$

5.2.2 Multi-antenna signal tracking methodology for calibration

The multi-antenna software receiver developed in Chapter 3 was used with the tracking architecture (Anantharamu et al 2012) shown in Figure 5-1. One of the antenna elements in the array acts as the reference antenna. Satellite signals were acquired and tracked using the IF signals collected at the reference antenna. The Doppler and code delays thus obtained were used to despread the signals from other antennas so that relative phase values between the antenna elements were maintained. The correlation values were normalized with respect to the reference antenna. The C/N_0 estimator method described in Chapter 2 was also implemented (Dierendonck 1996).

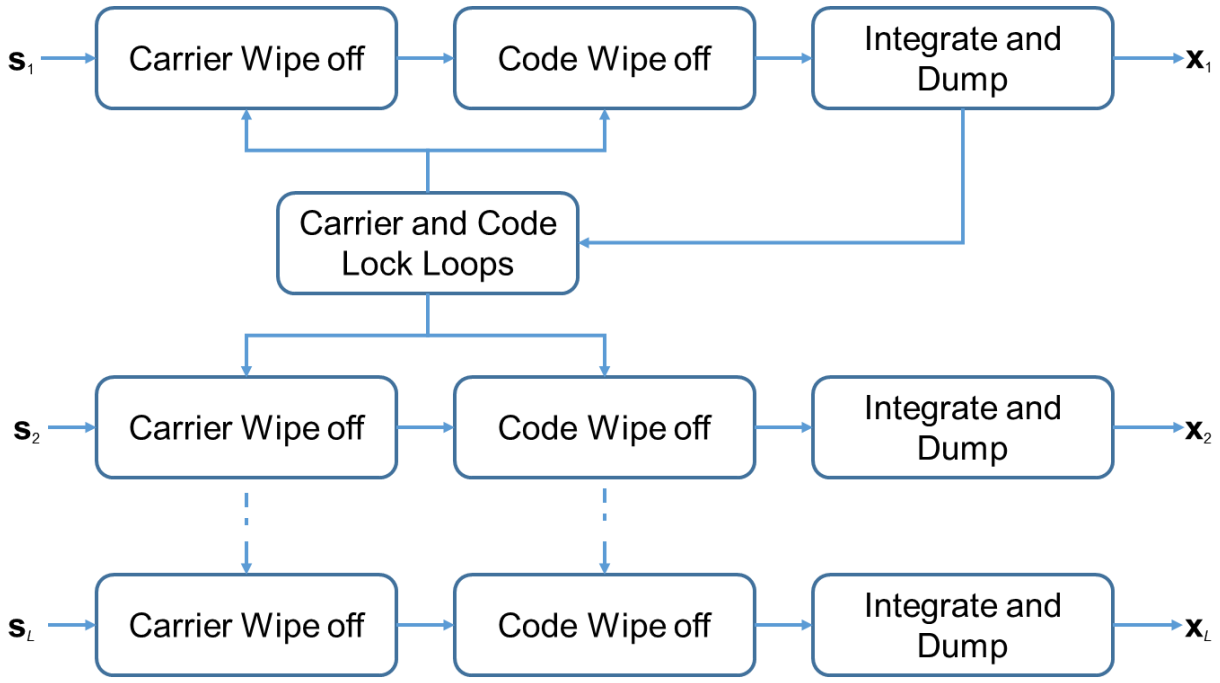

Figure 5-1: Multi-antenna GNSS signal tracking methodology

To reduce the multipath effect on calibration parameters the relative phase measurements between antenna elements are averaged over several multipath periods. Since there is a high correlation between C/N_0 variation and multipath period, the multipath period is calculated by monitoring C/N_0 variation. The averaging period should meet channel coherence time as well. Here, channel coherence time refers to the time for which relative phase measurements are time invariant.

5.3 Simulation results

The receiver was moving in linear fashion with a constant speed of 0.5 m/s. The errors due to atmosphere and multipath were disabled while collecting IF data samples from the hardware simulator. The IF samples were used by the multi-antenna software simulator

to generate multi-antenna signals. Multipath signals were also simulated through the software multipath simulator and their effects on antenna array calibration were analyzed. A constellation of seven GPS satellites was simulated and the corresponding sky plot is shown in Figure 5-2.

A rectangular antenna array of 3x2 elements was considered in the simulation. As multipath effect on calibration is studied in this research, it is assumed that the antenna elements are identical with isotropic radiation pattern having no mutual coupling among them. In the simulated calibration matrix, it is assumed that gain is the same across antenna elements and only phase variations are considered. It is also assumed that phase variations are independent of the directions of arrival of the signals. A complex normal distribution is used to generate the phase mismatches between the antenna elements, and captured in the calibration matrix. GPS data is simulated in two different conditions as described in Table 5-1.

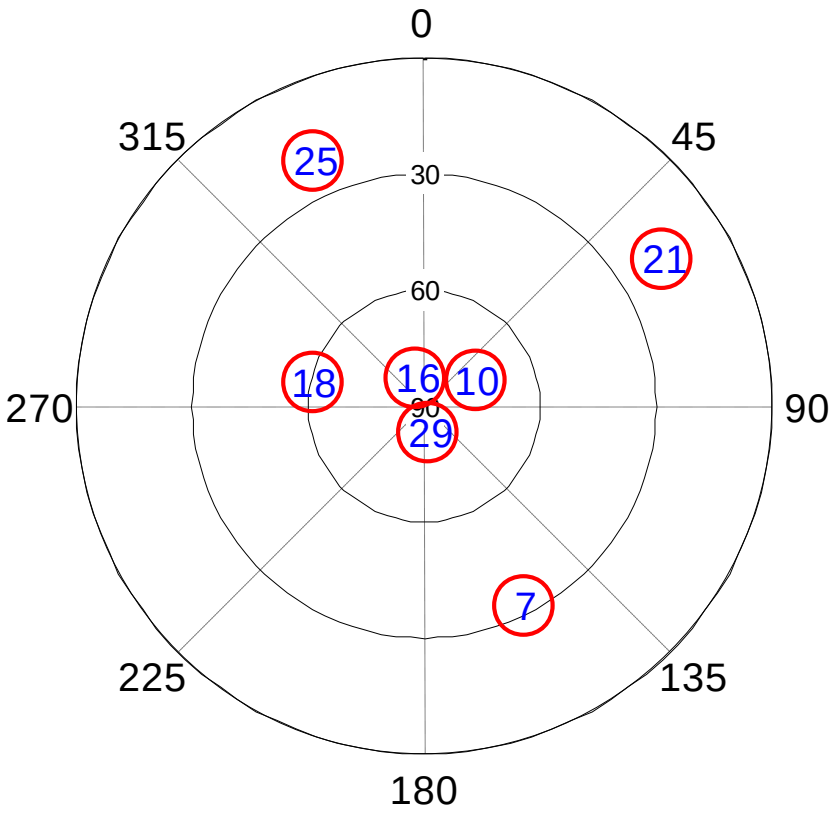

Figure 5-2: Sky plot for multi-antenna GPS signal simulation

Table 5-1: Description of GPS data simulations

Dataset	Description of the simulation environment
Dataset S1	Open sky conditions with no multipath for any of the satellites.
Dataset S2	Multipath condition with PRN 21 observing specular multipath reflections.

For Dataset S2, the reflector is placed such that PRN 21 is affected by multipath while the others are not. The reflector is kept at a distance of 30 m from the user. Reflectors are assumed to have smooth surfaces and provide specular reflections. The amplitude of the multipath signal is attenuated by 3 dB as compared to the direct signal. Based on the

user motion profile, a Doppler difference of 2 Hz is observed between LOS and multipath signals.

The simulated multi-antenna IF samples are processed using the multi-antenna tracking architecture shown in Figure 5-1 to generate prompt in-phase and quadrature-phase tracking values for all visible satellites and all antennas. The correlation outputs were generated using 20 ms coherent integration time. As Doppler and code phase estimates from the reference antenna were used to despread signals from other antennas, the measured phase from the correlation values for the reference antenna is zero (plus tracking loop noise). The measured phase values from the other antenna elements provide the relative phase differences between the antenna elements, which represent the steering vector perturbed by the calibration matrix. PRN 21, which is affected by multipath, is considered for analysis.

The measured relative phases between the antenna elements for Dataset S1 are shown in Figure 5-3(a). It is observed that the relative phase remains constant over time. The C/N_0 from the reference antenna of the array is shown in Figure 5-3(b) and is constant over time. An histogram of Antenna 5 phase values (using 5 s of data) is shown in Figure 5-3(c). Similar observations can be made with other antenna phase measurements.

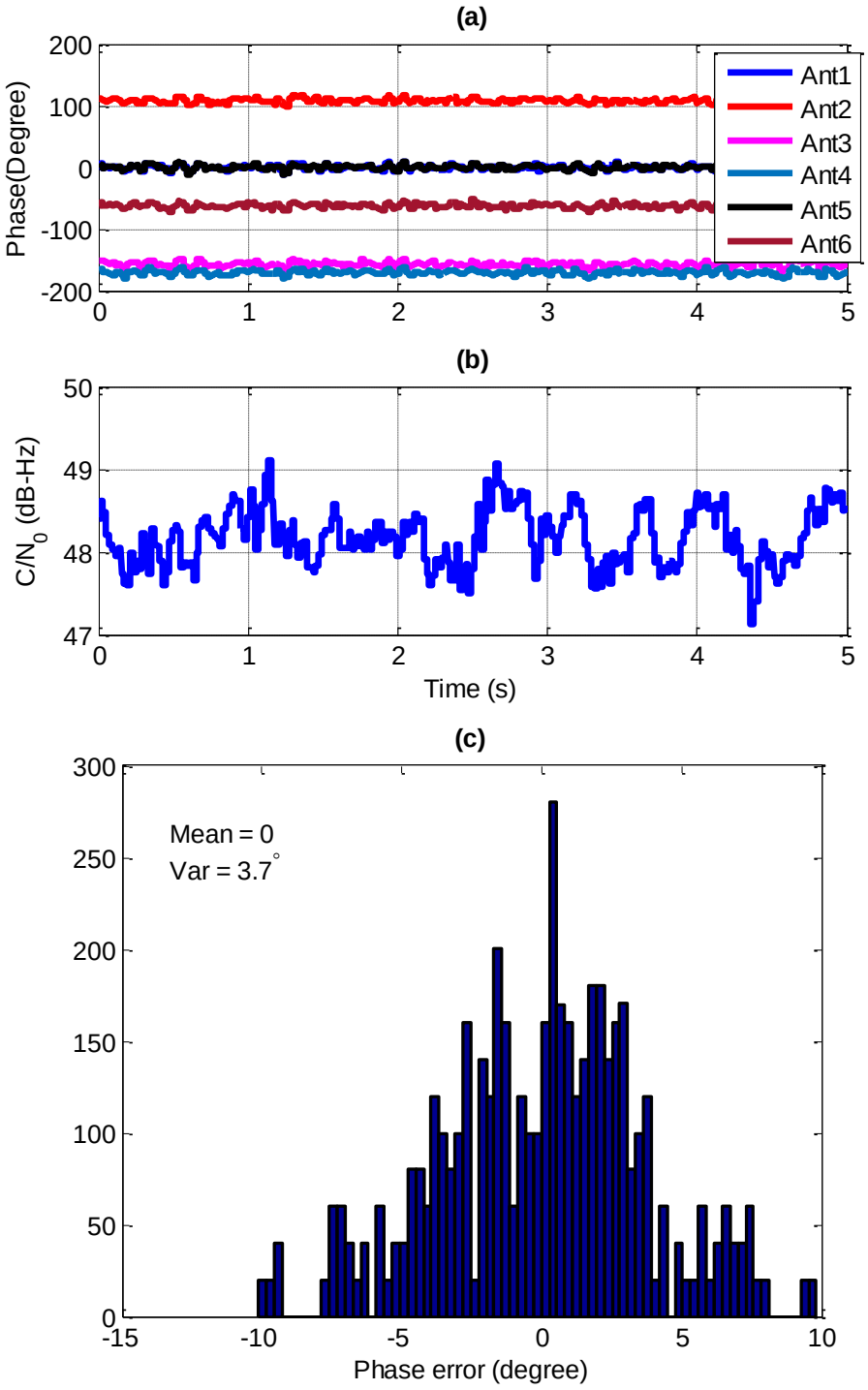

Figure 5-3: PRN 21 Results for multipath free case: (a) Measured relative phases between antenna elements, (b) C/N$_0$ of array reference antenna (c) Histogram of the phase values of Antenna 5

The relative phases between the antenna elements for Dataset S2 are shown in Figure 5-4(a). Due to constructive and destructive multipath, the relative phases vary periodically. In Figure 5-4(a), measured phases (from the correlator outputs) are shown as MSR and correct phases are shown as CRC. Correct phases (CRC) are computed using the known satellite DOA and calibration matrix. It can be observed that during multipath, the phase values fluctuate with respect to the true values. Similar periodic C/N_0 variations can be observed as shown in Figure 5-4(b). The variation periodicity depends on the Doppler difference between LOS and multipath and in this case, it is nearly 0.5 seconds. The periodicity of the phase variations corresponds to that of C/N_0 variations. The mean of the measured phases over several multipath periods corresponds to the true value observed in Figure 5-4(a). This can be seen through the histogram of the phase values (using 5 s of data) of Antenna 5 shown in Figure 5-4(c), where the mean is near zero and the variance has increased due to multipath. Therefore, by averaging the phase measurements over several multipath cycles, one can improve relative phase estimation.

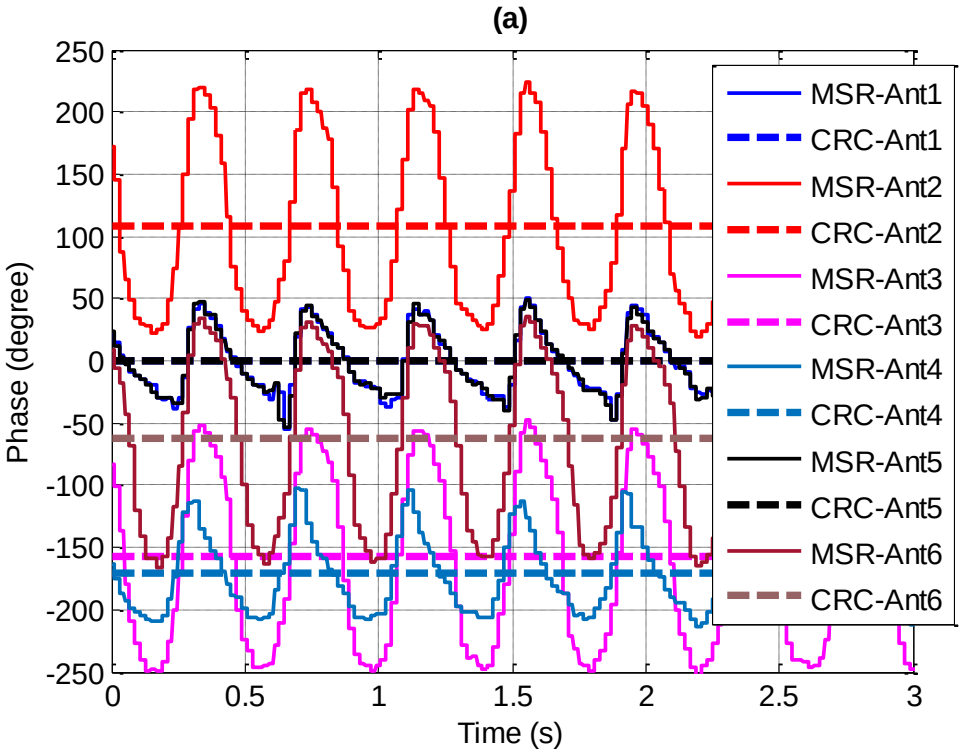
(a)
Phase (degree)
Time (s)
MSR-Ant1
CRC-Ant1
MSR-Ant2
CRC-Ant2
MSR-Ant3
CRC-Ant3
MSR-Ant4
CRC-Ant4
MSR-Ant5
CRC-Ant5
MSR-Ant6
CRC-Ant6

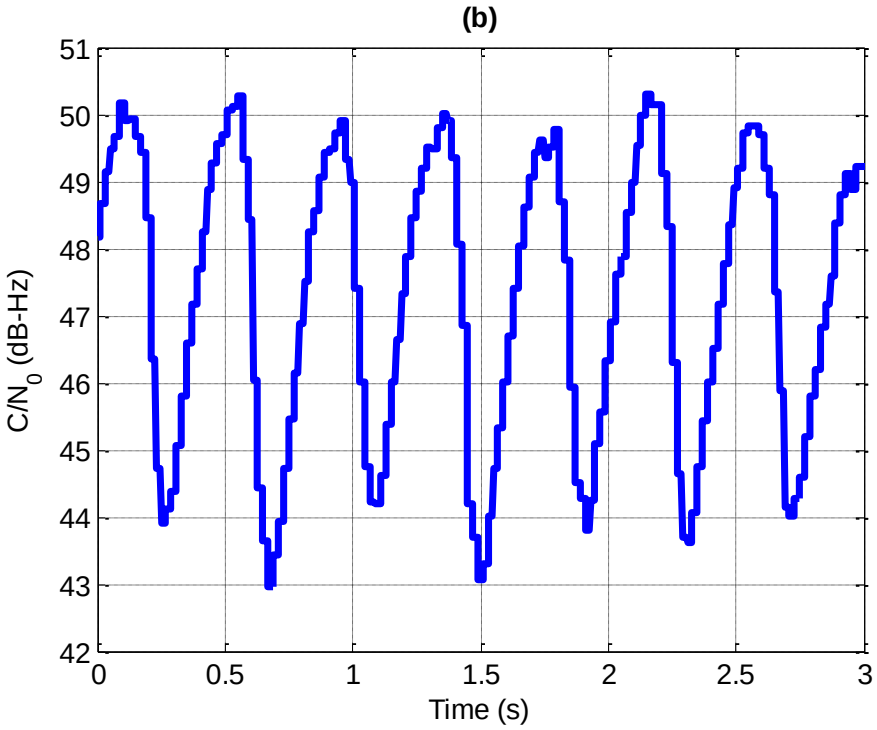
(b)
C/N0 (dB-Hz)
Time (s)

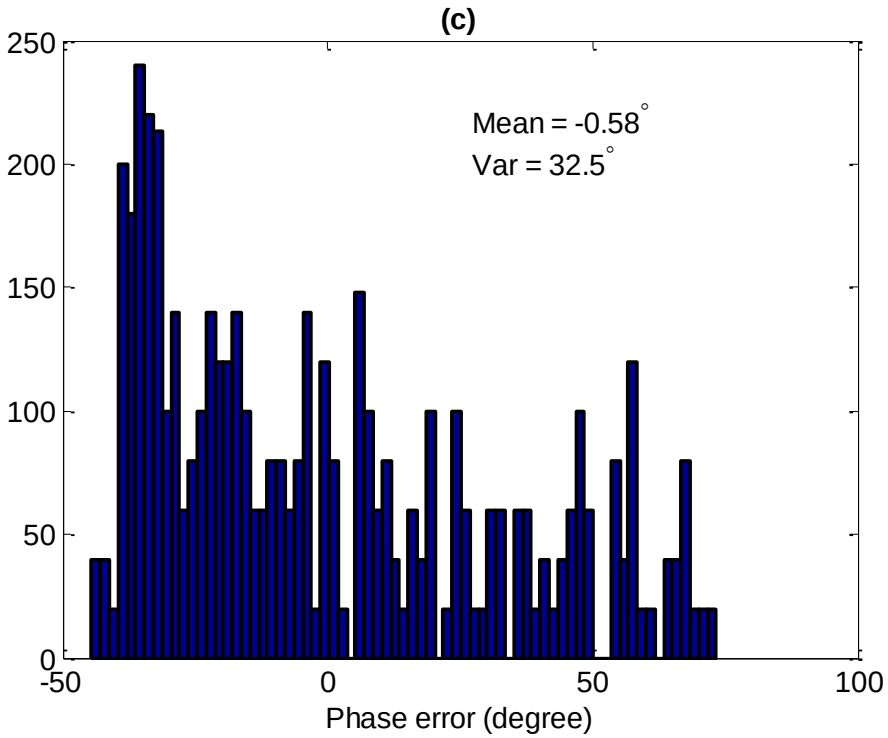

Figure 5-4: PRN 21 results for multipath case: (a) Measured relative phases between antenna elements [MSR – measured phase, CRC – correct phase], (b) C/N0 of array reference antenna (c) Histogram of Antenna 5 phase values

In order to evaluate the effect of multipath on calibration, Dataset S2 is considered. The calibration was performed using least squares and all seven satellites were used in the computation. Calibration parameters were estimated in two different ways. First, the calibration vector was obtained by choosing measured phases for an arbitrary time sample. In order to show the error induced by multipath on calibration, time instant where phase variations are the largest is considered. Let this calibration matrix be C1. The second calibration matrix is obtained by using the averaged phase measurements from each of the satellites. The averaging is done over several multipath periods of PRN 21.

Let this calibration matrix be C2. Here, averaging is performed over 5 seconds to remove the multipath effect.

The computed calibration matrices C1 and C2 were evaluated by performing DAS beamforming (Van Trees 2002) on one of the PRNs. Here, PRN 25 is considered because it is not affected by multipath. The beam patterns from conventional beamforming using calibration matrices C1 and C2 are shown in Figure 5-5. It can be observed that using C1 without averaging, the array main beampattern is displaced from the direction of arrival of the satellite signal. However, with averaging, the beampattern has maximum gain in the direction of the satellite. The true direction of the satellite is indicated with '**+**' marks on the array pattern plots. This indicates that averaging the phase measurements in multipath environments provides better estimation of the calibration parameters.

In the above analysis only one satellite affected by multipath was considered. However, it can be shown that averaging the phase measurements with multiple satellites affected by multipath improves estimation of calibration parameters. Averaging the phase measurements should improve the calibration, which is validated in the next section through actual measurements.

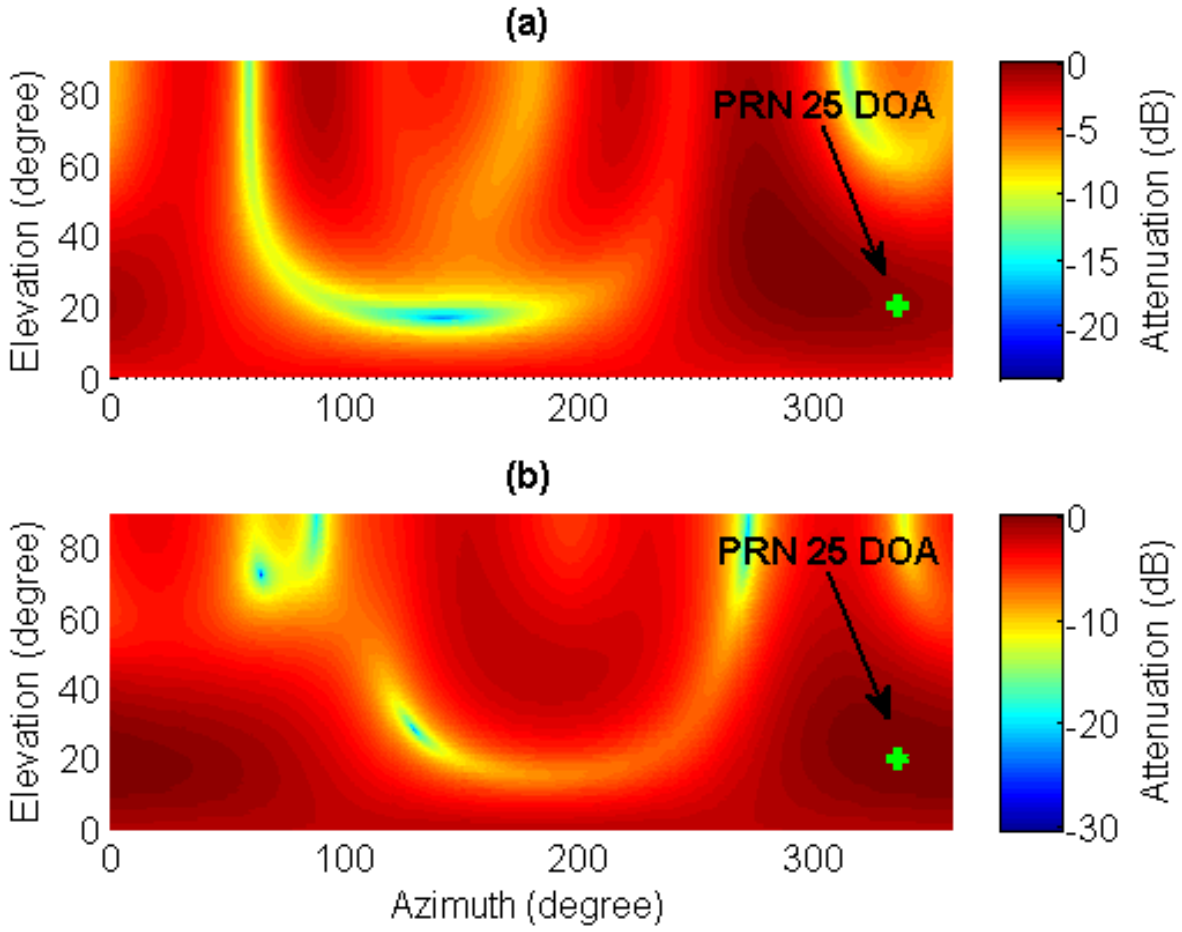

Figure 5-5: Array patterns for PRN 25: (a) Calibration matrix is estimated without averaging phase measurements (Calibration matrix C1); (b) Calibration matrix is estimated after averaging phase measurements (Calibration matrix C2)

5.4 Field-test tesults

This section describes the data collection environment and results. A six-element rectangular antenna array was assembled using Novatel 501 antennas as shown in Figure 5-6(a). The distance between the antenna elements is 0.11 m. The antenna array is mounted on a wooden platform on a vehicle. Baseband samples were collected at the antenna elements using a Fraunhofer RF front-end, which can collect data from all channels simultaneously. In order to obtain the attitude of the array and the reference

trajectory, a NovAtel Synchronous Position, Attitude and Navigation (SPAN)^{TM} LCI, which includes a NovAtel SPAN® enabled GNSS/INS receiver (SPAN SE) and a tactical grade Inertial Measurement Unit (IMU) LCI, was mounted on the same platform as that of the antenna array. One of the antenna elements of the array was chosen as a reference antenna to serve as origin of the body frame coordinate system. The data collection site and corresponding sky plot of the visible satellites are shown in Figure 5-6(b). Multi-story glass buildings surrounded the data collection site. A sampling frequency of 20.25 MHz was used. Data was collected in two different environments as described in Table 5-2.

(a)

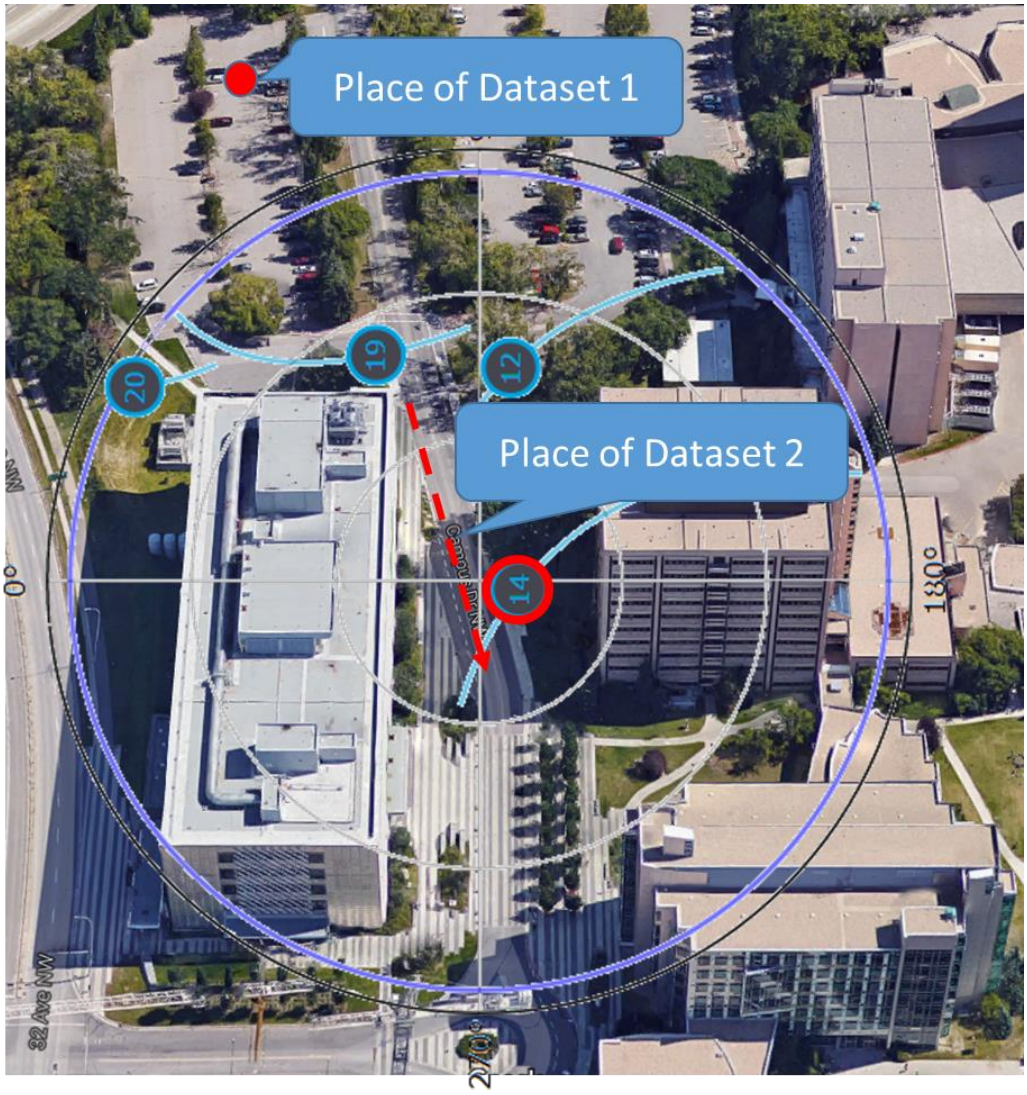

(b)

Figure 5-6: Field test data collection (a) Setup used for actual GPS data collection (b) Sky plot and locations of data collections

Table 5-2: Field test data collection scenarios

Dataset	Description of the multipath environment
Dataset F1	Data was collected in open sky conditions for a static user where multipath was low.
Dataset F2	Data was collected in a slow moving vehicle between glass-covered buildings. The glass planes act as reflecting surfaces and generate specular reflections. The vehicle moved at constant speed and relatively constant attitude.

The baseband samples collected were processed using the multi-antenna GNSS software receiver to generate prompt correlation values from all the antenna elements. The objective is to observe the behavior of measured relative phases between different antenna elements and their correlation with C/N_0 variations. The relative phase values for PRN 14 are compared for Dataset F1 and Dataset F2. The relative phases and C/N_0 variations for Dataset F1 are shown in Figure 5-7 and the same for Dataset F2 is shown in Figure 5-8. The C/N_0 remains constant for Dataset F1 where multipath is low. For Dataset F2, it fluctuates periodically due to constructive and destructive effect of multipath signals. Like C/N_0, the relative phases between the antenna elements also remain constant for Dataset F1. However, in significant multipath environments, relative phase values fluctuate depending on the multipath reflections. Phase variations up to ±30˚ were observed. The mean and the standard deviations for Dataset F1 and Dataset F2 are shown in Table 5-3 where it can be observed that the standard deviations increase for the multipath scenarios. The mean phase values in Dataset F1 and F2 differ due to the

different DOA values of the satellite signals. Even though the phase variations are higher in Dataset F2, it can be observed that the errors in phase measurements have a periodic pattern with zero mean. The mean phase errors computed for Dataset F2 are shown Table 5-3. The mean phase errors are computed by taking the difference between measured mean phase value and correct phase value. The correct phase value was computed using the known satellite DOA, array attitude and calibration parameters computed from the dataset F1.

The variations in the phase measurements can be nearly eliminated by observing phases for several multipath periods and averaging them. It is assumed that the satellite DOA values do not change during averaging period. As multipath phases received are different for different antenna elements, the relative phase measurement variations observed are also different for each antenna.

Table 5-3: Mean and standard deviations of antenna relative phase values

Antenna No	**Dataset F1**		**Dataset F2**		
	Mean phase (deg)	Phase standard deviation (deg)	Mean phase (deg)	Mean phase error (deg)	Phase standard deviation (deg)
Antenna 1	0	3.5	0	0	4.0
Antenna 2	18.6	4.1	20.2	1.6	11.1
Antenna 3	-85.6	4.2	-82.0	4.4	12.2
Antenna 4	100.8	3.7	94.2	0.1	7.7
Antenna 5	103.4	4.6	97.7	1.8	10.3
Antenna 6	31.9	4.2	30.8	4.0	12.6

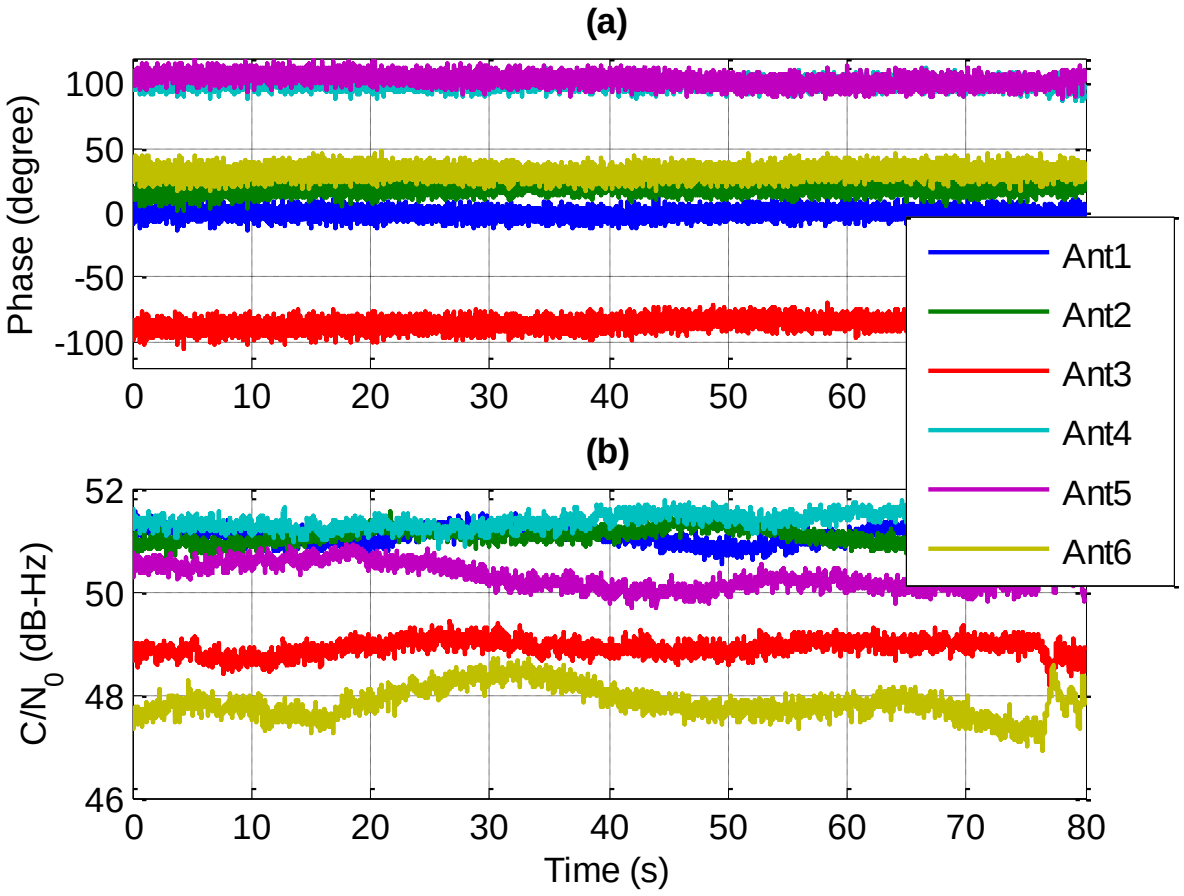

Figure 5-7: Results from Dataset 1 (a) Measured relative phases between antenna elements (b) Antenna elements C/N_0

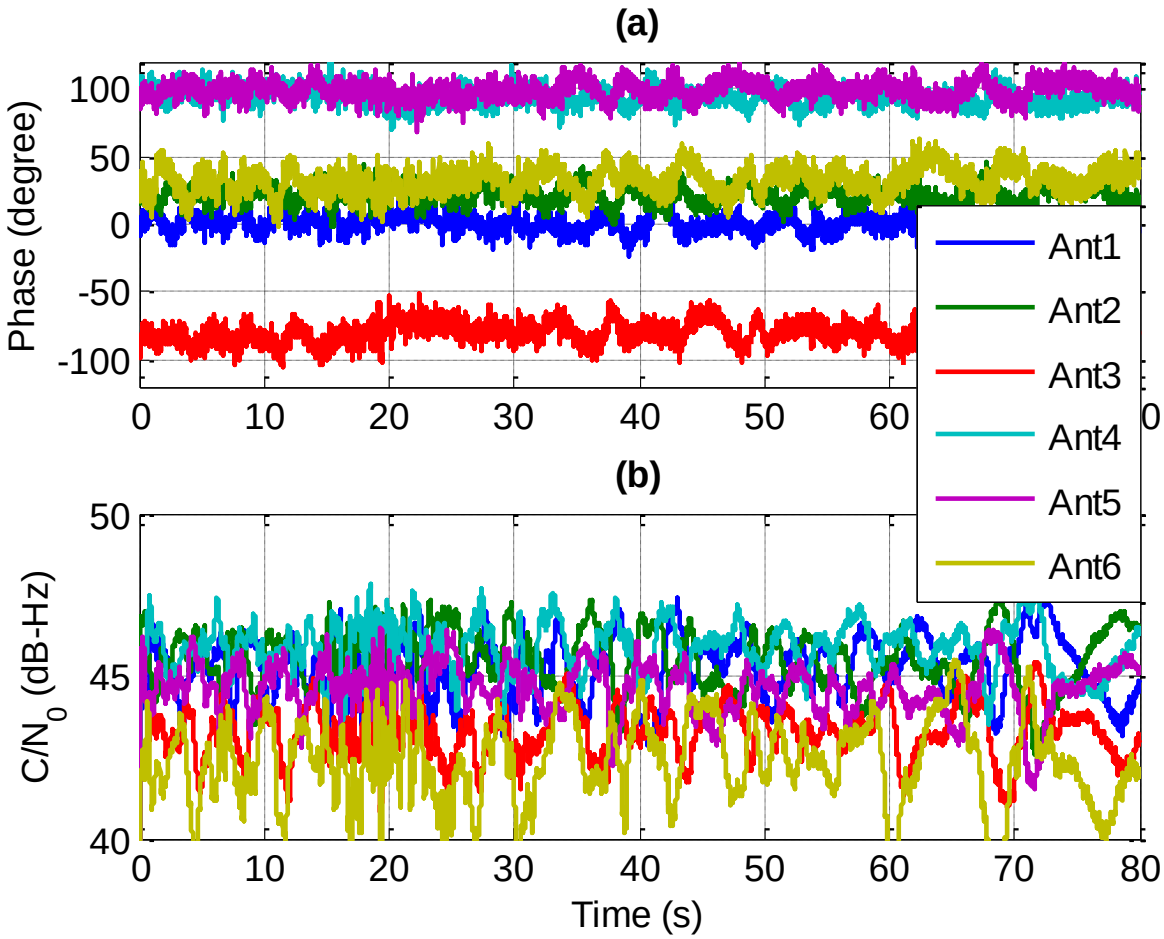

Figure 5-8: Results from Dataset 2 (a) Measured relative phases between the antenna elements (b) Antenna element C/N_0

Herein, the calibration analysis focused on one satellite affected by multipath (PRN 14). With the assumption of zero mutual coupling, a calibration vector is estimated instead of a calibration matrix. In order to compute the satellite azimuth and elevation properly, ephemeris information and known user position from the SPAN^{TM} receiver were used. The ephemeris information was used to compute satellite positions for transmit time corresponding to PRN 14. Using these satellite and user positions, the azimuth and elevation angles were computed in the ENU coordinate system. However, the relative

phases measured between the antenna elements are in the body frame. Therefore, the azimuth and elevation angles need to be converted into that frame. The rotation matrix to convert from ENU to the body frame was obtained by using the attitude of the array. Relative positions of the antenna elements with respect to reference antenna were measured in the body frame. Using the relative antenna positions and satellite DOA information, the steering vector was constructed in the body frame. The steering vector provides the actual or true phase difference between the antenna elements for a signal coming from the satellite direction. However, measured relative phase values between antenna elements do not correspond to the true phase differences as provided by the steering vector. Thus, by taking the difference between measured relative phases and the ones obtained using the true steering vector, the calibration matrix was estimated. As only one satellite was used, the mutual coupling between the antennas cannot be estimated and thus was not accounted in the calibration process.

To start with, the calibration vector was estimated using Dataset F1. It was observed that the calibration vector estimated from one sample and from averaged phase measurements were the almost same. This may not be the case in higher multipath scenarios due to phase fluctuations. Therefore, to validate calibration performance, the calibration vector was estimated in two different ways. For the first calibration vector (C1), an arbitrary sample was chosen in Dataset F2 and the phase measurements during that time instant were chosen to obtain the calibration vector. The second calibration vector (C2) was obtained by averaging the phase measurements of each antenna in Dataset F2. Using these two calibration vectors, the angle of arrival of the satellite signal using conventional beamforming was estimated on Dataset F1. The azimuth and elevation

estimation errors using calibration vectors C1 and C2 are shown in Figure 5-9. Errors in azimuth estimation are higher for C1 than for C2. The mean and standard deviations of the DOA errors are provided in Table 5-4. The mean error in azimuth was reduced by nearly 14˚ after averaging the phase estimates. As an arbitrary sample was chosen to compute C1, error statistics will be different for different samples. However, it should be noted that averaging the phase measurements provides DOA estimation due to better estimation of the calibration vector.

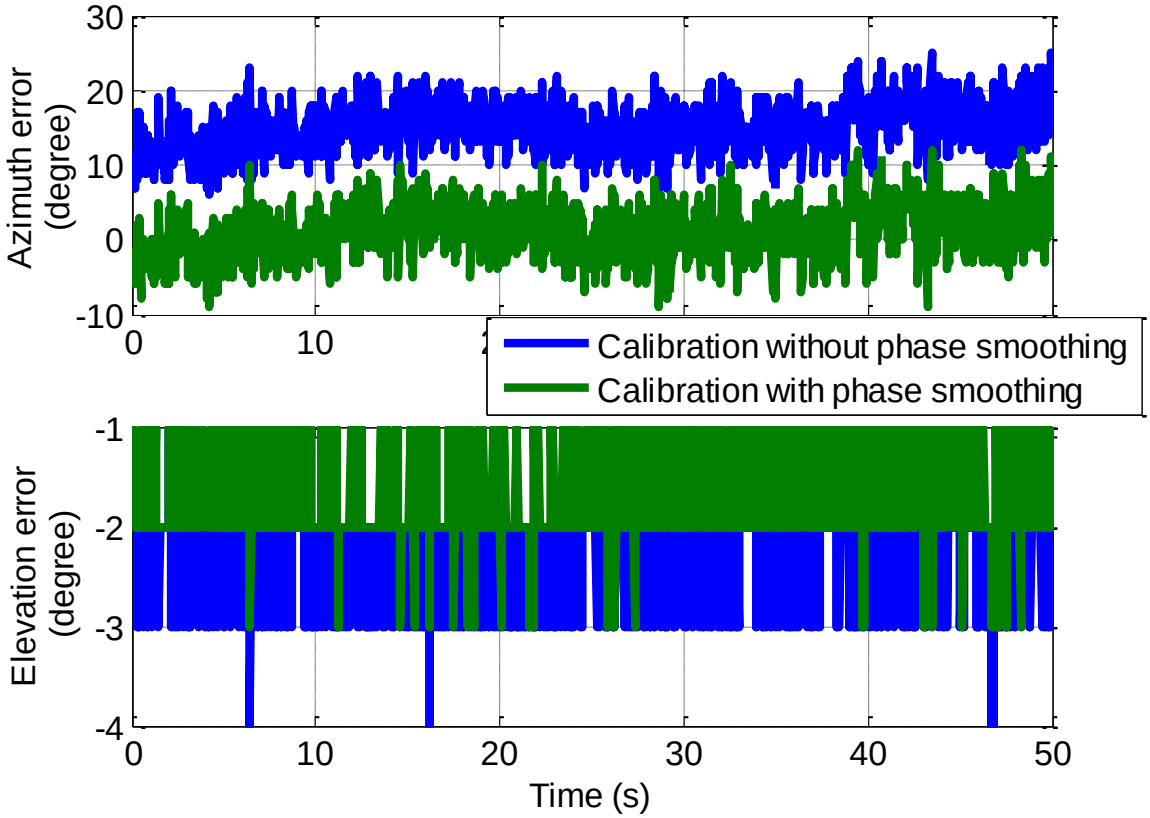

Figure 5-9: DOA estimation errors for PRN 14 (a) Azimuth angle errors (b) Elevation angle errors

Table 5-4: Mean and standard deviations of DOA estimation errors for PRN 14

Calibration Vector	Azimuth error (deg)		Elevation error (deg)	
	Mean	Standard Deviation	Mean	Standard Deviation
C1	14.4	4.8	-2.3	0.6
C2	0.5	4.8	-1.8	0.6

Even though the calibration performance was analyzed using a single satellite affected by multipath, performance can also be examined using multiple satellites simultaneously affected by multipath. In this case, the multipath period of various PRNs is different. Thus, one can choose the averaging period based on PRNs having longer multipath periods. Using these averaged phase measurements from all the satellites, the calibration parameters can be computed using Equation 5-6.

5.5 Summary

Antenna array calibration in multipath environments was analyzed. The effect of carrier phase multipath on the estimation of antenna array calibration parameters was demonstrated through simulation and actual data. Through simulations, it was shown that relative phase measurements are periodic with zero mean for specular multipath conditions. Calibration parameters estimated after averaging the phase measurements showed maximum gain in satellite directions, indicating improvement in the calibration parameters. An improvement up to 14˚ was shown in DOA estimation after averaging the phase measurements using the actual data collected in specular multipath conditions.

Chapter Six: GNSS ANTENNA ARRAY RECEIVER PERFORMANCE UNDER ELECTRONIC INTERFERENCE

6.1 Introduction

Antenna array processing induces distortions in code and carrier phase measurements in the presence of electronic interference (Chuang et al 2013, Church et al 2007**,** De Lorenzo et al 2006). For high precision applications, antenna array processing should not only protect against electronic interference but should also maintain quality of the measurements. There are different sources that can affect measurement quality, namely type of interference, GNSS receiver hardware (RF front-end delays, group delay, uneven cable lengths), receiver architecture and array processing techniques. Kim (2000) provided a detailed study of the hardware induced code and carrier phase biases due to different phase and group delays of the individual antennas. Some of the hardware induced biases can be corrected in the calibration process. Chuang et al (2013) studied induced code and carrier phase measurement biases through mathematical models. However, the performance of multi-antenna GNSS receivers in terms of measurement and position distortions has not been throughly studied. In this research, the performance of the multi-antenna GNSS receiver described in previous chapters under different types of electronic interference and different array processing techniques is evaluated in terms of carrier tracking, measurement distortions and position distortions. Both narrow band and wide band interference sources are considered. Two array processing techniques, namely blind beamformer, which does not take DOA of satellites into consideration, and distortionless beamformer, which uses DOA of satellites, are considered. The

methodology for evaluating possible distortions in the measurements is described and followed by a discussion of the results from simulated and actual data processing. The performance evaluations are carried out using GPS signals.

6.2 Methodology

This section describes the GNSS and interference signal simulations, multi-antenna signal processing method and the methodology to characterize the code and carrier phase measurement distortions.

6.2.1 Multi-antenna signal simulation

The multi-antenna signal simulator described in Chapter 3 was used to generate multi-antenna signals with different types of interference. For the simulations, it was assumed that antenna elements are identical and there is no mutual coupling. A static user scenario was considered and the interference source was also assumed to be static.

6.2.2 Multi-antenna signal processing

The simulated signals are processed using modified the multi-antenna GSNRx^{TM} software receiver is used to generate code and carrier phase measurements. The software receiver was modified to incorporate power minimization and MPDR processing techniques. The power minimization was implemented in the precorrelation stage and the receiver architecture is shown in Figure 6-1. The same beamformed signal will be tracked by all tracking channels. Also, antenna array calibration is not required for power minimization.

MPDR was performed at the postcorrelation stage and the receiver architecture with MPDR is shown in Figure 6-2. Here, signals from all the antennas are fed to each tracking channel. In each tracking channel, the code and carrier replica signals from the beamformed data to despread other antenna signals to maintain the relative phase differences between the antenna elements. The covariance matrix was computed at the precorrelation stage because at the postcorrelation stage, interference power might be reduced due to the correlation process affecting beamformer performance. The combined correlator outputs will be used to generate code and carrier phase measurements. The MPDR beamformer requires antenna array calibration.

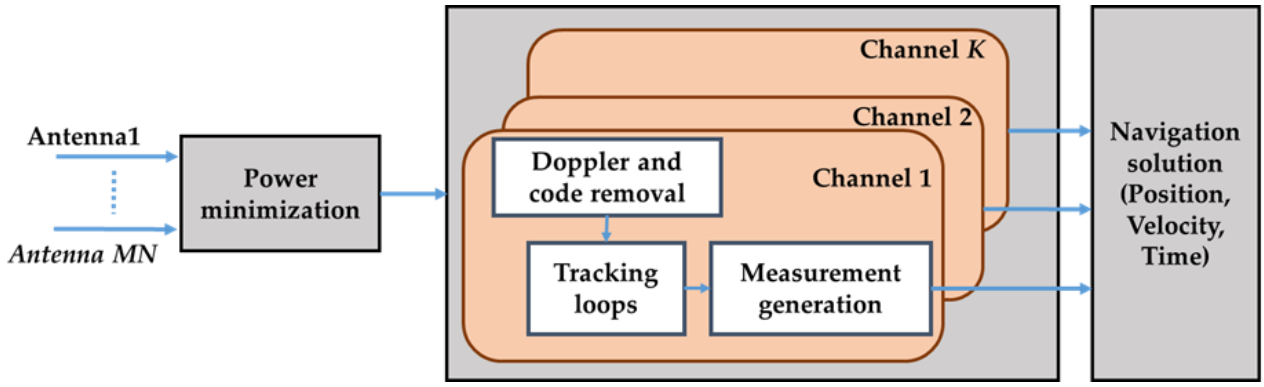

Figure 6-1: Multi-antenna processing using power minimization approach

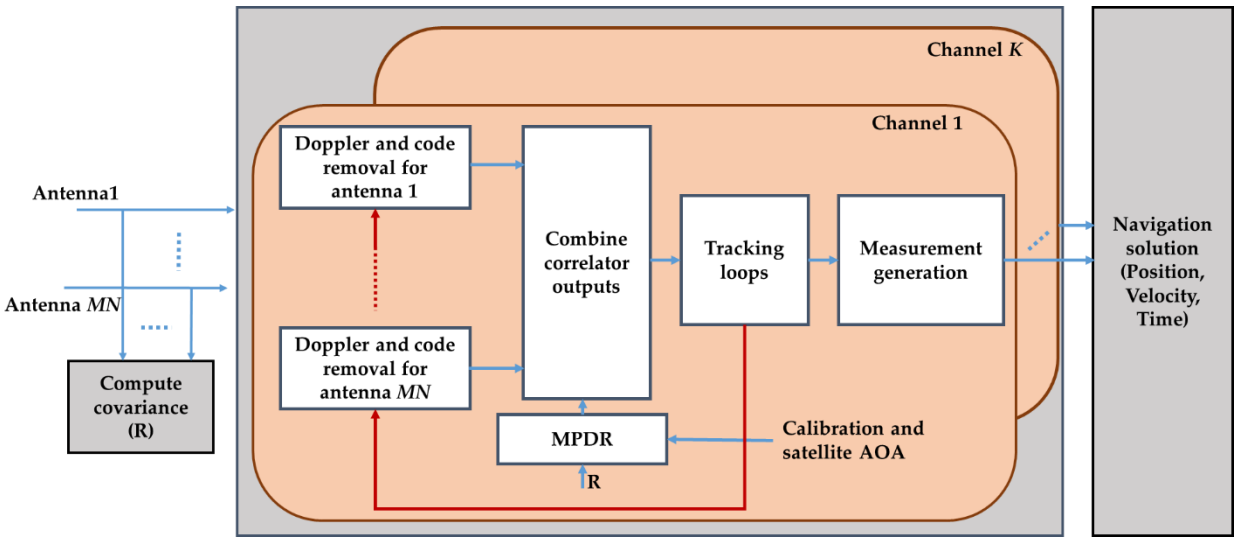

Figure 6-2: Multi-antenna processing approach using power minimization

6.2.3 Measurement distortion analysis

The goal is now to characterize the biases in the code and carrier phase measurements from the beamformed data in the presence of interference. A differential technique is used to evaluate the measurement biases. Measurements from one of the array antenna with clean data without interference acts as reference. Single differencing between reference antenna measurements (with clean data) and those from the beamformed data (in the presence of interference) acts as a zero base line test. The steering vector will be constructed with respect to a reference antenna position and the effective antenna array position will be the same as the reference antenna. The resulting single difference should ideally have a zero mean if there are no distortions in the measurements from the antenna array processing. In the rest of the chapter, measurement distortions refer to the distortions caused by the multi-antenna GNSS receiver in the presence of interference.

The pseudorange measuremnets of the i^{th} satellite after beamforming in the presence of interference can be expressed as

$$PR^i_{array} = \rho^i + d\rho^i + c(dt^i - dT) + d^i_{iono} + d^i_{tropo} + \rho^i_{bias} + \varepsilon^i_\rho \quad (6\text{-}1)$$

where, ρ^i is the true range, $d\rho^i$ is the orbital error, dt^i and dT are the satellite and receiver clock errors, d^i_{iono} is the ionosphere error, d^i_{tropo} is the tropospheric delay, ε_ρ is the receiver noise and ρ^i_{bias} is the possible bias introduced by antenna array processing.

The pseudorange from the i^{th} satellite for the reference antenna without interference can be expressed as

$$PR^i_{ref} = \rho^i + d\rho^i + c(dt^i - dT) + d^i_{iono} + d^i_{tropo} + \varepsilon^i_\rho \quad (6\text{-}2)$$

The single difference between the pseudorange measurements obtained from reference antenna and after beamforming is

$$\Delta PR^i = PR^i_{ref} - PR^i_{array} = \rho^i_{bias} + \varepsilon^i_{\Delta\rho} \quad (6\text{-}3)$$

Since this single differencing acts like a zero-baseline, the atmospheric errors and user clock bias cancel out. The code noise and pseudorange bias will remain after single differencing. The code noise standard deviation depends on receiver tracking strategies such as chip spacing and the discriminators used and it should ideally be zero mean. Hence, one can estimate the pseudorange bias induced by the antenna array processing in the presence of interference. It is assumed that the residual multipath effect is small compared to the antenna array induced biases. In the simulations, GPS signals were simulated in multipath free conditions. In the case of actual data collection, a low multipath environment was selected.

Similar to pseudorange measurement bias estimation, the carrier phase measurement bias can also be estimated by performing single differencing between the reference antenna and beamformed carrier phase measurements. Single difference carrier phase measurements are obtained as

$$\Delta\Phi^i = \Delta\phi^i_{bias} + \varepsilon^i_{\Delta\phi} \tag{6-4}$$

As in the pseudorange case, carrier phase noise is ideally zero mean and therefore any bias observed using single differencing can be attributed to array processing in the presence of interference.

6.3 Simulation results

The effect of different interference sources and array processing approaches are now studied through GPS signal simulations. Simulations are carried out considering different interference types. In order to evaluate the effect of different kinds of interference, it is assumed that only one interference source is present at the time in each simulation scenario. The interference sources considered are CW interference, chirp interference and band-limited additive white Gaussian noise. The effect of these interference sources on GNSS receiver operation differs due to their spectral characteristics. Therefore, it is of interest to check the performance of the array based receiver under different interference types.

The input IF data file for the multi-antenna software simulator was collected from a Spirent hardware GPS simulator by disabling multipath and atmospheric errors. A static user scenario was used for collecting IF data samples at a 5 MHz sampling rate. The multi-

antenna GPS signals were generated using the multi-antenna signal simulator and interference was added later to the clean IF samples. The six-element rectangular antenna array described earlier was considered for the simulations. The interference source was assumed to be static and was added after 15 seconds in order for the receiver to acquire and track the signals (for the post-correlation beamforming). The sky plot of the simulated GPS satellites is shown in Figure 6-3 and shows the interference source direction. The characteristics of the interference sources are given in Table 6-1. In all the simulation scenarios, the interference source direction is the same.

The simulated signals were processed using the multi-antenna GSNRx^{TM} software receiver with architectures shown in Figure 6-1 and Figure 6-2 to generate tracking parameters and measurements. Here, power minimization was performed from the beginning of the dataset as it was done in the pre-correlation stage. In the case of the MPDR beamformer, the receiver was made to operate with a single antenna for the initial 10 seconds, after which beamforming was performed before the occurrence of interference. This was done to ensure that the receiver operates in beamforming mode when interference affects the IF samples. In both power minimization and MPDR approaches, correlator spacing of 0.4 between early and late arms and non-coherent early-minus late discriminators were used. Carrier tracking was performed using a third order PLL with a 15 Hz bandwidth.

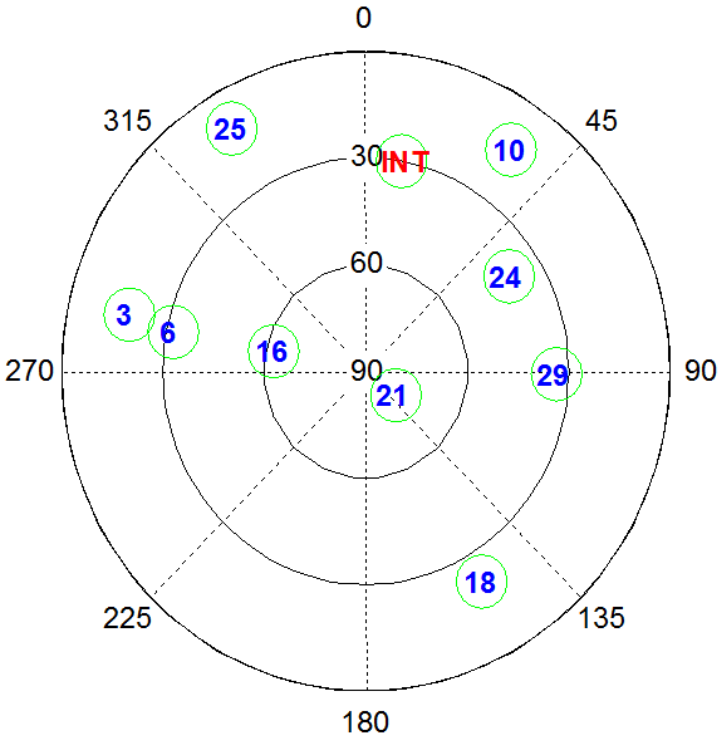

PRN	Elevation (Degree)	Azimuth (Degree)
3	18.2	282.8
6	31.8	281.2
10	14.1	34.6
16	62.3	282.1
18	21.5	149.8
21	78.9	128.0
24	40.1	57.8
25	10.9	330.1
29	33.7	90.6
INT	30	10

Figure 6-3: Sky plot of simulated GPS satellites and interference source

Table 6-1: Interference sources considered in the simulations and their characteristics

Simulation scenarios	Interference type	Interference characteristics
Scenario 1	CW interference	The frequency of the CW interference is 500 Hz away from IF (420 kHz). Jammer-to-signal power is assumed to be 30 dB.
Scenario 2	Chirp interference	Chirp signal bandwidth is 11.8 MHz with a chipping rate of 11.7 μs. These values are basically chosen from commercially available in-car jammers (Bauernfeind et al 2014). Jammer-to-signal power is 30 dB.
Scenario 3	Band limited white Gaussian noise	White Gaussian noise is generated through MATLAB^{TM} *awgn*() function with a bandwidth of 5 MHz and jammer-to-signal power of 30 dB.

6.3.1 Tracking domain analysis

In this section, tracking performance in terms of carrier Doppler estimation, C/N_0 and PLI is evaluated. Initially, data affected by interference from the reference antenna of the array was processed and corresponding results are discussed in subsequent sections. Since PRN 6 and PRN 16 are more affected by CW interference, these two PRNs are used to analyze tracking performance of the array-based receiver.

The tracking performance of PRN 6 in the presence of CW interference is discussed first to show the effectiveness of the beamformer. The tracking outputs for single antenna with interference and after beamforming are shown in Figure 6-4 where 'Single Antenna' corresponds to the tracking outputs of the reference antenna of the array in the presence of interference. For the initial 15 seconds, there was no interference; as mentioned earlier,

power minimization was performed from the beginning of the data and MPDR was performed after 10 seconds.

Let's first consider the initial 15 s of data without interference. After MPDR beamforming, a C/N_0 gain of 7.5 dB is observed. As six antenna elements were used, a gain of 7.7 dB [$10*\log_{10}$(number of antennas)] is expected and one can observe the same with MPDR beamforming. With power minimization, a gain of 1.5 dB is observed; in this case, since there is no accounting for satellite signal DOA, the gain depends on the beampattern, which in turn depends on the interference direction and array geometry. However, the same C/N_0 should occur even during interference.

Consider the data with interference (after 15 seconds) in the figure. As soon as interference is injected, the C/N_0 of the single antenna drops by 8 dB. However, the same C/N_0 as that without interference was maintained through MPDR and power minimization. This ensured successful mitigation of the interference. If one considers the C/N_0 gain in the presence of interference, MPDR was able to deliver nearly 15.5 dB with respect to the single antenna. The gain observed from power minimization was around 9.5 dB. The Doppler errors increase and PLI degrades for the single antenna after interference was injected. However, MPDR and power minimization were able to provide the same performance as that for the interference-free case. To compute the carrier Doppler errors shown in Figure 6-4, the Doppler values obtained from the reference antenna with clean data were used as reference.

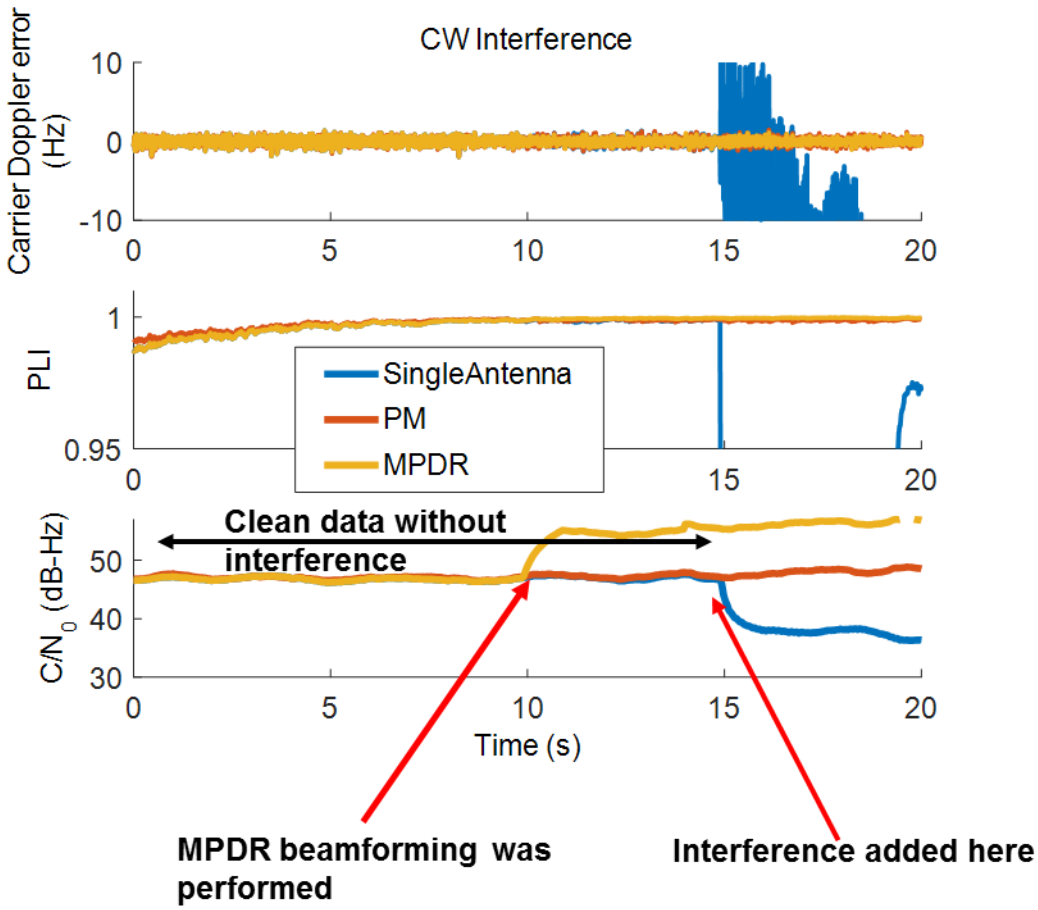

Figure 6-4: Tracking performance of PRN 6 with CW interference

The carrier tracking performance of PRN 6 for different interference simulation scenarios is shown in Figure 6-5. MPDR was able to provide 15.5 dB of gain even in the presence of chirp and BWGN interference. Even power minimization was able to provide 9.5 dB of gain in the presence of the same interference. The Doppler error variance is lower after beamforming; this can be clearly observed in Figure 6-5 (c) in the presence of BWGN interference. The receiver was able to maintain PLI values of 0.99 after beamforming in all interference scenarios indicating reliable tracking of the carrier phase.

The carrier tracking performance of PRN 16 for different interference simulation scenarios is shown in Figure 6-6. Even for this PRN, MPDR was able to provide 7.5 dB

of gain with clean data and 15.5 dB of gain with interference data. This was observed with all types of interference simulation scenarios as shown in the figure. However, no gain was observed for power minimization with clean data. However, in the presence of interference, power minimization was able to maintain the same C/N_0 as that of clean data. Similar to PRN 6, tracking performance improved after beamforming in terms of reduced Doppler errors and better PLI.

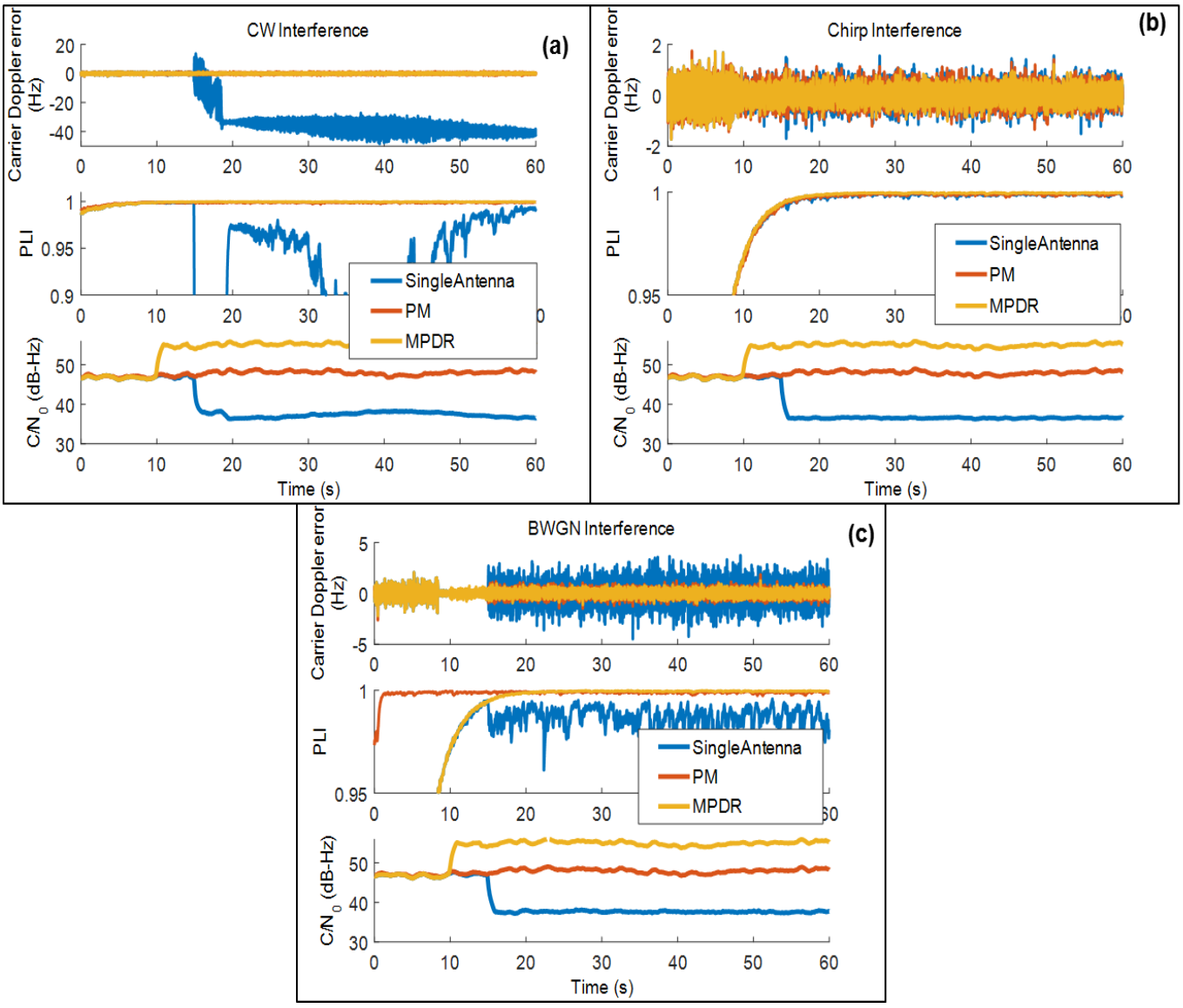

Figure 6-5: Carrier tracking performance of PRN 6 with (a) CW interference (b) Chirp interference (c) Bandlimitted white gaussian noise

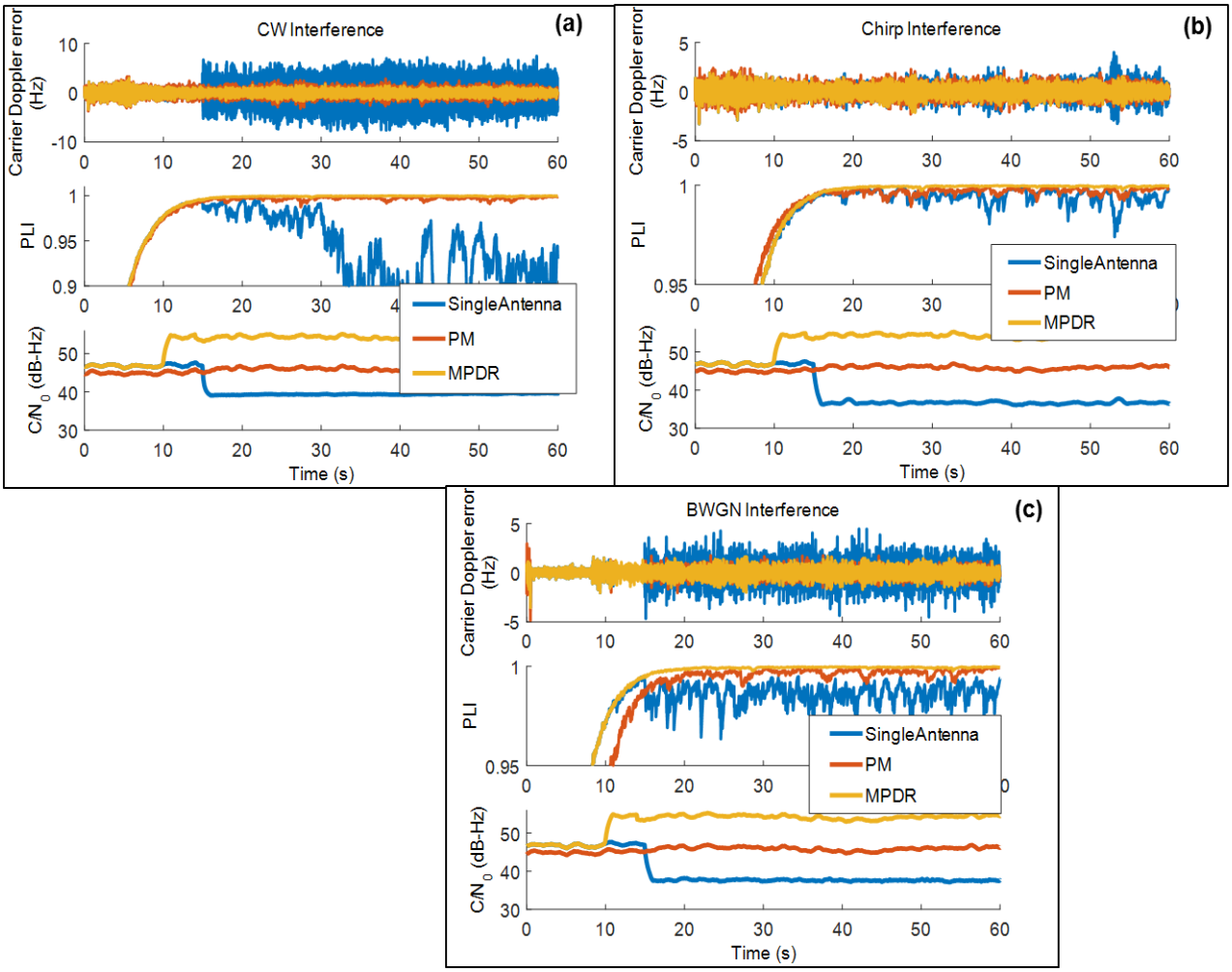

Figure 6-6: Carrier tracking performance of PRN 16 with (a) CW interference (b) Chirp interference (c) Bandlimited white Gaussian noise

The performance results of different PRNs in terms of RMSE Doppler error, C/N_0 gain and mean PLI for CW interference are listed in Table 6-2. These values were computed using the tracking outputs in the presence of interference. For computing RMSE Doppler errors, the Doppler values obtained from the reference antenna with clean data were used as true values. The tracking performance results of different PRNs in the presence of chirp jammer are provided in Table 6-3 and those in the presence of BWGN are provided in Table 6-4. It can be observed that compared to single antenna results, RMSE Doppler

errors are reduced in both beamformers for all simulation scenarios. However, However, the MPDR RMSE Doppler errors were lower by 0.1 Hz as compared to power minimization, a relative improvement of 25%. It is observed that the same C/N_0 gain occurs for all PRNs in all the interference scenarios for MPDR.

Table 6-2: Tracking performance of different PRNs in the presence of CW interference

PRN	Single Antenna			Power minimization			MPDR		
	RMSE Doppler error (Hz)	Mean PLI	Mean C/N_0 (dB-Hz)	RMSE Doppler error (Hz)	Mean PLI	Mean C/N_0 (dB-Hz)	RMSE Doppler error (Hz)	Mean PLI	Mean C/N_0 (dB-Hz)
PRN 3	0.51	0.99	33.4	0.42	0.99	48.9	0.34	0.99	54.69
PRN 6	36.14	0.89	37.3	0.42	0.99	48.02	0.33	0.99	54.59
PRN 16	3.25	0.93	39.4	0.75	0.99	45.92	0.51	0.99	54.26
PRN 18	0.80	0.99	36.25	0.51	0.99	47.38	0.40	0.99	54.26
PRN 21	1.97	0.98	37.01	0.47	0.99	48.56	0.35	0.99	54.66
PRN 24	0.57	0.99	34.79	0.46	0.99	47.66	0.37	0.99	54.80
PRN 25	0.49	0.99	35.6	0.46	0.99	47.08	0.39	0.99	54.29
PRN 29	0.90	0.99	34.8	0.67	0.99	45.43	0.51	0.99	54.27

Table 6-3: Tracking performance of different PRNs in the presence of chirp interference

PRN	Single Antenna			Power minimization			MPDR		
	RMSE Doppler error (Hz)	Mean PLI	Mean C/N_0 (dB-Hz)	RMSE Doppler error (Hz)	Mean PLI	Mean C/N_0 (dB-Hz)	RMSE Doppler error (Hz)	Mean PLI	Mean C/N_0 (dB-Hz)
PRN 3	0.45	0.99	36.6	0.32	0.99	48.9	0.26	0.99	54.9
PRN 6	0.40	0.99	36.6	0.36	0.99	48.0	0.28	0.99	54.7
PRN 16	0.74	0.99	36.7	0.61	0.99	45.9	0.51	0.99	54.4
PRN 18	0.43	0.99	36.7	0.40	0.99	47.3	0.35	0.99	54.4
PRN 21	0.42	0.99	36.7	0.35	0.99	48.5	0.33	0.99	54.8
PRN 24	0.48	0.99	36.6	0.46	0.99	47.6	0.36	0.99	54.0
PRN 25	0.47	0.99	36.7	0.43	0.99	47.0	0.33	0.99	54.9
PRN 29	0.55	0.99	36.7	0.49	0.99	45.4	0.46	0.99	54.4

Table 6-4: Tracking performances of different PRNs in the presence of BWGN interference

PRN	Single Antenna			Power minimization			MPDR		
	RMSE Doppler error (Hz)	Mean PLI	Mean C/N_0 (dB-Hz)	RMSE Doppler error (Hz)	Mean PLI	Mean C/N_0 (dB-Hz)	RMSE Doppler error (Hz)	Mean PLI	Mean C/N_0 (dB-Hz)
PRN 3	1.10	0.98	37.7	0.32	0.99	48.9	0.26	0.99	54.4
PRN 6	1.10	0.98	37.7	0.36	0.99	48.0	0.29	0.99	54.3
PRN 16	1.14	0.98	37.7	0.46	0.99	45.9	0.52	0.99	54.0
PRN 18	1.08	0.98	37.7	0.39	0.99	47.3	0.35	0.99	54.0
PRN 21	1.10	0.98	37.7	0.35	0.99	48.5	0.33	0.99	54.3
PRN 24	1.15	0.98	37.7	0.37	0.99	47.6	0.35	0.99	54.5
PRN 25	1.09	0.98	37.7	0.40	0.99	47.0	0.33	0.99	54.3
PRN 29	1.17	0.98	37.7	0.50	0.99	45.4	0.46	0.99	54.0

6.3.2 Measurement domain analysis

This section analyzes pseudorange and carrier phase measurement errors. The measurement domain results in the presence of chirp interference are provided here. The measurement differencing technique described in the methodology section is used here to obtain pseudorange and carrier phase measurement errors.

Time series plot of the pseudorange and carrier phase measurement errors for both power minimization and MPDR are shown in Figure 6-7. The mean and standard deviations of the pseudorange errors for all the PRNs are provided in Table 6-5. First consider the power minimization approach. It can be seen from Table 6-5 that power minimization induces pseudorange biases of the order of 30 cm to 50 cm for different

PRNs. It can also be observed that the biases observed are different for different PRNs. It can be seen from Figure 6-7 that the PRN 10 distortions in the measurements in terms of mean and standard deviation are higher than those of other PRNs. This is because the interference source location is near PRN 10 as shown in the sky plot of Figure 6-3. Now consider the MPDR beamformer; it induces up to 4 cm of pseudorange bias, which is nearly that same as the code phase measurement standard deviation. For PRN 10, which is near the interference source, standard deviations of the measurement errors have increased compared to other PRNs. The higher standard deviations in pseudorange measurements in both power minimization and MPDR are due to the tracking architecture used (0.4 chip spacing between early and late). It can be observed that mean pseudorange bias values are higher for power minimization than MPDR.

The mean and standard deviations of the carrier phase measurement errors for different PRNs are listed in Table 6-6. It can be observed from Figure 6-7 that power minimization induces different biases for different PRNs. The bias for a particular PRN remains the same for the entire test duration. This may be because the interference source location was fixed and the beamformer weights are not changing. However, if the interference direction is changed, the beamformer weights also change and different biases might be observed for the same PRN. The 30 mm PRN 10 bias is higher than that of other PRNs. The carrier phase measurement biases for the MPDR beamformer are minimal as listed in Table 6-6.

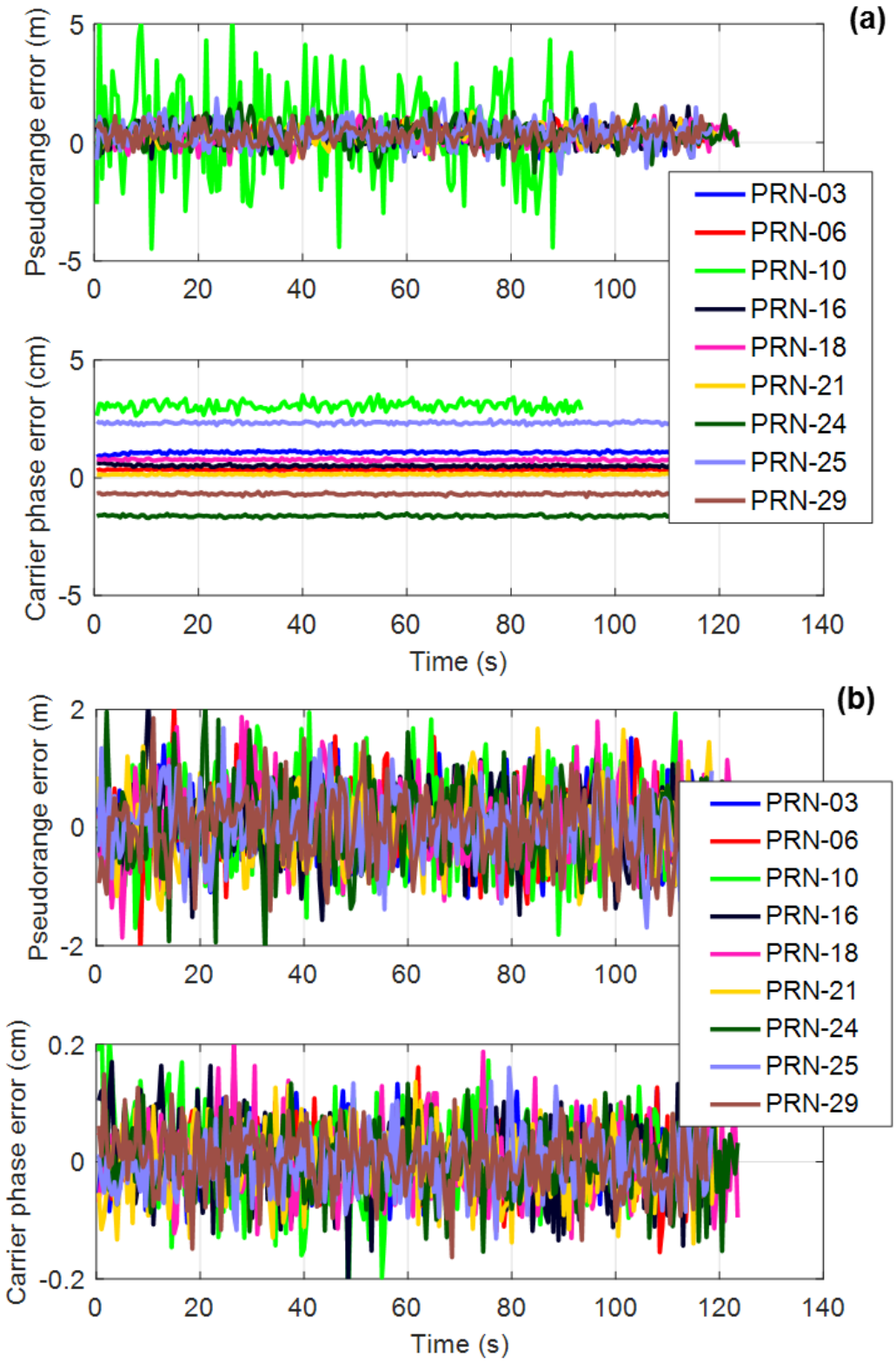

Figure 6-7: Time series plot of the pseudorange and carrier phase measurement errors using (a) Power minimization (b) MPDR

Table 6-5: Pseudorange measurement errors for power minimization and MPDR in the presence of chirp interference

PRN	Power minimization		MPDR	
	Mean (m)	Standard deviation(m)	Mean (m)	Standard deviation(m)
PRN 3	0.27	0.31	0.02	0.55
PRN 6	0.33	0.27	0.02	0.59
PRN 10	0.50	1.93	0.08	0.75
PRN 16	0.31	0.36	0.01	0.59
PRN 18	0.28	0.33	0.02	0.69
PRN 21	0.31	0.30	-0.04	0.58
PRN 24	0.35	0.49	0.02	0.65
PRN 25	0.38	0.55	0.04	0.55
PRN 29	0.31	0.40	-0.01	0.60

Table 6-6: Carrier phase measurement errors using power minimization and MPDR in the presence of chirp interference

PRN	Power minimization		MPDR	
	Mean (mm)	Standard deviation(mm)	Mean(mm)	Standard deviation(mm)
PRN 3	10.7	0.4	0.04	0.4
PRN 6	3.4	0.2	-0.01	0.4
PRN 10	30.5	1.8	0.07	0.7
PRN 16	5.0	0.4	0.05	0.6
PRN 18	7.6	0.3	-0.01	0.5
PRN 21	1.4	0.2	-0.05	0.5
PRN 24	-16.2	0.4	0.01	0.5
PRN 25	23.3	0.4	-0.03	0.5
PRN 29	-6.9	0.3	0.03	0.5

6.3.3 Position domain analysis

For the position domain analysis, the code and carrier phase measurements are processed using the RTKLib open source software. The measurements generated using the reference antenna of the array without interference were used as the base observations for the RTK software. The remote observations were generated from the beamformed data affected by interference. This kind of processing acts like zero baseline and any distortion in the measurements affects the position solution. The open source software was used without any modifications. In the RTKLib, the continuous ambiguity resolution mode was selected and forward-backward processing was performed.

The east, north and height position errors for power minimization and MPDR are shown in Figure 6-8. The RTK software outputs quality flag for each solution update indicating fixed or float solution. Power minimization was not able to provide fixed solutions and position errors of the order of 10 cm occur. MPDR was able to provide fixed solutions and position errors were at the sub-millimetre level. The mean and standard deviations of the position errors observed for both beamformers are provided in Table 6-7. In the power minimization case, satellite directions are not considered in the optimization criterion and the antenna phase values are not added coherently. This will have adverse effect on the carrier phase measurements as discussed in the measurement analysis section. These biased measurements will affect carrier phase based positioning. Also, it should be noted that if the biases are same for all PRNs, they can be pre-calibrated to avoid affecting the position solutions. However, with power minimization, different biases are observed for different PRNs and these have adverse effects on position solutions.

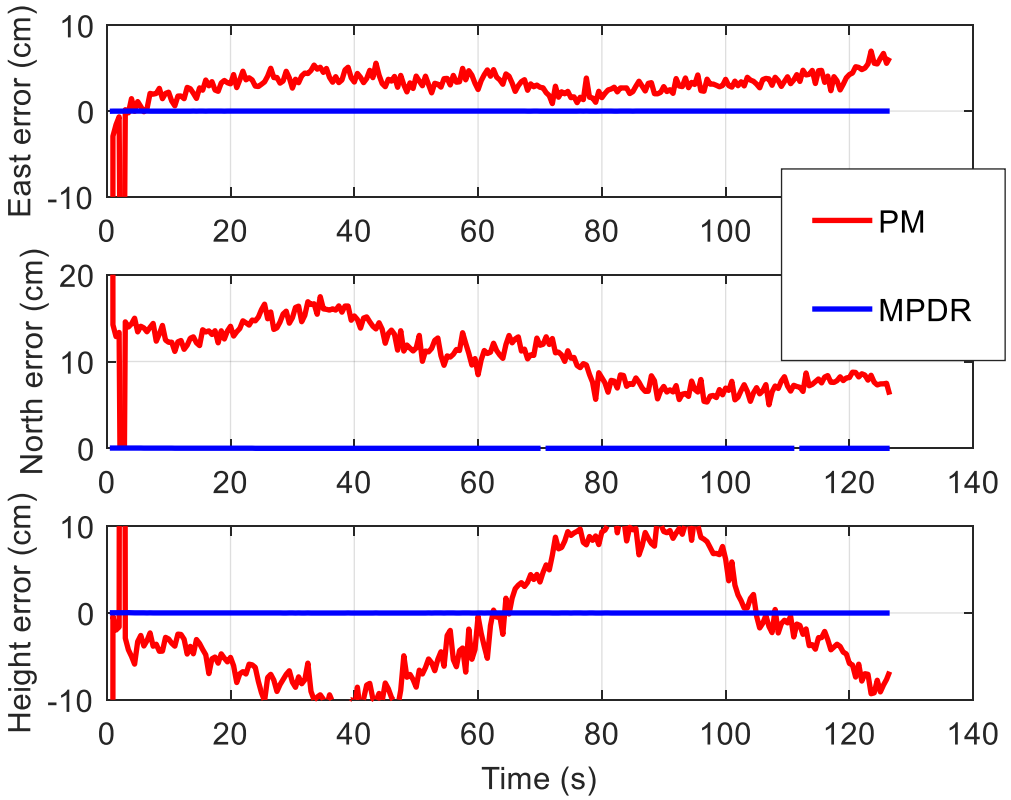

Figure 6-8: Carrier phase position errors with power minimization and MPDR (Processed using RTKLib open source software)

Table 6-7: Carrier phase position errors with power minimization and MPDR

Position errors	Power minimization		MPDR	
	Mean	Standard deviation	Mean	Standard deviation
East error (cm)	3.2	1.1	-0.001	0.003
North error (cm)	10.6	3.3	0.002	0.005
Height error (cm)	-1.4	6.8	-0.005	0.005

6.3.4 Effect of interference source DOA on measurements

The relative direction between jammer and satellite signals plays a critical role in anti-jamming applications using antenna arrays. The effect of changing the DOA of the

interference source is therefore analyzed. It is assumed that only one chirp interference source is present. Time series plots of the pseudorange and carrier phase measurements in the presence of chirp interference for PM and MPDR are shown in Figure 6-9. The interference direction is changed after 65 seconds. For the initial 65 seconds, the interference is located at (elevation=30°, azimuth=10°) and then changed to (elevation=30°, azimuth =225°). Carrier phase biases observed in PM changes when the interference direction changes. However, the MPDR beamformer does not induce any biases in the carrier phase measurements, irrespective of the interference source DOA. For the initial 65 seconds, interference location was near PRN 10 and due to this, the standard deviation of the pseudorange measurements for PRN 10 is high. After 65 seconds, the interference direction was farther away from PRN 10 and the standard deviation decreased.

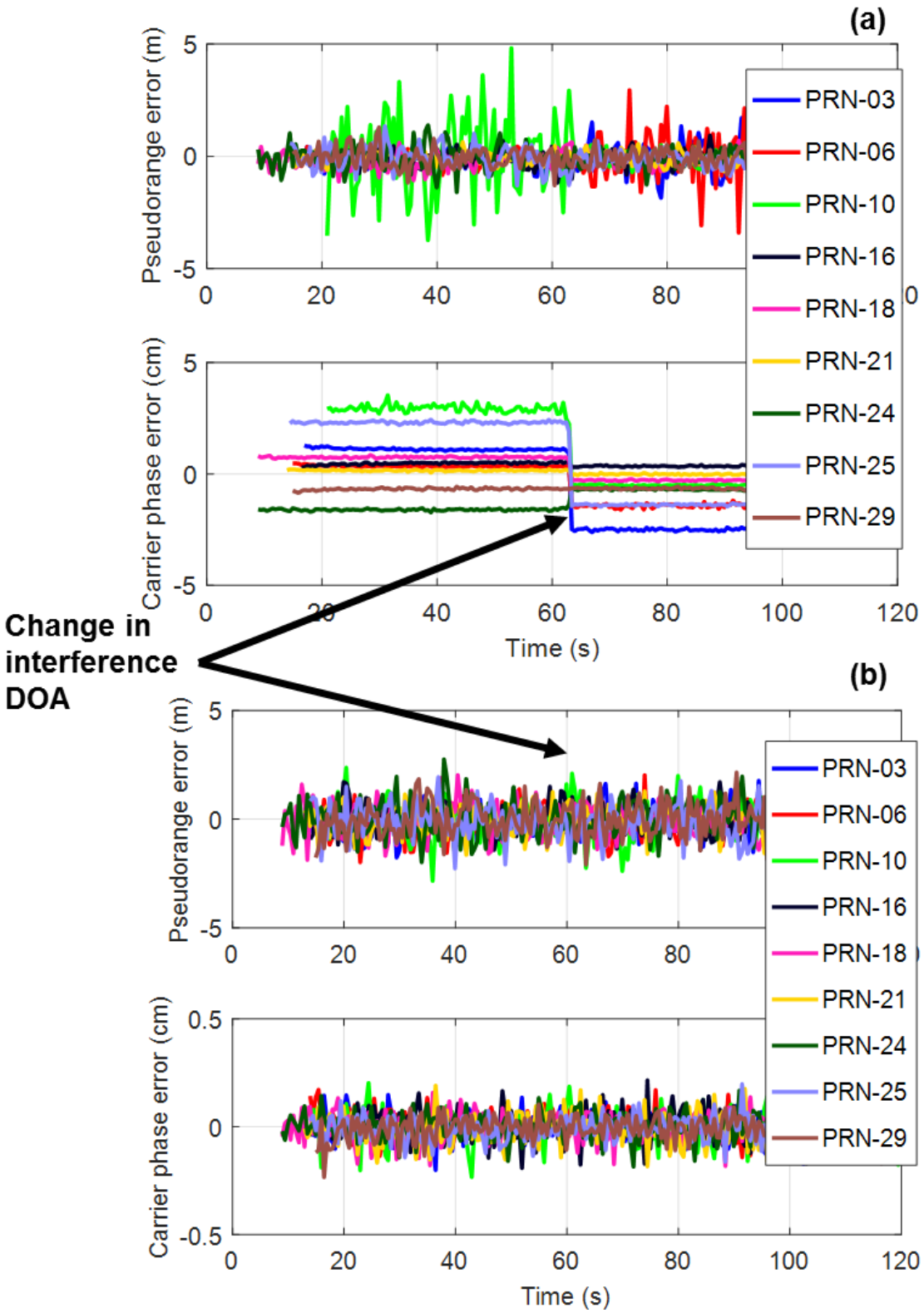

Figure 6-9: Effect of change in interference source DOA on pseudorange and carrier phase measurements for (a) PM and (b) MPDR

6.4 Field-test results

This section describes field test results using power minimization and MPDR beamforming. Unlike the case in the simulation section, the signals received by different antennas depend on actual antenna characteristics such as phase centre variations and offsets, and mutual coupling. In the simulations, it was assumed that the signal strength observed by different antennas was the same for all PRNs. However, for actual signals, different signal strengths are observed for different antennas in the array.

The rectangular array with six antenna elements shown in Figure 6-10 was used for the data collection. The setup used and sky plot of the visible GPS satellites are shown in Figure 6-10. A SPAN LCI mounted on the array platform was used to obtain the array attitude used for calibration and MPDR beamforming. A Fraunhofer Multi-antenna RF front-end was used to collect data from all the six antennas simultaneously in an open sky environment and low multipath conditions. The Initial few seconds of the data were used to perform the antenna array calibration. Interference was added to the collected data through a MATLAB^{TM} software script. Although interference was added later to the actual data as in the case of simulations, the difference between these simulations and field tests is the calibration of an actual array and mutual coupling which might affect the performance of the beamformer. The interference source is assumed to be static with a jammer-to-signal power of 30 dB. The analysis was performed considering one chirp interference.

The collected data without interference and after adding interference were processed using the multi-antenna GSNRx^{TM} software receiver to generate tracking parameters and measurements. A correlator spacing of 0.2 between early and late arms and non-coherent

early-minus late discriminator was used. Carrier tracking was performed using a third order PLL with 15 Hz bandwidth.

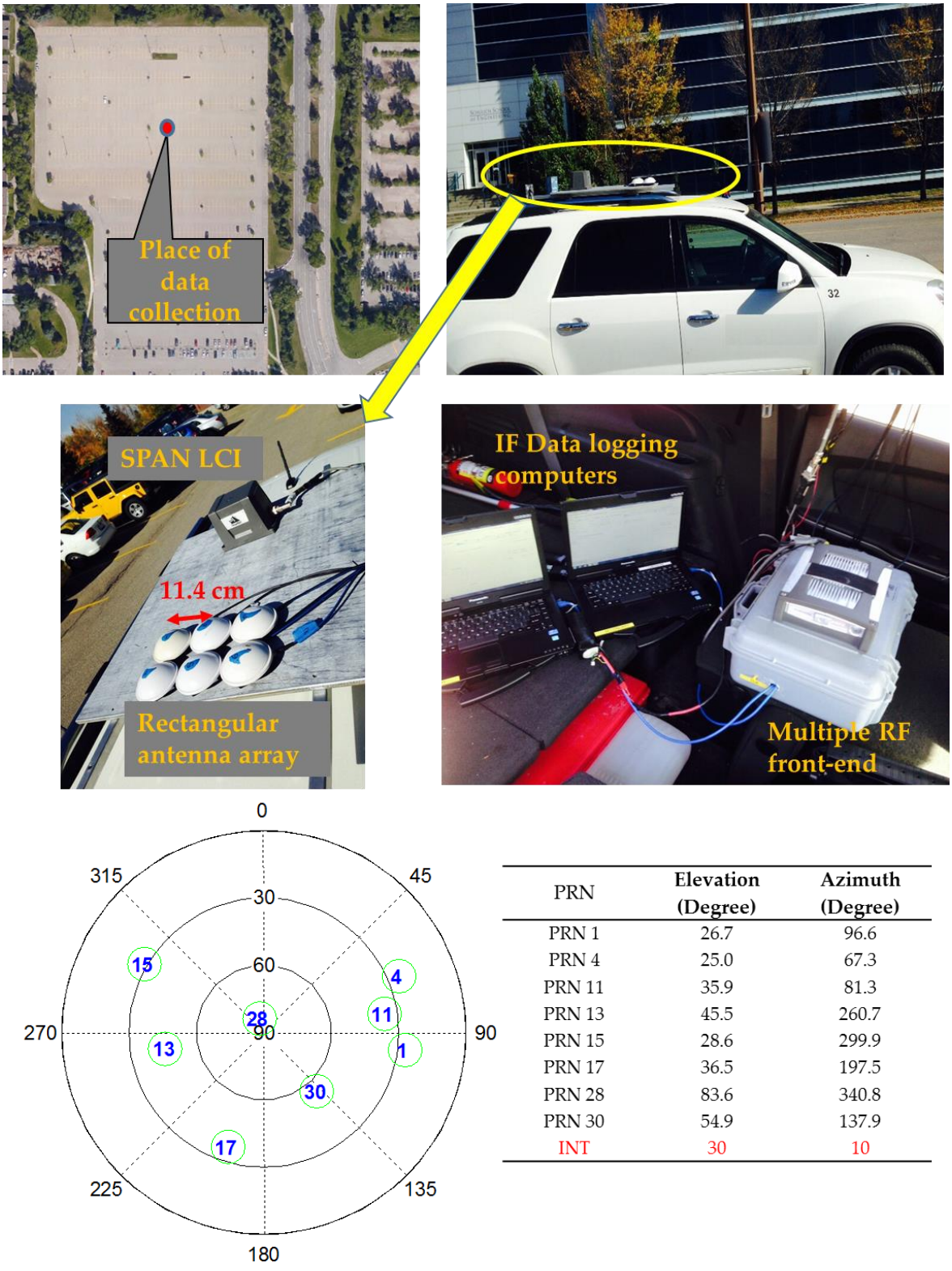

PRN	Elevation (Degree)	Azimuth (Degree)
PRN 1	26.7	96.6
PRN 4	25.0	67.3
PRN 11	35.9	81.3
PRN 13	45.5	260.7
PRN 15	28.6	299.9
PRN 17	36.5	197.5
PRN 28	83.6	340.8
PRN 30	54.9	137.9
INT	30	10

Figure 6-10: Field data collection setup and sky plot of visible GPS satellites

6.4.1 Tracking performance

The power minimization beamforming was performed from the beginning of the data and MPDR was performed after 10 seconds. The interference was added to the collected data after 15 seconds. Here, tracking performances of PRN 4, which is at lower elevation and PRN 28 which is at higher elevation are considered. The tracking performances for these PRNs are shown Figure 6-11. MPDR beamforming performed on clean data from 10 seconds to 15 seconds showed nearly 6 dB of gain with respect to single antenna. In the presence of interference MPDR was able to maintain the gain. However, the gain obtained was higher in the presence of interference and was observed to be around 12 dB with respect to single antenna. The C/N_0 gain observed with power minimization in the presence of interference was about 7 dB. The carrier Doppler errors were computed by taking the difference between the reference antenna Doppler with clean data without interference and beamformed data in the presence of interference. The Doppler RMSE errors, PLI and C/N_0 gain for different PRNs are shown in Table 6-8. These values are computed from the tracking results in the presence of interference. The RMSE Doppler errors are slightly higher for MPDR than single antenna with interference. This could be due to the residual phase errors from the calibration. For all the PRNs, PLL was able to maintain lock even in the presence of interference.

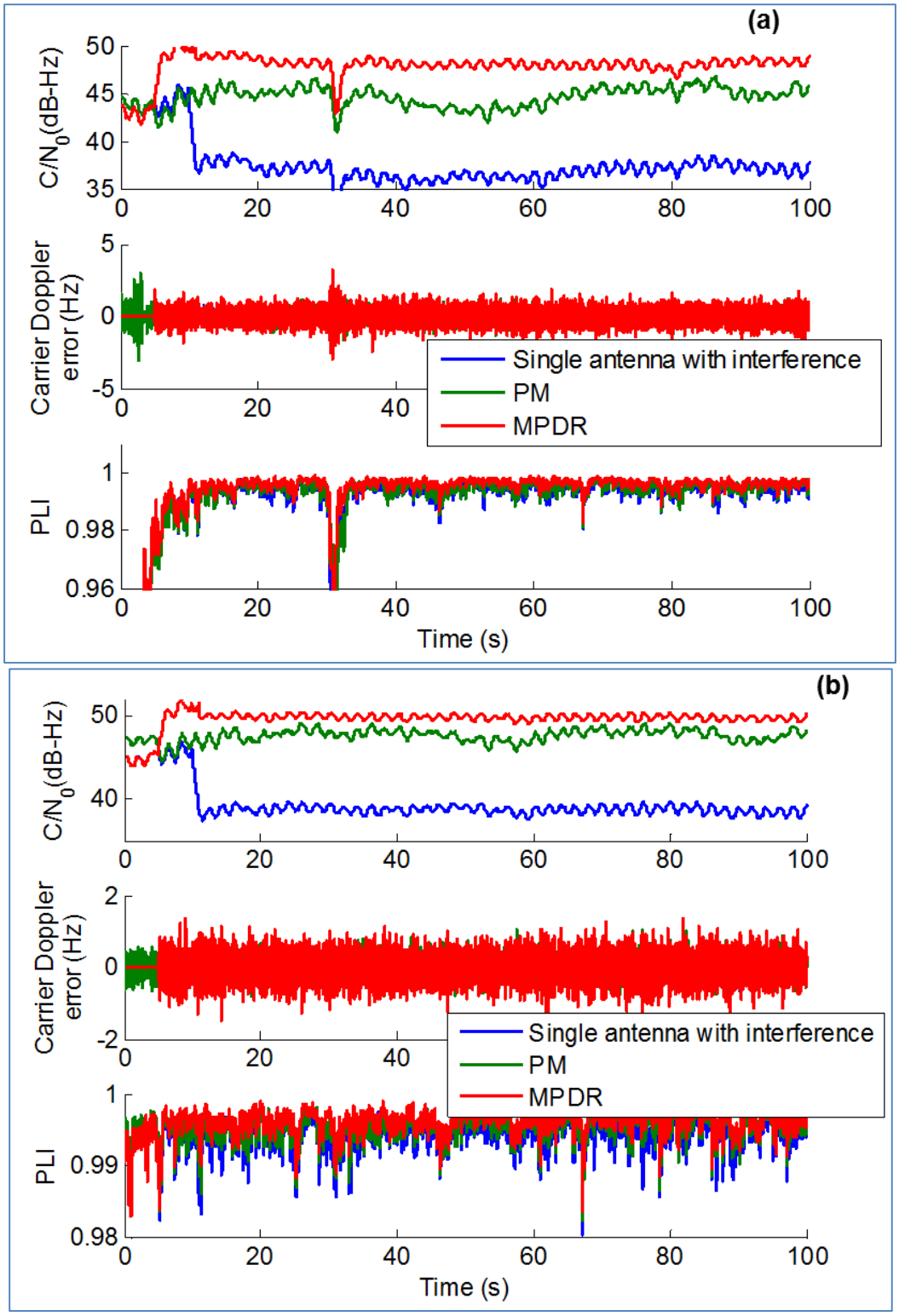

Figure 6-11: Tracking performance of PRN 4 and PRN 28 with power minimization and MPDR beamformer using actual data

Table 6-8: Tracking performance of different PRNs with power minimization and MPDR in the presence of chirp interference

PRN	Single antenna with interference			Power minimization			MPDR		
	RMSE Doppler error (Hz)	Mean PLI	Mean C/N_0 (dB-Hz)	RMSE Doppler error (Hz)	Mean PLI	Mean C/N_0 (dB-Hz)	RMSE Doppler error (Hz)	Mean PLI	Mean C/N_0 (dB-Hz)
PRN 1	0.98	0.98	34.1	0.43	0.99	44.9	0.66	0.99	46.5
PRN 4	0.97	0.98	36.7	0.45	0.99	44.7	0.49	0.99	48.1
PRN 11	0.91	0.97	37.6	0.45	0.99	46.8	0.31	0.99	49.1
PRN 13	0.89	0.97	37.5	0.45	0.99	48.2	0.28	0.99	50.9
PRN 15	0092	0.97	33.8	0.85	0.99	43.4	0.64	0.99	48.6
PRN 17	0.92	0.97	38.2	0.28	0.99	45.5	0.47	0.99	47.7
PRN 28	0.92	0.97	38.7	0.23	0.99	47.7	0.34	0.99	49.8
PRN 30	0.98	0.99	41.1	0.60	0.99	44.7	0.29	0.99	52.7

6.4.2 Measurement domain analysis

The measurements generated by the interference free reference antenna data acts as reference measurements in this case. Differences between these measurements and those generated after beamforming were compared for power minimization and MPDR. The resulting time series plot of the pseudorange and carrier phase measurement errors are shown in Figure 6-12. In the case of power minimization, there are abrupt errors in both pseudorange and carrier phase measurements. Therefore, error statistics were computed without considering these large errors. Pseudorange biases up to 2 m are observed in both power minimization and MPDR beamformers. However, the biases

observed are different for different PRNs. Carrier phase biases are minimal (less than 0.1 mm) with MPDR beamformer for all PRNs, which agrees with the simulation results. With power minimization, different biases are observed for different PRNs as seen from Figure 6-12 (a) and they reach 1.5 cm. The results with power minimization also agree with simulation results where different biases were observed for different PRNs. Pseudorange and carrier phase biases of different PRNs are provided in Tables 6-9 and 6-10.

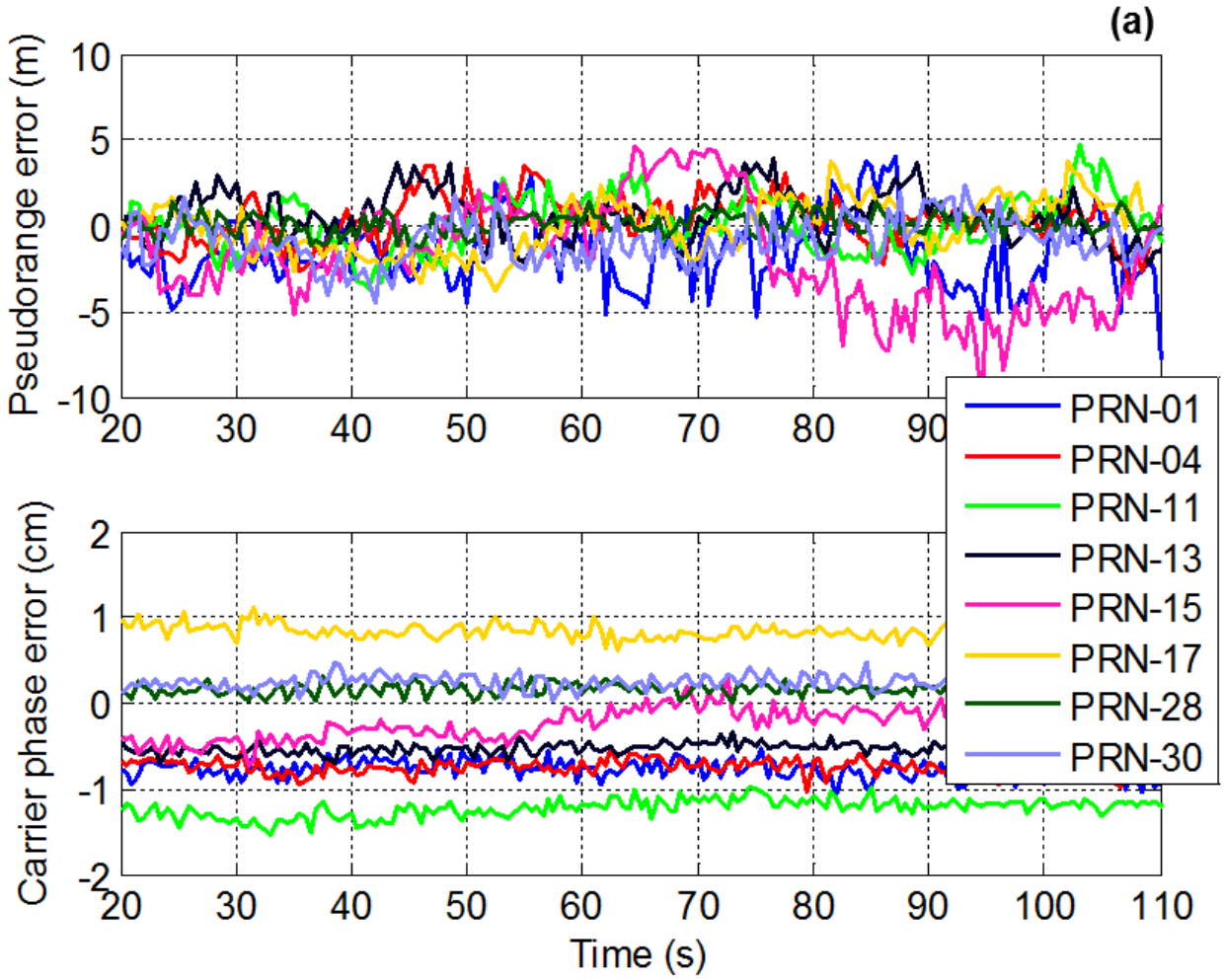

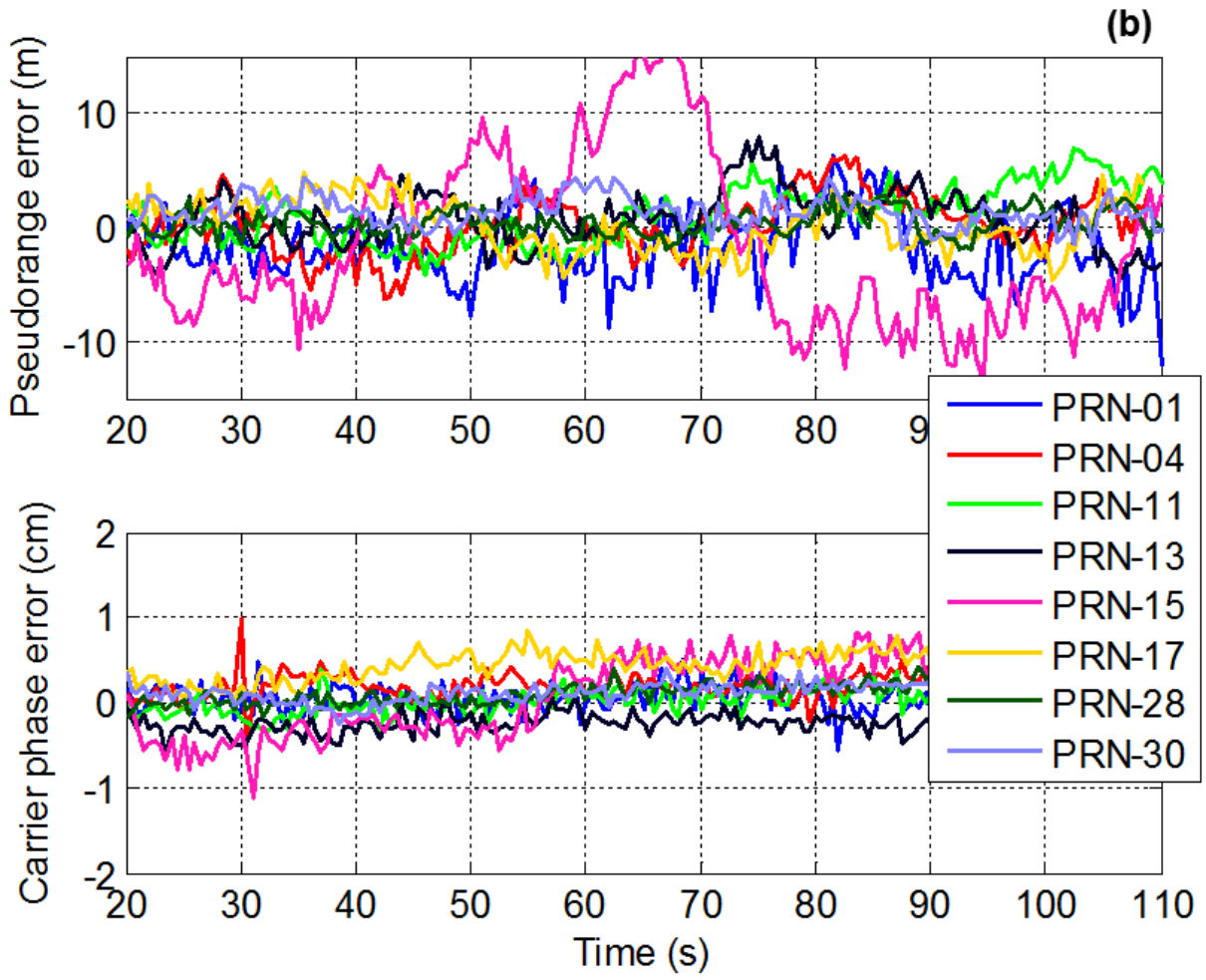

Figure 6-12: Pseudorange and carrier phase measurement errors for power minimization and MPDR with actual data

Table 6-9: Pseudorange measurement errors for PM and MPDR with chirp interference

PRN	PM		MPDR	
	Mean (m)	Std (m)	Mean (m)	Std (m)
PRN 1	-1.42	1.94	-1.71	2.92
PRN 4	0.34	1.32	0.26	2.40
PRN 11	0.22	1.49	1.27	2.42
PRN 13	0.48	1.33	0.47	2.38
PRN 15	-1.05	3.31	-0.55	3.21
PRN 17	-0.06	1.48	0.24	2.01
PRN 28	-0.01	0.69	0.29	1.11
PRN 30	-0.69	1.31	1.12	1.35

Table 6-10: Carrier phase measurement errors using PM and MPDR with chirp interference

PRN	PM		MPDR	
	Mean (mm)	**Std(mm)**	**Mean(mm)**	**Std(mm)**
PRN 1	-7.3	2.0	0.3	1.6
PRN 4	7.1	1.7	0.9	2.0
PRN 11	-10.9	3.8	0.2	1.4
PRN 13	-5.0	1.3	-0.8	1.3
PRN 15	-2.3	1.8	1.0	1.7
PRN 17	8.2	1.9	0.5	2.1
PRN 28	1.6	0.8	0.9	1.1
PRN 30	2.3	1.1	0.5	1.5

6.4.3 Position domain analysis

Carrier phase based positioning was performed using RTKLib open source software. The position errors using power minimization and MPDR are shown in Figure 6-13 and the error statistics in Table 6-11. MPDR is able to provide fixed solutions as seen from Figure 6-13. However, power minimization was not able to provide fixed solution and errors upto 1 m are observed.

Table 6-11: Carrier phase based position errors with actual data

Position errors	**Power minimization**		**MPDR**	
	Mean	Standard deviation	Mean	Standard deviation
East error (cm)	-63.4	36.2	-0.04	0.08
North error (cm)	104.5	65.0	-0.25	0.06
Height error (cm)	-5.09	78.6	-0.06	0.16

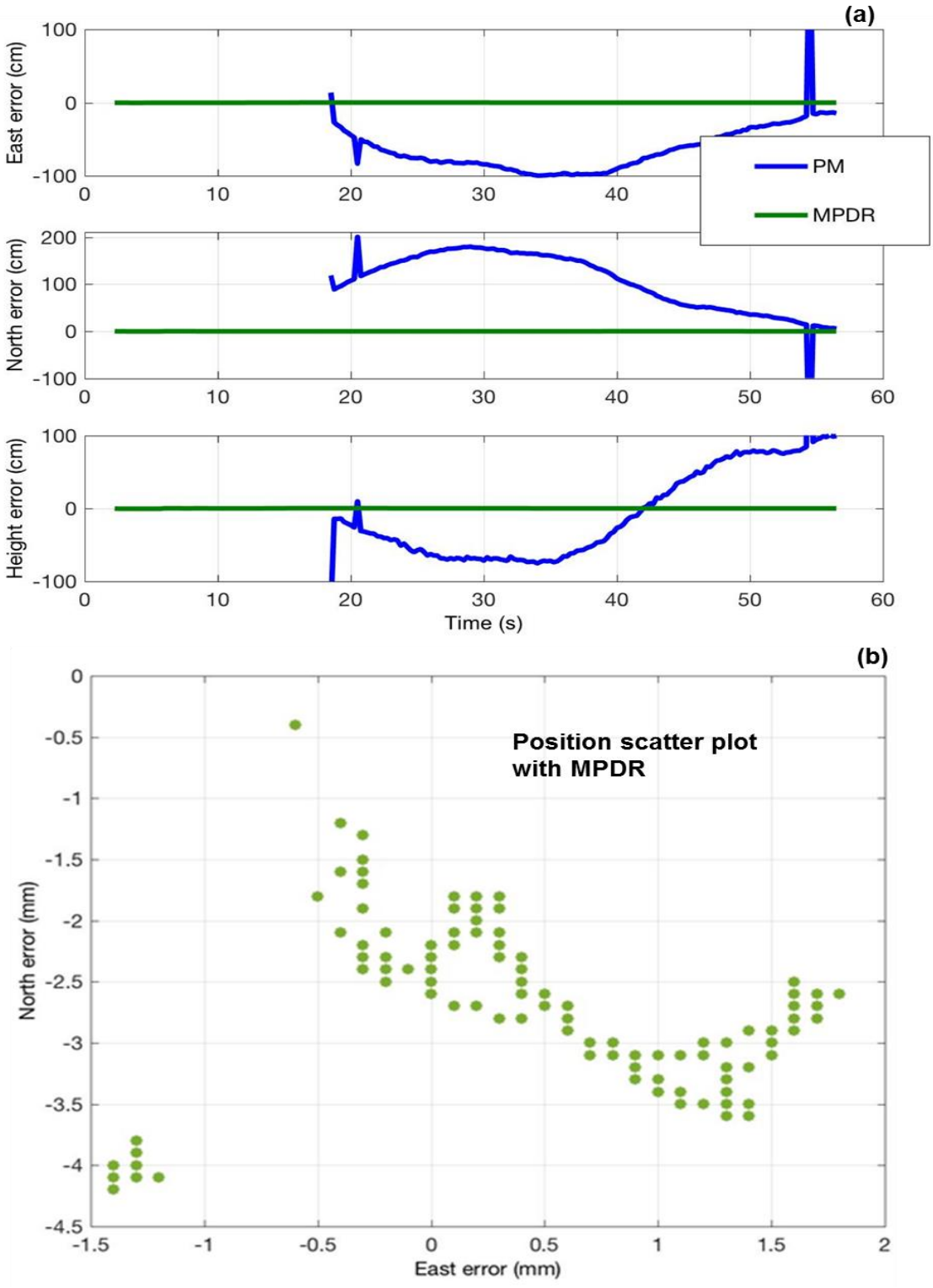

Figure 6-13: Carrier phase based position errors with actual data using power minimization and MPDR

6.5 Summary

This chapter investigated the performance of a multi-antenna GNSS receiver in different electronic interference scenarios. The receiver performance in terms of tracking, measurement distortions and position distortions was analyzed for power minimization and MPDR. A number of GPS signal simulations with different interference sources was performed to evaluate measurement distortions. It was observed that MPDR induced measurement distortions were very minimal (less than mm for carrier phase and few cm for pseudorange measurements) in the simulations. With actual data, carrier phase measurement biases were minimal and pseudorange measurement errors up to 2 m were observed. However, with power minimization, pseudorange biases up 50 cm were observed in the simulations and up to 2 m with actual data. Carrier phase measurement biases up to few cm were observed with power minimization in both simulations and actual data processing. The biases observed were different for different PRNs. Carrier phase positioning performance with MPDR was better than power minimization; the latter was unable to provide fixed solutions. With power minimization, position errors up to 10 cm were observed in simulations and up to 1 m with actual data.

Chapter Seven: CONCLUSIONS AND RECOMMENDATIONS

Based on the results and analyzes provided in the previous chapters, the following conclusions are made. Recommendations for future work are then presented.

7.1 Conclusions

The main motivation for this research was to analyze and characterize the performance of antenna array based GNSS receivers under different interference conditions. Conclusions are provided in terms of four major topics discussed in the previous chapters. These are multi-antenna GNSS signal simulator, performance of antenna array based GNSS receivers under multipath conditions, antenna array calibration in multipath environments and performance of antenna array based GNSS receivers under electronic interference.

7.1.1 Multi-antenna GNSS signal simulator

A novel method of simulating multi-antenna GNSS signals was provided in Chapter 3. From the results presented, the following points can be made:

1. The proposed simulation method can be used to generate single antenna as well as multi-antenna GNSS signals affected by interference.
2. The simulated multi-antenna signals can be used to characterize the performance of different spatial processing techniques in antenna array based GNSS receivers. This includes applications such as antenna array calibration, controlled reception

pattern antenna applications under different electronic interference, characterization of measurement distortions, etc.

3. From the positioning results presented, it can be concluded that this multi-antenna software simulator can be a good choice for high performance carrier phase based positioning application performance analysis.

7.1.2 Performance of multi-antenna GNSS receivers under multipath conditions

Based on the results from the simulations and actual data collections in multipath environments, the following conclusions can be made regarding the performance of antenna array based GNSS receivers:

1. The numerical simulation results showed that performance of MPDR and MPDRSS beamformers improves as the correlation between LOS and multipath signals decreases.
2. It was observed through numerical simulations that for a rectangular array with six antenna elements, the MPDRSS beamformer provides better multipath mitigation than MPDR. It was also observed that MPDRSS performance was better for higher elevation satellites. As only six antenna elements were used, only one spatial smoothing can be performed. Due to this, the decorrelation obtained for low elevation satellites is not sufficient to provide better multipath mitigation.
3. Using the simulated GPS signals, it was observed that pseudorange errors can be reduced by up to tens of metres in high multipath environments, thereby improving position accuracy. The MPDRSS beamformer was found to perform better than the MPDR and DAS beamformers.

4. Using the simulated signals, it was also shown that carrier phase multipath can be reduced significantly employing an antenna array. Even in the case of carrier phase multipath, MPDRSS performance was better than MPDR and DAS beamformers.
5. With actual GPS L1 signals collected in a moderate specular multipath scenario, a reduction of 10 m in RMS pseudorange error was observed for satellites affected by multipath signals. Pseudorange error reduction was reflected in the position solutions, with easting errors reduced by 8 m and height errors reduced by 10 m.
6. Finally, it was shown that a practically realizable six-antenna rectangular array is effective to mitigate short-range multipath signals and provide an improved navigation solution, based on the data used in the analysis.

7.1.3 Performance of antenna array calibration in multipath environments

1. It was shown that GNSS antenna array calibration using live signals is challenging in multipath environments because the latter induce significant gain and phase errors in the calibration parameters.
2. It was observed that the errors in the relative phases between the antenna elements are periodic with zero mean. Based on this observation a method was proposed to improve the estimation of the measured steering vector which is being used in the calibration.
3. It was proposed that averaging the relative phase measurements over several multipath cycles improves the estimation of measured steering vector. By using

this improved steering vector in the calibration process, the calibration parameter errors can be reduced.

4. The periodicity of the errors in the relative phase measurements were shown through simulation and actual data collected in specular multipath conditions. In high multipath environments, these measurements may not be periodic. However, the errors in the measurements will be zero mean.
5. It was shown by processing the actual data that by employing the averaging method, the calibration can be improved, as shown through the improvement in DOA estimation.

7.1.4 Performance of multi-antenna GNSS receivers under electronic interference conditions

An extensive analysis of the array based GNSS receiver used herein under electronic interference conditions was performed and based on the results, the following conclusions can be made:

1. Improved tracking performance was observed in terms of Doppler estimation after beamforming. The tracking performance of MPDR was better than power minimization.
2. For single interference scenarios, it was observed that the interference type has no effect on tracking, measurement and position errors after beamforming.
3. Through GPS signal simulations, it was observed that MPDR does not significantly distort the measurements. However, power minimization induces more distortions in the code and carrier phase measurements.

4. It was also shown that satellites that are in the direction of the interference suffer more distortions in both code and carrier phase measurements than other satellites.
5. After MPDR beamforming, carrier phase integer ambiguities could be resolved and fixed ambiguity solutions could be provided. However, with power minimization, ambiguity resolution was not successful using actual and simulated data.
6. Based on the results obtained, for high precision applications, MPDR beamforming is a better option albeit with higher implementation complexity.

7.2 Recommendations

Recommendations for future work are as follows:

1. Even though the proposed multi-antenna signal simulator can be used for different user scenarios such as static and dynamic, the results presented in the current research were limited to static user. Few tests for validating dynamic user scenarios were carried out. However, extensive testing should be performed to evaluate the simulator functionality.
2. While simulating multipath signals, reflectors with smooth surfaces were considered. It would be interesting to verify the multipath simulations for different reflector surfaces and incorporating a method to model the attenuation factor of the multipath signals. Also, work can be extended to incorporate different multipath models.

3. Spoofing is another type of interference which also affects the receiver performance. The proposed software simulator can be extended to simulate spoofing signals in a controlled environment.
4. The multipath mitigation performance was analyzed for a static user. In the case of a moving user, further decorrelation between the LOS and multipath signals can be obtained which would improve beamformer performance.
5. The performance was evaluated by collecting actual data in specular multipath conditions. The developed receiver software incorporating different beamforming techniques could also be tested in high multipath conditions such as semi-urban environments.
6. Carrier phase multipath has been evaluated in terms of reduction in measurement errors. This could be extended to the position domain and the suitability of antenna array based GNSS receivers for high precision applications (in multipath environments) could be evaluated.
7. In Chapter 5, the array calibration was performed considering only a single satellite affected by multipath. However, in actual environments, many satellites will be affected by multipath. The proposed method could be tested by taking multiple satellites into consideration. For the analysis only specular multipath conditions were considered. Further tests could be performed by collecting data in more complex multipath environments.
8. In Chapter 6, only single interference scenarios were considered to evaluate the performance of the antenna array based GNSS receiver. This could be extended to multiple interference scenarios. For the actual data, interference was added

through software script. It would be interesting to assess performance with data collected in actual interference conditions. Also, carrier phase tracking performance and RTK positioning performance require additional investigations using real data.

9. In all the tests, for measuring the attitude of the array, a high-grade Novatel SPAN LCI system which has gyro performance of 1 degree/hour (in-run bias drift) was used as it was readily available and easy to incorporate in test set-up. However, the feasibility of using other quality MEMS sensors with different in-run bias drifts could also be investigated to reduce cost.

References

Allen, B. and M. Ghavami (2005). *Adaptive Array Systems Fundamentals and Applications*. John Wiley & Sons, Ltd, ISBN 0-470-86189-4.

Amin, M.G., X. Wang, Y. D. Zhang, F. Ahmad, and E. Aboutanios (2016) "Sparse Arrays and Sampling for Interference Mitigation and DOA Estimation in GNSS," in *Proceedings of the IEEE* , vol.PP, no.99, pp.1-16.

Amin, M.G. and W. Sun (2005) "A novel interference suppression scheme for global navigation satellite systems using antenna array", in *IEEE Journal on Selected Areas in Communications*, vol. 23, no. 5. pp. 999-1012, May 2005. doi: 10.1109/JSAC.2005.845404

Anantharamu, P. B., D. Borio, and G. Lachapelle (2012) "Self-Contained Antenna Array Calibration using GNSS Signals", in *NAVIGATION, Journal of The Institute of Navigation*, Vol. 59, No. 3, Fall 2012, pp. 209-220.

Arribas, J., P. Closas, and C. Fernández-Prades (2014) "Interference mitigation in GNSS receivers by array signal processing: A software radio approach" in *2014 IEEE 8th Sensor Array and Multichannel Signal Processing Workshop (SAM)*, A Coruna, 2014, pp. 121-124.

Arribas, J., C. Fernandez-Prades, and P. Closas (2013) "Antenna Array Based GNSS Signal Acquisition for Interference Mitigation" in *IEEE Transactions on Aerospace and Electronic Systems*, vol. 49, no. 1, pp. 223-243, Jan. 2013.

Backén, S., D. M. Akos, and M. L. Nordenvaad (2008) “Post-processing Dynamic GNSS Antenna Array Calibration and Deterministic Beamforming” in *Proceedings of the 21st*

International Technical Meeting of the Satellite Division of The Institute of Navigation (ION GNSS 2008), Savannah, GA, USA, 16–19 September 2008; pp. 2806–2814.

Balai, A. T., A. G. Dempster, and L. L. Presti (2009) "Characterization of the Effects of CW and Pulse CW Interference on the GPS Signal Quality," in *IEEE Transactions on Aerospace and Electronic Systems*, Vol. 45, October 2009, pp. 1418 - 1431.

Bauernfeind, R. and B. Eissfeller (2014) “Softwrare-Defined Radio based Roadside Jammer Detector: Architecture and Results,” *2014 IEEE/ION Position, Location and Navigation Symposium - PLANS 2014*, Monterey, CA, 2014, pp. 1293-1300. doi: 10.1109/PLANS.2014.6851504

Bauernfeind, T. Kraus, A. S. Ayaz, D. Dotterbock, and B. Eissfeller (2012), “Analysis, Detection and Mitigation of Incar GNSS Jammer Interference in Intelligent Transport Systems,” in Deutsche Gesellschaft fur Luft-und Raumfahrt-Lilienthal-Oberth eV, 2013.

Borre, K. and D.Akos (2005) "A Software-Defined GPS and Galileo Receiver:Single-Frequency Approach," in *Proc.of the Institute of Navigation GNSS 18th. International Technical Meeting of the Satellite Division*, Long Beach,CA,Sept.13-16,2005, pp.1632-1637.

Braasch, M. S. (1996) “Multipath Effects,” [Chapter 14] in Global Positioning Systems: Theory and Applications, American Institute of Aeronautics and Astronautics, Vol. 1, Chapter 14, pp. 547-568.

Broumandan, A., A. Jafarnia-Jahromi, S. Daneshmand, and G. Lachapelle (2016), "Overview of Spatial Processing Approaches for GNSS Structural Interference Detection and Mitigation," in *Proceedings of the IEEE* , vol. 104, no. 6, pp. 1246-1257, June 2016. doi: 10.1109/JPROC.2016.2529600

Brown, A. (2000) "Multipath Rejection Through Spatial Processing" in *Proceedings of the 13th International Technical Meeting of the Satellite Division of The Institute of Navigation (ION GPS 2000)*, pp. 2330-2337, Salt Lake City, UT.

Borio, D., L. Camoriano, and L. Lo Presti (2008) “Two Pole and Multi Pole Notch Filters: A Computationally Effective Solution for GNSS Interference Detection and Mitigation,” in *IEEE Systems Journal*, Vol. 2, No. 1, pp. 38-47.

Bu-hong, W. (2004) "Array Calibration in the presence of multipath based on CODE Criterion”, in *International Symposium on Antennas and Propagation*, Vol 1, pp 439-442, June 2004.

Burns, J. R., C. Cutright, and M. Braasch (2002) "Investigation of GPS Software Radio Performance in Combating Narrow Band Interference", in *ION 58 Annual Meeting/CIGTF 21 Guidance Test Symposium*, Albuquerque, NM, pp.523-530.

G. Carrié, F. Vincent, T. Deloues, D. Pietin, and A. Renard (2005) “A new blind adaptive antenna array for GNSS interference cancellation,” in *Proceedings of 39th Asilomar Conference, Signals, Systems, Comput.*, Pacific Grove, CA, USA, Oct. 28–Nov. 1, 2005, pp. 1326–1330. doi: 10.1109/ACSSC.2005.1599978

Chen, Y., J. Juang, J. Seo, S. Lo, D. Akos, D. De Lorenzo, and Enge, P. (2012) "Design and Implementation of Real-Time Software Radio for Anti-Interference GPS/WAAS Sensors" in *Sensors* 2012, 12, pp. 13417-13440.

Chuang, Y. and I.J. Gupta (2013) "Antenna Induced Biases in GNSS Receiver Measurements" in *Proceedings of the 2013 International Technical Meeting of The Institute of Navigation*, pp. 164-171, January 2013, San Diego, California.

Chuang, Y., M. Buchanan, A. O'Brien, and I.J. Gupta (2014) "Prediction of Antenna Induced Biases for Precision GNSS Receivers" in *Proceedings of the 2014 International Technical Meeting of The Institute of Navigation*, pp. 898-903, San Diego, California.

Church, C. M. and I.J. Gupta (2009) "Estimation of Adaptive Antenna Induced Code and Carrier Phase Bias in GNSS Receivers" in *NAVIGATION, Journal of The Institute of Navigation*, 56.3, 151-160.

Church, C. M., I.J. Gupta, and A. O'Brien (2007) "Adaptive Antenna Induced Biases in GNSS Receivers" in *Proceedings of the 63rd Annual Meeting of The Institute of Navigation*, pp. 204 - 212, Cambridge, MA.

Citron, T. and T. Kailath (1984) "An improved eigenvector beamformer. IEEE International Conference onAcoustics, Speech, and Signal Processing", in *ICASSP 84,* pp. 718-721, San Diego, CA.

Cuntz, M., A. Konovaltsev and M. Meurer (2016) "Concepts, Development, and Validation of Multiantenna GNSS Receivers for Resilient Navigation," in *Proceedings of the IEEE* , vol.PP, no.99, pp.1-14.

Daneshmand, S. (2013) *GNSS Interference Mitigation Using Antenna Array Processing,* PhD Thesis, Department of Geomatics Engineering, University of Calgary, Canada (Available at http://plan.geomatics.ucalgary.ca).

Daneshmand, S., N. Sokhandan, M. Zaeri-Amirani, and G. Lachapelle (2014) "Precise Calibration of a GNSS Antenna Array for Adaptive Beamforming Applications", in *Sensors* 14.6(2014): 9669-9691.

de Bakker, P. F. (2007) *Effects of Radio Frequency Interference on GNSS Receiver Output,* Masters Thesis, Faculty of Aerospace Engineering, Delft University of Technology, Netherlands (Available at http://www.tudelft.nl/fileadmin/Faculteit/ CiTG/Over_de_faculteit/Afdelingen/Afdeling_Geoscience_and_Remote_Sensing/MSc_theses/de_bakker07_msc.pdf)

De Jong, Y. and M. Herben (1999) "High-resolution angle-of-arrival measurement of the mobile radio channel" in *IEEE Transactions on Antennas and Propagation*, 47, 1677-1687.

De Lorenzo, D., S. C. Lo, P. K. Enge, and J. Rife (2011) “Calibrating adaptive antenna arrays for high-integrity GPS,” in *GPS Solutions*, vol. 16, no. 2, pp. 221–220, Apr. 2011

De Lorenzo, D., J. Rife, P. Enge, and D. Akos (2006) "Navigation Accuracy and Interference Rejection for an Adaptive GPS Antenna Array" in *Proceedings of the 19th International Technical Meeting of the Satellite Division of The Institute of Navigation (ION GNSS 2006)*, pp. 763-773, Fort Worth, TX.

De Lorenzo, D., J. Gautier, J. Rife, P. Enge,and D. Akos (2005) "Adaptive Array Processing for GPS Interference Rejection". in *Proceedings of the The Institute of Navigation*, 13-16 September, Long Beach CA, pp. 618-627, US, Institute of Navigation.

Dong, L. (2003) *IF GPS Signal Simulator Development and Verification*, M.Sc. Thesis, UCGE 20184 (URL: http://www.geomatics.ucalgary.ca/links/GradTheses.ht ml).

Dovis, F. (Ed.) (2015) *GNSS Interference Threats and Countermeasures,* Artech House, Boston, USA, ISBN-13: 978-1-60807-810-3.

Evans, J., J. Johnson, and D. Sun (1982) "Application of advanced signal processing techniques to angle of arrival estimation in ATC navigation and surveillance systems", Technical Report, M.I.T. Lincoln Laboratory, Lexington, Massachusetts.

Fernández-Prades,C., J. Arribas, and P. Closas (2016) “Robust GNSS Receivers by Array Signal Processing: Theory and Implementation”, In *Proceedings of the IEEE*, vol. 104, no. 6, pp. 1207-1220, June 2016. doi: 10.1109/JPROC.2016.2532963

Fernández-Prades, C., P. Closas, and J. Arribas (2011) "Eigenbeamforming for interference mitigation in GNSS receivers" in *International Conference on Localization and GNSS 2011,* pp. 93 - 97, Tampere.

Garlin, L., F. van Digelen, and J.M. Rousseau (1996) "Strobe and Edge Correlaor Multipath Mitigation for COde," in *Proceedings of the Proceedings of the 9th International Technical Meeting of the Satellite Dicision of The Institute of Navigation*, , Kansas City, MO, pp. 657-664.

Giordanengo, G. (2009) *Impact of Notch Filtering on Tracking Loops for GNSS Applications*, Master Thesis, Facoltà di Ingegneria dell'infromazione, Politecnico di Torino (Available at http://plan.geomatics.ucalgary.ca).

Gupta,I.J., I. M. Weiss and A. W. Morrison (2016), "Desired Features of Adaptive Antenna Arrays for GNSS Receivers," in *Proceedings of the IEEE* , vol. 104, no. 6, pp. 1195-1206, June 2016. doi: 10.1109/JPROC.2016.2524416

GPS-ICD (2013) *Navstar GPS Space Segment/Navigation User Interfaces*, Interface Specification, IS-GPS-200H. ICD. Retrieved from http://www.gps.gov/technical/icwg/IS-GPS-200H.pdf

Groves, P. D., Z. Jiang, M. Rudi, and P. Strode (2013), “A Portfolio Approach to NLOS and Multipath Mitigation in Dense Urban Areas”, in *Proceeding of ION GNSS 2013*, September 16-20, Nashville, TN, Institute of Navigation.

Haber, F. and M. Zoltowski (1986) "Spatial spectrum estimation in a coherent signal environment using an array in motion" in *IEEE Transactions on Antennas and Propagation*, vol. 34, no. 3, pp. 301-310, Mar 1986. doi: 10.1109/TAP.1986.1143831

Hu, Y., D. Yang, Y. Zhang, and Q. Zhang (2009) "Development of a software-based IF GPS signal simulator**"** in Proceedings of the SPIE, The International Society for Optical Engineering, vol. 7651, December 2009.

Irsigler, M. and B. Eissfeller (2003) “Comparison of multipath mitigation techniques with consideration of future signal structures,” in *Proceedings of the 16th International Technical Meeting of the Satellite Division of the Institute of Navigation*, 9-12 September, Portland OR, USA pp. 2584–2592

Joosten, P., T. Pany, and J. Winkel (2002) "The impact of unmodelled multipath on ambiguity resolution," in *Proceedings of the Proceedings of the 15th International Technical Meeting of the Satellite Division of The Institute of Navigation (ION GPS 2002)*, , Oregon Convention Center, Portland, OR, pp. 953 – 961

Julien, O., B. Zheng, L. Dong, and G. Lachapelle (2004), "A Complete Software-Based IF GNSS Signal Generator for Software Receiver Development", in *Proceedings of the ION GNSS 17th International Technical Meeting of the Satellite Division*, Long Beach, California, USA, pp. 2146-2157, September 21-24, 2004

Kalyanaraman, S. K. and M.S. Braasch (2010) "GPS Adaptive Array Phase Compensation Using a Software Radio Architecture" in *NAVIGATION, Journal of The Institute of Navigation*, vol. 57, No. 1 Spring 2010, pp. 53-68.

Kamel, A.M., V. Renaudin, J. Nielsen and G. Lachapelle (2013) "INS Assisted Fuzzy Tracking Loop for GPS-Guided Missiles and Vehicular Applications," in *International Journal of Navigation and Observation*, 2013, pp.1-17.

Kaplan, E. D. and C. J. Hegarty (2006) *Understanding GPS - Principles and Applications*, Artech House, Inc, Norwood, USA.

Kappen, G., C. Haettich, and M. Meurer (2012) "Towards a robust multi-antenna mass market GNSS receiver" in *Proceedings of the 2012 IEEE/ION Position Location and Navigation Symposium (PLANS)*, Myrtle Beach, SC, USA, 23–26 April 2012; pp. 291–300.

Kim, U. S., D. De Lorenzo, D. Akos, J. Gautier, P. Enge,and J. Orr (2004) "Precise phase calibration of a controlled reception pattern GPS antenna for JPALS" in *Position Location and Navigation Symposium*, PLANS 2004 (pp. 478-485). IEEE.

Kim, J.W., Dong-Hwan Hwang, and S.J. Lee (2007) "Performance Evaluation of INS Velocity-Aided Tracking Loop and Deeply Coupled GPS/INS Integration System in Jamming Environment," in *ION 63rd Annual Meeting*, April 23-25, 2007, Cambridge, Massachusetts pp.742–748.

Konovaltsev, A., M. Cuntz, L. Greda, M. Heckler, and M. Meurer (2010) “Antenna and RF front end calibration in a GNSS array receiver,” in *Proc. IEEE Intl. Microwave Workshop Series on RF Front-ends for Software Defined and Cognitive Radio Solutions*, Aveiro, Portugal, Feb. 2010, pp 1-4. doi: 10.1109/IMWS.2010.5440984

Lambert, J. R., C. A. Balanis and D. DeCarlo (2009), "Spherical Cap Adaptive Antennas for GPS," in *IEEE Transactions on Antennas and Propagation*, vol. 57, no. 2, pp. 406-413, Feb. 2009. doi: 10.1109/TAP.2008.2011219

Landry, R. J. and A. Renard (1997) "Analysis of Potential Interference Sources And Assessment of Present Solutions For GPS/GNSS Receivers," in *Proceedings of the 4th International Conference on Integrated Navigation Systems*, 26-28 May, St. Petersburg, 13 pages

Leshem, A. and M. Wax (2000), “Array Calibration in the Presence of Multipath”, in *IEEE Transactions on Signal Processing*, Vol 48, No 1, January 2000.

Lau, L. and P. A. Cross (2007) "Development and testing of a new rigorous ray tracing approach to GNSS carrier phase multipath modelling" in *Journal of Geodedy*, 81(11), 713–732. doi:10.1007/s00190-00007-00139-z.

Li, M., A. G. Dempster, A. T. Balaei, C. Rizos, and F. Wang (2011) “Switchable beam steering/null steering algorithm for CW interference mitigation in GPS C/A code receivers,” in *IEEE Trans. Aerosp. Electron. Syst.*, vol. 47, no. 3, pp. 1564–1579, Jul. 2011, doi: 10.1109/TAES.2011.5937250.

Lorenz, R. G. and S. P. Boyd (2006) “Robust minimum variance beamformer,” in *Robust Adaptive Beamforming,* J. Li and P. Stoica, Eds. Hoboken, NJ, USA: Wiley, 2006 ch. 1, pp. 1–46

McGraw, G. A. and M. S. Braasch (1999) “GNSS multipath mitigation using gated and high resolution correlator concepts,” in *Proceedings of the The National Technical Meeting of the Satellite Division of the Institute of Navigation*, 25-27 January, San Diego CA, USA, pp. 333-342

Misra, P. and P. Enge (2001) *Global Positioning System - Signals, Measurements, and Performance*, Ganga-Jamuna Press, Lincoln, USA

Moelker, D.J. (1998) *Interference in satellite navigation and mobile communication, Dissertation*, TU Delft, http://repository.tudelft.nl/view/ir/uuid%3A93c5f66e-71c8- 4dc1-841c-9ab5426fbb8d/, last accessed November 07, 2015

Montloin, L. (2010) *Impact of Interference Mitigation Techniques on a GNSS Receiver,* Memoire de fin d'Etudes, Ecole Nationale de l'Aviation Civile, Toulouse.

Morton, Y.T., L. L. Liou, D.M. Lin, J.B. Tsui, and Q. Zhou (2004) "Interference Cancellation Using Power Minimization and Self-coherence Properties of GPS Signals" in *Proceedings of the 17th International Technical Meeting of the Satellite Division of The Institute of Navigation (ION GNSS 2004)*, pp. 132-143, Long Beach, CA.

P. S. Naidu, *Sensor Array Signal Processing*, 2012, CRC Press, ISBN: 978-1-4200-7190-0.

NAVSYS Corporation, “White paper—High gain advanced GPS receiver,” 2002. Available at: http://www.navsys.com/ Papers/HAGR_White_Paper.pdf, Accessed June. 30, 2016

Ndili, A. and P. Enge (1998) “GPS Receiver Autonomous Interference Detection,” in *IEEE Position, Location and Navigation Symposium - PLANS’98*, April, Palm Springs, California, pp. 123-130.

Novatel. (1994). GPSAntenna Model 501. Datasheet, Novatel 501 antenna series, Novatel. Retrieved from http://www.novatel.com/assets/Documents/Manuals/om-20000001.pdf.

Parkinson, B. W. and J. J. Spilker Jr. (1996) Global Positioning System: Theory and Applications Volume I, American Institute of Aeronautics and Atronautics, Inc, Washington, USA, ISBN 1-56347-106-X.

Paulraj, A., V. Reddy, and T. Kailath (1987) "Analysis of Signal Cancellation Due To Multipath in Optimum Beamformers for Moving Arrays" in *IEEE Journal of Oceanic Engineering*, 12, 163-172.

Petovello, M. G., C. O'Driscoll, G. Lachapelle, D. Borio, and H. Murtaza (2008) "Architecture and Benefits of an Advanced GNSS Software Receiver" in *International Symposium on GPS/GNSS 2008*, November 11-14, Tokyo, Japan.

Pillai, S. and B. Kwon (1989) "Forward/backward spatial smoothing techniques for coherent signal identification" in *IEEE Transactions on Acoustics, Speech and Signal Processing*, vol. 37, pp. 8-15.

Rao, B. R. (2013). *GPS/GNSS antennas*. Boston: Artech House, ISBN-13: 978-1-59693-150-3.

Ray, J.K., M. E. Cannon, and P. Fenton (2001) "GPS code and carrier multipath mitigation using a multiantenna system" in *IEEE Transactions on Aerospace and Electronic Systems*, vol. 37, No. 1, pp 183-195, Jan 2001. doi: 10.1109/7.913677

Reddy, V., Paulraj, A., & Kailath, T. (1987) "Performance Analysis of the Optimum Beamformer in the Presence of Correlated Sources and Its Behavior Under Spatial Smoothing" in *IEEE Transactions on Acoustics, Speech, and Signal Processing,* vol. 35, no. 7, pp. 927-936, Jul 1987. doi: 10.1109/TASSP.1987.1165239

Rougerie, S., G. Carrie, F. Vincent, L. Ries, and M. Monnerat (2012) “A New Multipath Mitigation Method for GNSS Receivers Based on an Antenna Array,” in *International Journal of Navigation and Observation*, Hindawi Publishing Corporation, Vol. 2012, Article ID 804732

Sahmoudi, M. and M. G. Amin (2007) "Optimal Robust Beamforming for Interference and Multipath Mitigation in GNSS Arrays" in *IEEE International Conference on Acoustics, Speech and Signal Processing -ICASSP '07*, 2007, pp. III-693 - III-696, Honolulu. doi: 10.1109/ICASSP.2007.366774

Seco-Granados, G. and J. Fernandez Rubio, (1997) "Multipath and Interference Errors Reduction in GNSS by Joint pseudorange measurement and array beamforming" in *GNSS'97, First European Symposium on Global Navigation Satellite Systems*, 1997, April 21-25 , pp. 606-614, Munich, Germnany.

Seco-Granados, G., J. Fernandez-Rubioand C Fernández-Prades (2005) "ML estimator and hybrid beamformer for multipath and interference mitigation in GNSS receivers" in *IEEE Transactions on Signal Processing*, vol. 53, no. 3, pp. 1194-1208, March 2005. doi: 10.1109/TSP.2004.842193

Sgammini,M., F. Antreich, M. Meurer, L. Kurz, and T.G. Noll (2012) "Blind adaptive beamformer based on orthogonal projections for GNSS", in *Proceedings of the 25th International Technical Meeting of The Satellite Division of the Institute of Navigation (ION GNSS 2012),* Nashville, TN, September 2012, pp. 926-935.

Shan, T.J. & T. Kailath (1985) "Adaptive Beamforming for Coherent Signals and Interference" in *IEEE Transactions on Acoustics, Speech, and Signal Processing,* vol. 33, no. 3, pp. 527-536, Jun 1985. doi: 10.1109/TASSP.1985.1164583

Spirent Communications plc (2012) "Simgen Software User Manual," Paignton, 548 pages.

Soloviev, A., C. Toth and D. Grejner-Brzezinska (2011) “Performance of Deeply Integrated GPS/INS in Dense Forestry Areas”, in *Proceeding of ION/GNSS 2011*, September 20-23, Portland, Oregon.

Stöber, C., F. Kneissl, B. Eissfeller, and T. Pany (2011) “Analysis and verification of synthetic multicorrelators,” in *Proceedings of the 24th International Technical Meeting of The Satellite Division of the Institute of Navigation (ION GNSS)*, Portland, OR, September, pp. 2060-2069.

Takasu, T. (2007) *RTKLIB: An Open Source Program Package for GNSS Positioning*, Available at *http://www.rtklib.com/*

Thompson, R. J. R., J.H. Wu, A. T. Balaei, and A. G. Dempster (2010) “Detection of RF interference to GPS using day-to-day C/No differences”, in *International Symposium on GPS/GNSS*, Taipei, Taiwan, October pp. 26-28, 2010, http://www.gmat.unsw.edu.au/snap/publications/thompson_etal2010a.pdf

Tsui, J. B. (2000) *Fundamentals of Global Positioning System Receivers: A Software Approach*, John Willey & Sons, Inc.

Van Dierendonck, A.J. (1996) Parkinson, B. W. and J.J. Jr. Spilker, eds., *Global Positioning System: Theory and Applications*, vol.1, American Institute of Aeronautics, 370 L’Enfant Promenade, SW, Washington, DC, pp 393-394.

van Dierendonck, A. J., P. Fenton, and T. Ford (1992) “Theory and performance of narrow correlator spacing in a GPS receiver,” in *NAVIGATION, Journal of the Institute Of Navigation*, 39(3), Fall 1992, pp. 265-283.

van Diggelen, F. (2009) *A-GPS: Assisted GPS, GNSS, and SBAS,* Jan 1, Artech House, pp. 103-223, ISBN-13: 978-1596933743.

Van Nee, R., J. Siereceld, P. C. Fenton, and B. R. Townsend (1994) "Multipath Estimating Delay Lock Loop: Approaching Theoretical Accuracy Limits," in *Proceedings of the IEEE Position Location and Navigation Synopsium*, , Las Vegas, Nevada, pp. 246-251.

Van Trees, H. (2002). *Optimum Array Processing, Detection, Estimation, and Modulation Theory* Part IV (4th Edition ed.). New York: John Wiley & Sons.

Van Veen, B. D. and K. M. Buckley (1988) "Beamforming: A Versatile Approach to Spatial Filtering," in *IEEE ASSP Magazine*, vol. 5, no. 2, pp. 4-24, April 1988. doi: 10.1109/53.665

Vicario, J.L., M. Barcelo, M. Mañosas, G. Seco-Granados, F. Antreich, J.M. Cebrian, J. Picanyol, and F. Amarillo (2010), “A novel look into digital beamforming techniques for multipath and interference mitigation in Galileo ground stations”, in *2010 5th Advanced Satellite Multimedia Systems Conference and the 11th Signal Processing for Space Communications Workshop*, 2010, pp. 240-247.

Ward, P.W., J. W. Betz and C. J. Hegarty (2006) Kaplan, E. D. and C. J. Hegarty, eds., *Understanding GPS: Principle and Applications*, Second edition, Artech House, Boston, pp. 153-173

Widrow, B., K. Duvall, R. Gooch, and W. Newman (1982) "Signal Cacellation Phenomena in Adaptive Antennas: Causes and Cures" in *IEEE Transactions on Antennas and Propagation*, vol. 30, no. 3, pp. 469-478, May 1982. doi: 10.1109/TAP.1982.1142804

Weiss, J. P., P. Axelrad, and S. Anderson(2007) “A GNSS code multipath model for semi-urban, aircraft, and ship environments,” in *NAVIGATION, Journal of the Institute of Navigation*, vol. 54, no. 4, pp. 293–307, 2007.

Zoltowski, M., & Gecan, A. (1995) "Advanced adaptive null steering concepts for GPS" in *Military Communications Conference, 1995. MILCOM '95, Conference Record, IEEE,* San Diego, CA, 1995, pp. 1214-1218 vol.3. doi: 10.1109/MILCOM.1995.483688.